Masterthesis

Catalytic Degradation of Organic Molecules by Colloidal Hematite in a Silica Box *via* Fenton-like Reaction

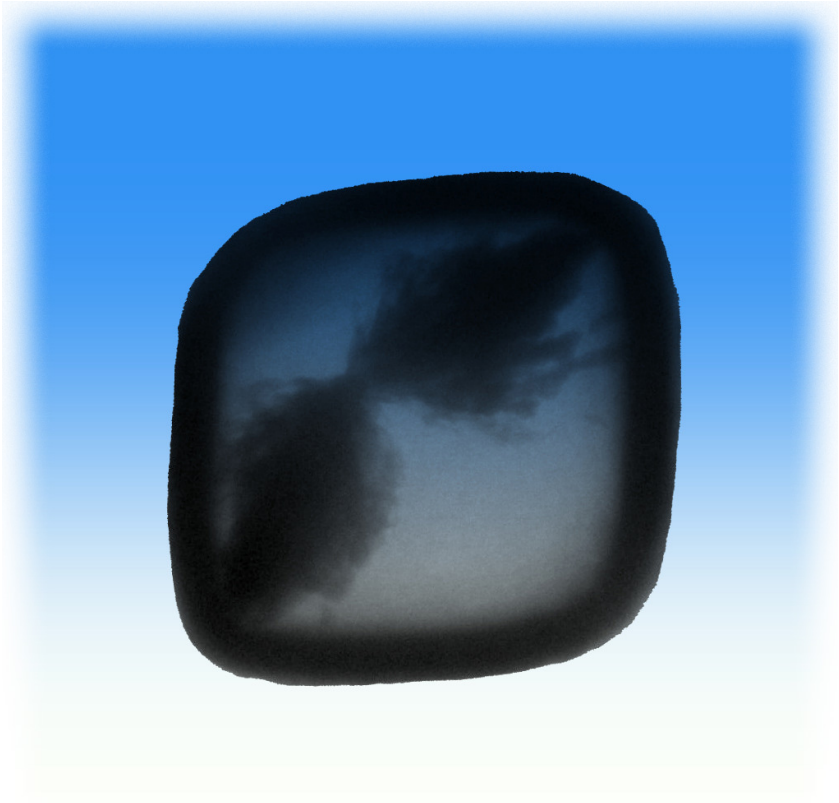

Lisette Pompe BSc

Supervisors:
Sonja Castillo MSc & Prof. Dr. Albert P. Philipse

Van 't Hoff Laboratory for Physical and Colloid Chemistry

Utrecht University

March 2013

Abstract

Fenton's reagent is the combination of ferrous ions (Fe^{2+}) and hydrogen peroxide and is commonly used for the degradation of organic molecules. The ferrous ions promote the formation of radicals from the hydrogen peroxide which degrade the organic molecules. In this research, colloidal hematite (α-Fe_2O_3) cubes are used as a source of iron ions. These cubes were synthesized according to an adjusted method of Sugimoto *et al.* and were coated with amorphous and porous silica, yielding colloidal hematite in a silica box. We find that in the presence of hydrogen peroxide these colloids accelerate the degradation of organic molecules in a fashion similar to Fenton's reagent. The degradation of the model organic molecules methylene blue and rhodamine B was followed by the eye and with UV-Vis spectroscopy to quantify the amount of remaining organic dye. Cubes immobilized on mica substrates were still able to accelerate the reaction, although the catalytic activity was less than for the cubes used in dispersed form. Unfortunately, not all the cubes remained on the support during the reaction. The adhesion was improved by thermally treating the substrates and it was observed that the silica shells were less brittle after the treatment. Nitrogen physisorption measurements were performed on the bare and silica coated hematite cubes to determine the surface area and pore sizes after etching the hematite core or the silica layer. Upon etching of the hematite core with hydrochloric acid the porosity of the hematite and the silica shell increased. A maximum in surface area for hematite during the etching with hydrochloric acid was not found.

Contents

Chapter 1

Introduction

1.1 Colloids

In this research, colloids of iron oxide coated with silica are used in combination with hydrogen peroxide for the degradation of organic molecules. Colloids are particles with at least one dimension between approximately 1 nm and 1 µm and are widely spread. For instance, mud is a dispersion of colloidal clay particles in water, fog consists of water droplets in air and also the fat droplets in milk and mayonnaise are of the colloidal size. Colloids are found in all kinds of shapes and are made of various materials [1]. They are used as model systems for atoms, because they show still Brownian motion, but can be much easier visualized with microscope techniques than individual atoms [2].

1.2 Fenton's reagent and Waste Water Treatment

Iron in the combination with hydrogen peroxide is known to form Fenton's reagent to degrade organic molecules [3]. In this research cubic shaped hematite (α-Fe_2O_3) colloids of $\sim$1 µm were used as a source of iron for the catalytic reaction. The cubes were synthesized *via* a precipitation reaction of iron(III) chloride and sodium hydroxide following the method of Sugimoto *et al.* [4, 5]. The hematite particles were coated with porous silica [6, 7] in order to make a porous box with an iron oxide core.

H.J.H. Fenton discovered the fast degradation reaction of organic molecules in the presence of Fe^{2+}-ions (ferrous ions) and hydrogen peroxide H_2O_2, known as the Fenton reaction, already in 1894 [3]. Although Fenton discovered the reaction, the mechanism was first described by F. Haber and J. Weiss in 1934 [8]. They discovered that the hydroxyl radicals were responsible for the degradation reaction of the organic molecules. In 1949, W.G. Barb *et al.* adjusted the reaction mechanism to what is still the most used explanation today [9, 10]. This reaction mechanism will be discussed in section 2.1.

During the reaction Fe^{2+}-ions act as a catalyst and promote the formation of radicals from hydrogen peroxide [11]. The most important radical is the hydroxyl radical ($OH^{\bullet}$), which has a very high reduction potential (see section 2.1.1.1). Therefore, it can degrade almost any organic molecule. In the Fenton process organic molecules are degraded into fragments mainly by reacting with this radical [11].

The Fenton reaction is known to be very efficient in waste water treatment and can be used for the degradation of a wild variety of organics and is applied in many industrial waste water treatments [11, 12].

1.3 Separation Membranes

Separation membranes are used to separate different species from each other, for example pollutants from waste water, discriminating on their size. Densely packed colloids can form a separation membrane for molecules. Since cubes have a 100 % theoretical packing, they are the perfect shape to form a membrane of.

In this thesis cubic shaped silica coated hematite (α-Fe_2O_3) colloids are applied for this aim. Stöber silica is a porous material through which liquids can pass, however large molecules can not. The cubes

are also filled with iron oxide, so the membrane will not only be able to filter but also to degrade organic molecules by a Fenton-like reaction. Figure 1.1 shows a schematic picture of membrane built up from porous silica boxes, functionalized with hematite for catalysis. The advantage of this membrane is that the silica boxes already contain the hematite core by the followed synthesis route.

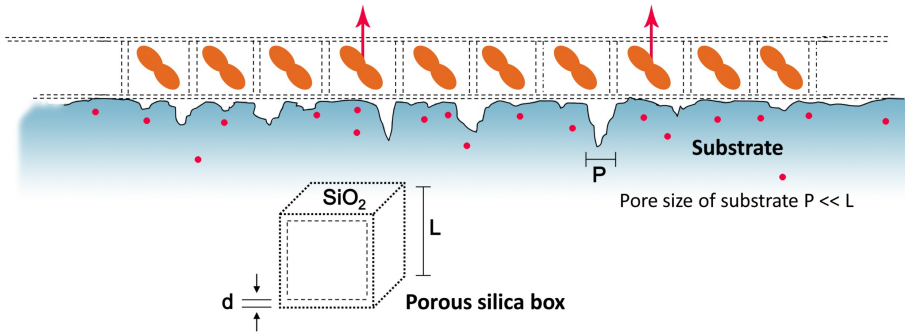

Figure 1.1: Schematic picture of a membrane of porous silica cubes containing hematite. Contaminated water flows from below through the membrane. Large organic molecules will be blocked by the porous silica boxes and small molecules are degraded inside due to the presence of iron oxide and hydrogen peroxide added to the solution.

Chapter 2

Theory

2.1 Fenton's reagent

2.1.1 Reaction Mechanism

The reaction mechanism of the Fenton reaction, the fast degradation of organic molecules in the presence of iron ions and hydrogen peroxide, is stated below [9, 10, 13]. The underlying redox reactions of this mechanism are listed in the next section.

$Fe^{2+} + H_2O_2 \longrightarrow Fe^{3+} + OH^\bullet + OH^-$
$Fe^{3+} + H_2O_2 \longrightarrow Fe^{2+} + OOH^\bullet + H^+$
$Fe^{3+} + OOH^\bullet \longrightarrow Fe^{2+} + O_2 + H^+$
$OH^\bullet + H_2O_2 \longrightarrow OOH^\bullet + H_2O$
$OH^\bullet +$ organic molecule $\longrightarrow$ fragments

First Fe^{2+} promotes the formation of hydroxyl radicals, although little can be found in literature about this specific reaction mechanism. The iron ions are regenerated by hydrogen peroxide to their original oxidation state and so iron can be considered as a catalyst in this reaction. The ratio of ferrous (Fe^{2+}) and ferric (Fe^{3+}) ions can, however, change during the reaction. Finally the produced radicals, and in particular the hydroxyl radicals, are responsible for the fragmentation and degradation of the organic molecules. When completely degraded, the final products from the organic molecules are water, carbon dioxide and inorganic salts [11].

In the case of the hematite (α-Fe_2O_3), which will be used in colloidal form in this research, iron is present as Fe^{3+} and the reaction will start at the second and third step where Fe^{2+} is formed. The Fenton reaction starting with iron(III) instead of iron(II) is called a Fenton-like reaction [11].

2.1.1.1 Redox Reactions

Below, a number of reduction potentials are given for species which play a role in the Fenton's reaction and of fluor as a reference which is known to be a strong oxidant [14]. The degradation of the model organic molecule methylene blue can not be achieved by a redox reaction between the iron ions and methylene blue or hydrogen peroxide and methylene blue, since the difference between the potentials of the oxidant and reductor has to be positive. The only redox reaction that can occur in the first place is between Fe^{3+} and hydrogen peroxide, due to the slightly positive difference in standard reduction potentials between the reduction and the oxidation reaction [14, 15]:

$$\Delta E^0 = E^0_{\text{reduction}} - E^0_{\text{oxidation}} = E^0_{Fe^{3+}} - E^0_{H_2O_2} = 0.77 - 0.70 = 0.07\,\text{V} \tag{2.1}$$

However, Barb *et al.* proposed a different mechanism for the reaction between the Fe^{3+} ions and hydrogen peroxide [10]. Hydrogen peroxide itself is in equilibrium with H^+ and OOH^-. The OOH^- ion can react with the ferric (Fe^{3+}) ion to form a ferrous and a neutral OOH radical. Subsequently the radical can react with another ferric ion.

The Fenton reaction has a optimum at an acidic pH. In literature, a pH of 3 is often stated as the optimum pH for the Fenton reaction [11, 16].

$F_2(g) + 2\,e^- \rightleftharpoons 2\,F^-$	E^0=2.89 V
$OH^\bullet + H^+ + e^- \rightleftharpoons H_2O$	E^0=2.56 V
$O_3(g) + 2\,H^+ + 2\,e^- \rightleftharpoons O_2(g) + H_2O$	E^0=2.08 V
$H_2O_2 + 2\,H^+ + 2\,e^- \rightleftharpoons 2\,H_2O$	E^0=1.76 V
$OOH^\bullet + H^+ + e^- \rightleftharpoons H_2O_2$	E^0=1.44 V
$\frac{1}{2}\,O_2(g) + 2\,H^+ + 2\,e^- \rightleftharpoons H_2O$	E^0=1.23 V
$Fe^{3+} + e^- \rightleftharpoons Fe^{2+}$	E^0=0.77 V
$O_2(g) + 2\,H^+ + 2\,e^- \rightleftharpoons H_2O_2$	E^0=0.70 V
methylene blue $+ 2\,H^+ + 2\,e^- \rightleftharpoons$ reduced state	E^0=0.53 V
$O_2(g) + H^+ + e^- \rightleftharpoons OOH^\bullet$	E^0=−0.05 V

2.2 Nitrogen Physisorption

Molecules and atoms can attach to surfaces in two different ways, covalent or non covalent. The covalent way is called chemisorption, which will only be discussed briefly. Chemisorption is the abbreviation of chemical adsorption and is the chemical bonding of a molecule or atom on a surface. Energy is needed to chemisorb a molecule and the distance from the adsorbate to the surface is much shorter than in physisorption, the other way of attaching a molecule or atom. In physisorption only the van der Waals attraction between the surface and the adsorbate plays a role. The binding energy is typically around $-20\,kJ\,mol^{-1}$, which is ten times smaller than the energy required for chemisorption (around $-200\,kJ\,mol^{-1}$). The binding energy involved in physisorption is not large enough to break a bond in the physisorbed molecule, therefore the adsorbate retains its identity, although the shape might be distorted by the surface [17].

Physisorption can be used to determine the surface area of a material and the presence of pores and their size. The most common used technique is nitrogen physisorption. Physisorption can also be done with other gases, however nitrogen is abundant, relatively cheap, the measurement temperature is well controllable and the molecules hardly change their shape and size when it adsorbed on an interface.

2.2.1 Operation of a Nitrogen Physisorption Apparatus

In figure 2.1 a schematic representation of a nitrogen physisorption apparatus is shown. The set-up consist of two compartments with a known volume; compartment one is empty and compartment two contains the material to be measured. First, vacuum is created in the two compartments to ensure that all adsorbed species on the material are removed. The left compartment is then filled with nitrogen while the right one is closed. Subsequently, the valve between the compartments is opened and the material in the right compartment takes up some gas. After equilibration, the pressure is measured and the valve between the two compartments is closed. The pressure in compartment one is increased and after equilibration between the two compartments the pressure is measured again. These steps are repeated until the condensation pressure of the gas is reached, which is one bar for nitrogen at 77 K. The amount of adsorbed gas can be calculated from the difference in pressure for each step and a plot of the amount of adsorbed gas as a function of the pressure is obtained. In this way the absorption curve is obtained, for the desorption curve the pressure in the first compartment is lowered in each step. The adsorption and desorption curves, and the difference between them, contains information about the surface area of the material and the pores in the material [18].

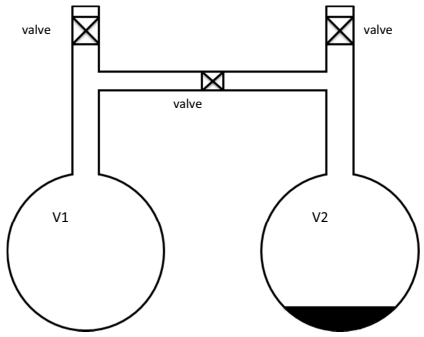

Figure 2.1: Schematic picture of the operation of a nitrogen physisorption apparatus. Compartment 2 (V2) is filled with the material being measured. The compartments can be opened and closed by the valves. Redrawn from [18].

2.2.2 Pores

The IUPAC (International Union of Pure and Applied Chemistry) defined pores in the three following classed, depending on their size [19]:

micropores	$<2\,\mathrm{nm}$
mesopores	2–50 nm
macropores	$>50\,\mathrm{nm}$

The size and the shape of the pores in a material can also be determined with nitrogen physisorption. Small pores fill at a lower pressure and hysteresis between the adsorption and the desorption curve contains information about the shape of the pores. First the capillary condensation in the pores is discussed according to the Kelvin equation, whereafter the different pore shapes are discussed.

2.2.2.1 Kelvin Equation

The Kelvin equation describes the equilibrium condition for curved surfaces of a liquid that is in equilibrium with the vapor phase [18]:

$$\ln \frac{p_\mathrm{r}}{p_0} = \frac{V_\mathrm{m}\gamma}{RT}\left(\frac{1}{r_1}+\frac{1}{r_2}\right) \tag{2.2}$$

Where p_r is the vapor pressure of a supersaturated gas that is in equilibrium with droplets with radius r, p_0 is the saturated vapor pressure, V_m the molar volume (in $\mathrm{cm^3/mol}$ or $\mathrm{m^3/mol}$) and γ the surface tension (in $\mathrm{J/m^2}$) both of the liquid. R is the gas constant, T the absolute temperature and r_1 and r_2 are the radii of curvature of the surface in two directions. Notice that the radius is positive for a convex surface and negative for a concave surface. The difference in the adsorption and the desorption isotherm will only be observed when meso- or marcropores are present. Micropores fill at low pressure and therefore no hysteresis occurs. Since the measurements are performed with nitrogen, $T = 77\,\mathrm{K}$, $\gamma = 0.0085\,\mathrm{J/m^2}$ and $V_\mathrm{m} = 30\,\mathrm{cm^3/mol}$.

A spherical and a cylindrical meniscus are shown in figure 2.2, these two types are common in adsorption of gasses. For the spherical meniscus in figure 2.2a the radii are equal and because the surface is concave, both are negative. The Kelvin equation for this surface then is:

$$p_\mathrm{r} = p_0 \exp\left(\frac{V_\mathrm{m}\gamma\left(-\frac{1}{r}-\frac{1}{r}\right)}{RT}\right) = p_0 \exp\left(-\frac{2V_\mathrm{m}\gamma}{rRT}\right) \tag{2.3}$$

For the surface in figure 2.2b the surface is curved in one direction and flat in the other direction. The Kelvin equation for this cylindrical surface is therefore:

$$p_r = p_0 \exp\left(\frac{V_m \gamma \left(-\frac{1}{r} + \frac{1}{\infty}\right)}{RT}\right) = p_0 \exp\left(-\frac{V_m \gamma}{rRT}\right) \tag{2.4}$$

For a flat surface between the liquid and vapor phase, p_r has to equal p_0 which also follows from the Kelvin equation:

$$p_r = p_0 \exp\left(\frac{V_m \gamma \left(\frac{1}{\infty} + \frac{1}{\infty}\right)}{RT}\right) = p_0 \tag{2.5}$$

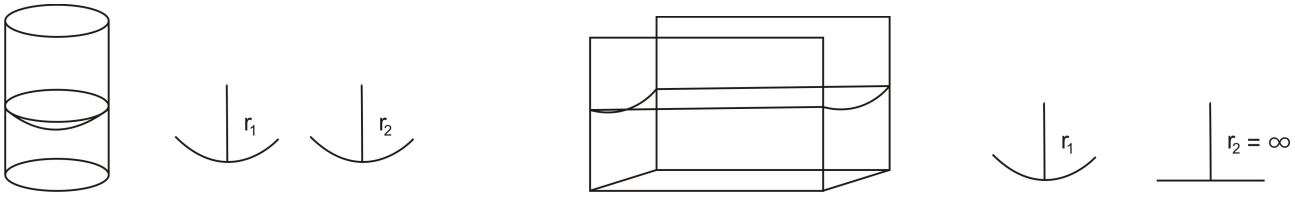

(a) Spherical mensiscus **(b)** Cylindrical meniscus

Figure 2.2: The spherical interface is curved in two directions, where the cylindrical interface is curved one direction and flat in the other direction. Redrawn from [18].

From these formulas it can be seen that the pressure above a spherical interface is smaller than above a cylindrical interface. Also the fact that small pores fill at low pressure can be understand using the Kelvin equation.

2.2.2.2 Slit-like Pores

In slit-like pores the thickness of the layer fill follow the normal absorption, depending on the material and the pressure. This adsorption can for instance be described by formula 2.12, which will be discussed later. The layers will touch when the thickness of the layer is half the diameter of the pore. However, for the desorption the interface is curved, as can be seen in figure 2.3, which results in emptying of the pore at a lower pressure.

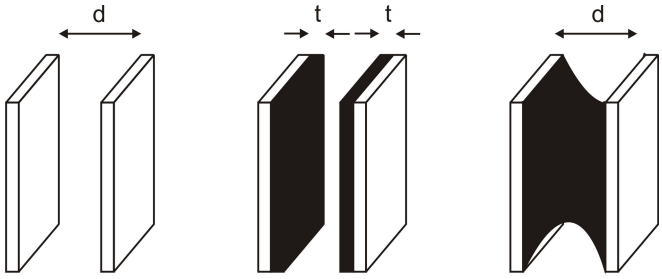

Figure 2.3: Adsorption and desorption of a slit-like pore. From left to right: empty slit-like pore, a slit-like pore during filling and a slit-like pore during emptying of the pore. Redrawn from [18].

2.2.2.3 Cylindrical Pores

There are two types of cylindrical pores: pores that are open at both sides and pores that are open at only one side. These two types show different behavior in the physisorption measurements. In the Kelvin equation r is replaced by $r_p - t_{cyl}$, the pore radius minus the adsorbed thickness, because the radii of cylindrical pores depend on thickness of the already adsorbed layer.

Open at Both Sides For pores open at both sides hysteresis is observed, the adsorption takes place at:

$$p_r = p_0 \exp\left(-\frac{2V_m\gamma}{(r_p - t_{cyl})RT}\right) \tag{2.6}$$

The desorption of the cylindrical pore takes place at:

$$p_r = p_0 \exp\left(\frac{V_m\gamma\left(-\frac{1}{r_p - t_{cyl}} + \frac{1}{\infty}\right)}{RT}\right) = p_0 \exp\left(-\frac{V_m\gamma}{(r_p - t_{cyl})RT}\right) \tag{2.7}$$

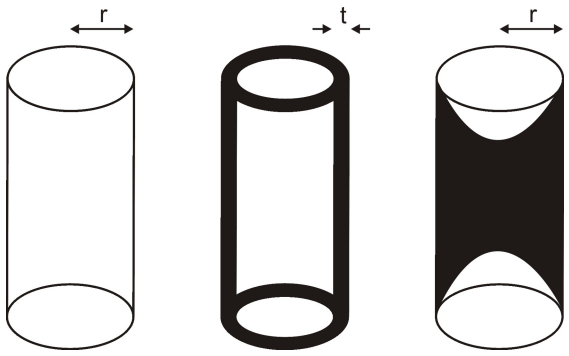

Figure 2.4: Schematic representation of adsorption and desorption of an open cylindrical pore. The interface is curved in one direction during the adsorption and is curved in two directions during the desorption. Redrawn from [18].

Open at One Side For one end open cylindrical pores there is no hysteresis between the adsorption and desorption curve, because the smallest curvatures are the same in adsorption and desorption. Therefore the filling and opening takes place at:

$$p_r = p_0 \exp\left(-\frac{2V_m\gamma}{(r_p - t_{cyl})RT}\right) \tag{2.8}$$

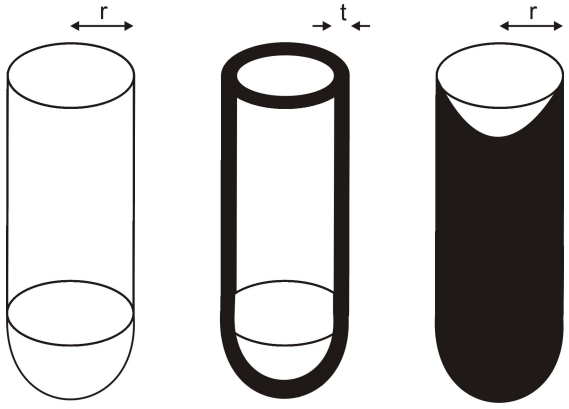

Figure 2.5: The interface of a one side closed pore is curved in two directions during adsorption and desorption. Redrawn from [18].

2.2.2.4 Ink Bottle Pores

For ink bottle pores, schematically drawn in figure 2.6, the moment of adsorption is determined by the radius of the large volume, while the point of desorption is determined by the relatively small radius of the cylinder. This results in a relatively large hysteresis compared to the hysteresis found for slit-like and cylindrical pores.

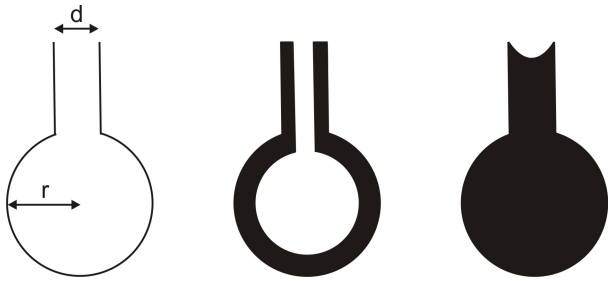

Figure 2.6: The radius of the large volume determines the adsorption pressure and the radius of the small end determines the desorption pressure. Both interfaces are curves in two directions. Redrawn from [18].

2.2.3 Isotherms

In this section, the Langmuir and BET theories for molecules adsorbing on a surface are discussed, as well as the t-plot method used for microporous materials.

2.2.3.1 IUPAC Classifications of Isotherms

Different materials give rise to different types of isotherms. IUPAC categorized physisorption isotherms in six types which are shown in figure 2.7 and will be discussed briefly here [20].

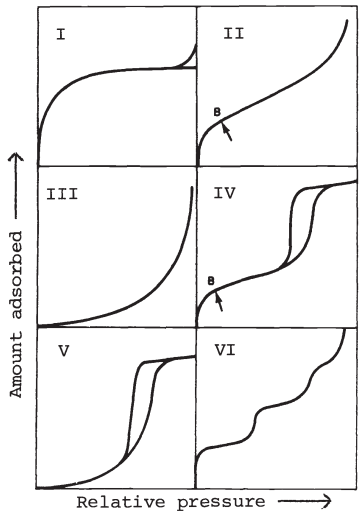

Figure 2.7: IUPAC classifications of physisorption isotherms, see the text for details [20].

Type I This isotherm is obtained by materials with a relatively low external surface and has the form of the Langmuir isotherm (section 2.2.3.2).

Type II This isotherm is often obtained for non-porous or macroporous materials.

Type III This type of isotherm is not very common, however it can be found when the interaction between the material and the adsorbed species is very weak.

Type IV This type is the equivalent of Type II for materials with mesopores. The mesopores cause the hystheresis in the isotherm, which is discussed in section 2.2.2.

Type V This isotherm is the equivalent of Type III for porous materials.

Type VI This isotherm shows stepwise multilayer adsorption. This form can be obtained with argon or krypton on graphitised carbon blacks at liquid nitrogen temperature.

2.2.3.2 Langmuir Isotherm

The Langmuir isotherm is one of the most simplest theories for adsorption and describes monolayer adsorption of gases on surfaces [21, 22]. Furthermore, this theory assumes that all adsorption sites on the surface are equal and there are no interactions between the adsorbed molecules. Formula 2.9 is the Langmuir isotherm and can be derived form thermodynamics and equilibrium reactions. In figure 2.8 the Langmuir isotherm is plotted for different values of K, the equilibrium constant. θ is the surface coverage, which equals one when the surface is completely covered and p is the pressure. Since θ is unitless K has the unit bar^{-1} when p has the unit bar.

$$\theta = \frac{Kp}{1 + Kp} \tag{2.9}$$

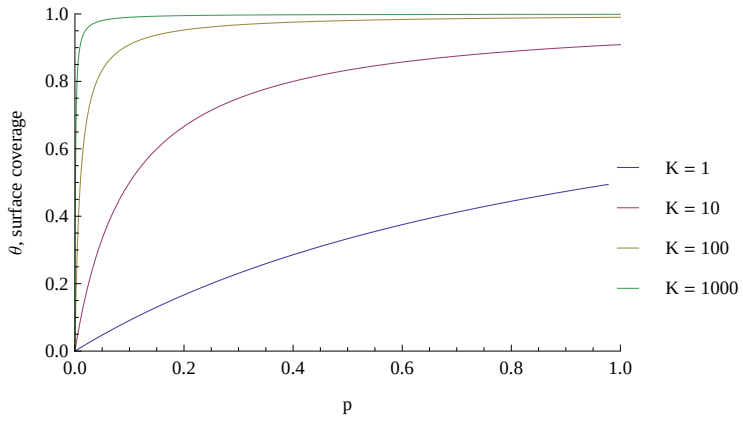

Figure 2.8: Langmuir isotherms for different equilibrium constants

2.2.3.3 BET-isotherm

The BET-isotherm (equation 2.10), named after and derived by Brunauer, Emmett and Teller is a theory describing multilayer adsorption [23]. In this formula V_{ad} is the adsorbed volume nitrogen in cm^3 or m^3 at 273 K and 1 atm, V_{ml} the volume of one monolayer in cm^3 or m^3 at 273 K and 1 atm, $c = \frac{K_1}{K_2}$, the BET-constant where K is the equilibrium constant between the adsorbed and the desorbed molecules in Pa^{-1}. Moreover, c compares the interaction for the first and the following layers and is a rough measure for the heat of adsorption for the first layer. When molecules adsorb easily at low pressure the c value is high, as also can be seen in figure 2.9. p/p_0 is the relative pressure and the condensation pressure is at $p/p_0 = 1$. The equation describes the adsorption of the number of molecules on a surface as a function of the pressure.

$$\frac{V_{\text{ad}}}{V_{\text{ml}}} = \frac{cp/p_0}{(1 - p/p_0 + cp/p_0)(1 - p/p_0)} \tag{2.10}$$

The BET-constant c is a measure for the interaction between the nitrogen molecules and the material. In figure 2.9 a few isotherms are given for several values of c.

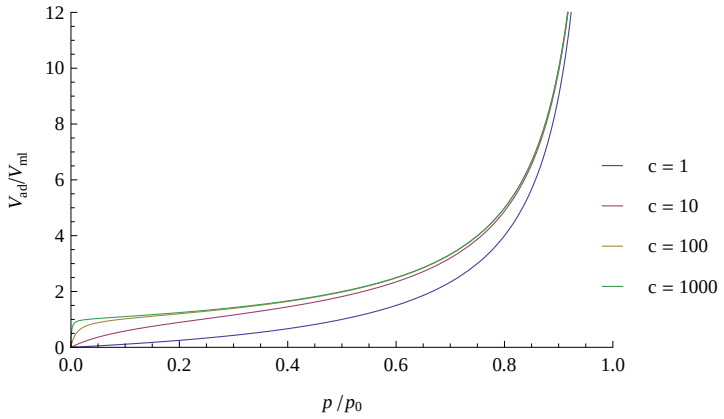

Figure 2.9: BET isotherm for different BET-constants.

The BET-isotherm is only valid when certain assumptions are made. The BET-isotherm assumes that all the nitrogen molecules adsorb on equal adsorption sites, but in practice some places on the surface will be favored. All the layers of adsorbed molecules are assumed to be equal and the heat of adsorbtion is assumed to be equal in all the layers except for the first layer adsorbed on the surface. In reality the second layer will be adsorbed more easily than for example the fourth layer. The interaction of molecules within a layer is assumed to be absent and therefore a molecule can not adsorb on a site in a layer when the place below is not occupied. A big disadvantage of the BET-isotherm is that is also assumes the absence of pores. This makes the BET-isotherm only a good description for the adsorbtion of the first few layers.

To determine the constants in the BET-isotherm it is useful to linearize equation 2.10 to formula 2.11.

$$\frac{p/p_0}{V_{ad}(1-p/p_0)} = \frac{1}{V_{ml}c} + \frac{c-1}{V_{ml}c}p/p_0 \tag{2.11}$$

Where $\frac{c-1}{V_{ml}c}$ is the slope and $\frac{1}{V_{ml}c}$ the intercept with the y-axis. The BET-isotherm is fitted in this way usually between $0.05 < p/p_0 < 0.3$.

2.2.3.4 t-plot Method

The t-plot method is used to determine the surface area and the pore volume of microporous materials. Due to the capillary condensation in the pores, more gas is adsorbed in porous materials than in non-porous materials. t in the following equations is the statistical thickness of an adsorbed monolayer at a certain pressure for a non-porous material. The statistical thickness is compared with the adsorbed amount of gas with one of the following formulas. From the linear ranges the surface area follows from the slope and the micropore volume from the intercept. The intercept and the slope are corrected by applying a correction factor. This correction factor is determined for a non-porous silica-alumina material.

The formulas are both plotted in figure 2.10, in this thesis the most commonly used Harkins–Jura–de Boer isotherm (equation 2.12) will be used to determine the pore volume [24, 25]. The second formula is the Dollimore–Heal equation [26, 27].

$$\text{HJB:} \quad t = \sqrt{\frac{0.1399}{0.034 - \log(p/p_0)}} \tag{2.12}$$

$$\text{DH:} \quad t = 0.354 \left(\frac{-5}{\ln(p/p_0)} \right)^{1/3} \tag{2.13}$$

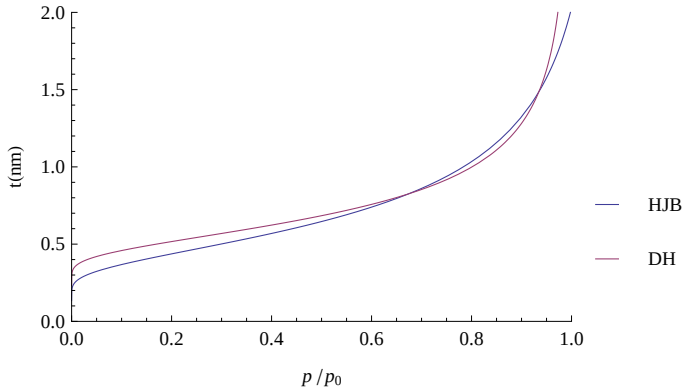

Figure 2.10: Plot of the Harkins–Jura–de Boer (HJB) and the Dollimore–Heal (DH) equations.

2.3 Self-assembly of Cubes

To block the major part of the contaminants in a feed solution by the membrane, the cubic shape particles have to (self-)assemble into a face centered cubic (fcc)-like structure. It has previously been found that silica cubes can assemble in cubic crystals by the use of a depletant, which forces the cubes together [28]. Nevertheless, silica coated hematite cubes can form densely packed structures in the absence of a depletant, which can be seen in figure 4.37. In this scanning electron microscope (SEM) picture silica coated hematite cubes were dried on a mica substrate, on which they also form ordered structures.

Jiao *et al.* modeled the optimal packing of 2D superdisks and 3D superballs [29, 30]. The colloidal hematite cubes have the superball shape, which can be described by equation 2.14. x, y and z are Cartesian coordinates and m is the shape parameter [31]. The shape parameter defines the deformation of the superball. For $m = 2$ a sphere is obtained and for $m = \infty$ a perfect cube.

$$(x)^m + (y)^m + (z)^m = 1 \tag{2.14}$$

Depending on the shape parameter the following structures were found for superballs by Jiao *et al.* [30]. In figure 2.11 two structures are shown for superballs with $m > 1$. For superballs with $m > 2.3$ the C_1-packing, shown in figure 2.11b, is found to be the most dense and favored packing. These dense packings of cubic particles would be ideal to form a separation membrane.

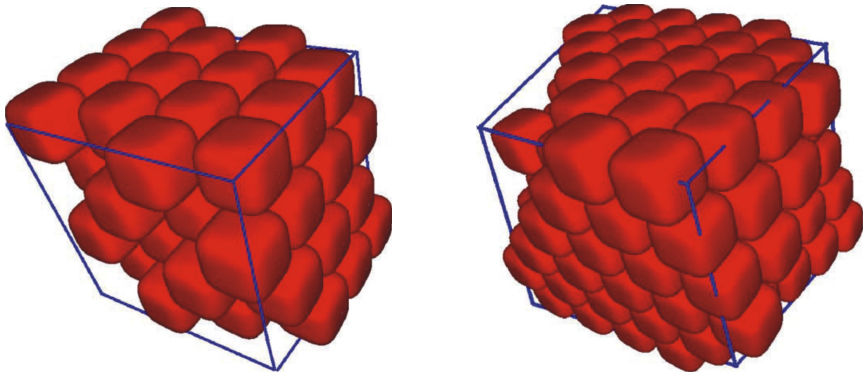

(a) C_0-packing for $m = 3.6$. **(b)** C_1-packing for $m = 4$.

Figure 2.11: Figures taken from [30].

2.4 Properties of Hematite

Hematite (α-Fe_2O_3) is, together with goethite (α-FeOOH), one of the most stable forms of iron oxide and is therefore the most common natural form of iron [32]. It appears red when it is finely divided and

black or grey when it is crystalline, see figure 2.12 [15]. The crystal structure of hematite is hexagonal (rhombohedral) [15, 33] and the density of the material is 5.26 g/cm^3 [32].

Figure 2.12: Hematite mineral [34].

2.4.1 Colloidal Hematite Cubes

Colloidal hematite cubes can be synthesized *via* a precipitation reaction of iron (III) cloride ($FeCl_3$) and sodium hydroxide (NaOH) to iron hydroxide ($Fe(OH)_3$) [4, 5]. During this synthesis, needles of akaganéite (β-FeOOOH) are formed which aggregate while the akaganéite dehydrates to form hematite [35]. The final internal structure of the particles still contains the needle structure [36]. Furthermore, the size of the colloidal particles can be controlled by the excess of Fe^{3+}. The excess of ferric ions (Fe_x^{3+}) can be calculated from the reaction equation with the following formula.

$$Fe_x^{3+} = Fe_{total}^{3+} - \frac{1}{3}OH_{total}^{-} \tag{2.15}$$

The larger the excess of Fe^{3+} ions, the larger the particles will become [4, 37]. The cubic shape of the hematite colloids is obtained by the absorption of chloride ions on the {012} crystal planes [38, 39]. Rossi has confirmed that obtained particles from this reaction are made solely of hematite by X-ray powder diffraction [40].

2.4.2 Acidity of Iron Ions

Solutions of iron chloride are highly acidic, because the iron ions in solution can form an aqua acid. This means that six water molecules coordinate to the iron ion as can be seen in figure 2.13. Subsequently, a proton can be repelled and an acidic solution is formed. Iron(II) ions can also form aqua complexes, however, due to their lower charge less protons will be repelled [41]. The equilibrium reaction for the hexaaquairon(III) ion is given by:

$$[Fe(OH_2)_6]^{3+}(aq) + H_2O(l) \rightleftharpoons [Fe(OH_2)_5(OH)]^{2+}(aq) + H_3O^{+}(aq) \tag{2.16}$$

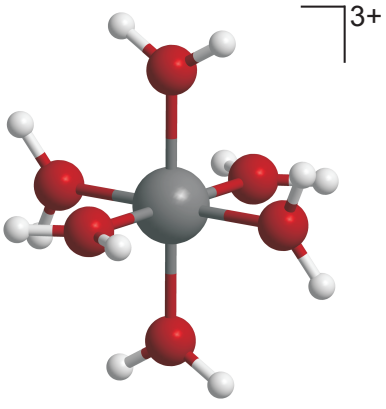

Figure 2.13: Iron water complex, hexaaquairon(III) ion

2.5 Properties of Stöber Silica

For the coating of the particles with silica, the silica precursor tetraethyl orthosilicate (TEOS) is used. TEOS can be hydrolyzed and subsequently condensated to form Stöber silica (SiO_2) following the total overall reaction given in equation 2.17 [6]. The formation of Stöber silica is catalyzed by a base although the hydrolyzation and condensation reaction can also be catalyzed by an acid. From this reaction in ethanol, porous silica is formed and when catalyzed by a base, having a porosity of 70 % and a specific surface area of 515 m^2/g [42]. The density of the silica is approximately 2 g/cm^3 [43].

$$Si(OC_2H_5)_4 + 2\,H_2O \longrightarrow SiO_2 + 4\,C_2H_5OH \tag{2.17}$$

The pH in the reaction mixtures with the hematite cubes, hydrogen peroxide and an organic molecule is quite low, around pH 3. This will be favorable for the silica coating, because the solubility in water of silica is less at low pH than at moderate or high pH [44].

It is known for Stöber silica to melt around 1150 °C and fuse into dense silica. However also at lower temperatures (upto 850 °C) the strength of silica is increased by the disappearance of silanol and ethoxy groups on the surface [45]. Unfortunately the porosity of the silica also disappears above 850–950 °C [46].

2.5.1 Surface Protected Water Etching of Silica

To make silica more porous, without affecting the shape of a colloidal particle, the silica can be etched by surface protected water etching [47, 48]. In figure 2.14 the procedure is schematically shown. First an adsorbing polymer is added to the particles, in this case polyvinylpyrrolidone (PVP). The polymer will protect the outer surface. The etching is carried out in water around its boiling point, whether or not in the presence of sodium hydroxide [48]. Silica dissolves in a basic environment and because the outer surface is protected by PVP the OH^--ions diffuse into the silica layer and dissolve the silica inside [44, 47]. Depending on the degree of etching the particles can be made hollow.

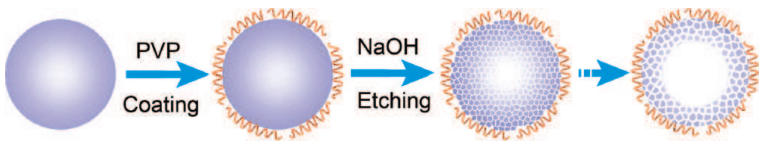

Figure 2.14: Schematic picture of the surface protected water etching process. First PVP is adsorbed on silica particles to protect the outer surface. Subsequently the (basic) solution in heated leaving a porous and optionally hollow silica particle. Taken from [47].

2.6 Analytical techniques

In the following sections the analytical techniques used during this research are briefly explained.

2.6.1 Electron Microscopy

Using electron microscopy a higher resolution is obtained than using light microscopy. Instead of light electrons are used to visualize materials. The wavelength of particles with a high speed is namely smaller than the wavelength of visible light and is determined by the De Broglie wavelength [49]:

$$\lambda = \frac{h}{mv} \tag{2.18}$$

Electron microscopy was used for the visual observation of the particles. Both transmission and scanning electron microscopy were used to observe individual particles and determine their size. In the next figure the operation of the microscopes is shown schematically, which will be discussed in the next two sections.

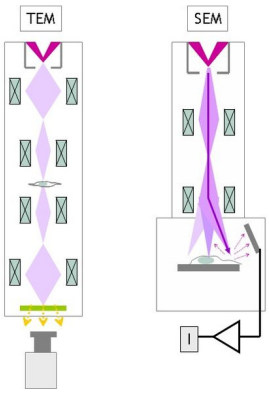

Figure 2.15: Schematic picture of (left) TEM and (right) SEM. In the TEM electrons pass through the sample whereafter the electrons are detected. In the SEM the backscattered electrons are detected. The magnetic lenses are denoted in the figure by the rectangles with crosses and focus the electron beam. Figure taken from [50].

2.6.1.1 TEM

In a transmission electron microscope (TEM) electrons are emitted by an electron gun, usually a tungsten filament. The electrons are accelerated by a high voltage and are focused by the magnetic lenses. The electrons pass through the sample, therefore a thin sample is needed, otherwise no electrons can be detected. Electrons encountering a thin specimen are often diffracted and can be detected in the so-called dark field mode, electrons encountering a thick specimen are not transmitted nor detected. A contrast image is formed by detecting the transmitted electrons [49].

2.6.1.2 SEM

In the case of a scanning electron microscope (SEM) no thin sample is needed. In a SEM also electrons are accelerated and hit the specimen. Because the backscattered and not the transmitted electrons are detected, the surface morphology of the sample can be viewed by a quasi 3D image. For SEM there is no need of a thin sample, however the sample has to be conducting. Therefore the surface is usually coated with a thin layer of metal [49].

2.6.2 UV-Vis Spectroscopy

In a UV-Vis spectrometer the difference in intensity of the incident beam (I_0) and the intensity of the transmitted beam (I_e) is measured for each wavelength, usually between 200 and 700 nm. The transmission is determined by equation 2.19 and the absorption by equation 2.20.

$$\text{Transmission} = T = I_e/I_0 \tag{2.19}$$

$$\text{Absorption} = 100 - T \tag{2.20}$$

However, it is convenient to use the absorbance (equation 2.21), because the absorbance is linear with concentration as given by the law of Lamber–Beer in equation 2.22.

$$\text{Absorbance} = A = -\log T = -\log I_e/I_0 \tag{2.21}$$

$$A = \epsilon c l \tag{2.22}$$

Where ϵ is the molar extinction coefficient in $M^{-1}cm^{-1}$, c the concentration in M and l the length of the cuvet in cm (usually 1 cm) [14]. In this research UV-Vis spectroscopy is used to quantify the remaining amount of dye during the catalytic degradation reaction of the dye molecules methylene blue and rhodamine B in the presence of hematite cubes and hydrogen peroxide.

2.6.2.1 Reaction Speed

The absorbance for one peak is plotted versus the time, the slope is a measure for the reaction speed of the degradation of the organic molecules by the Fenton reaction. The absorbance decreases namely during the degradation reaction. The slope is given by:

$$\text{reaction speed} = \frac{\Delta A}{\Delta t} \tag{2.23}$$

Finally the conversion of organic molecules is liked to be known, in molecules degraded per second, and is calculated by:

$$\text{speed (molecules/second)} = \frac{\Delta A}{\epsilon\, \Delta t} \frac{\text{total reaction volume (mL)} \cdot N_{\text{av}}}{1000 \cdot 86400} \tag{2.24}$$

This equation gives the total number of molecules converted in the reaction mixture. ΔA is the difference in absorbance over a time Δt (in days). ϵ is the molar extinction coefficient for the defined peak in $\text{M}^{-1}\text{cm}^{-1}$ and N_{av} is Avogadro's constant. From this speed also the theoretical degradation time can be calculated, wherein no color would be observed anymore. The result should be divided by the path length of the light, which is the thickness of the cuvet used in the experiment, to obtain the right units. The used path length throughout this thesis is 1 cm and therefore is left out of the formula in equation 2.24.

Also the number of converted molecules per cube per second can be calculated. Therefore number of cubes present in the reaction mixtures were approximated using the weight percentage of the dispersion, the volume of a perfect cube and the percentage of etched away silica and/or hematite by:

$$\text{number of cubes} = \frac{m_{\text{total}}}{m_{\text{single cube}}} \approx \frac{\text{mL of dispersion} \cdot \text{weight \%}/100}{d^3 \cdot \rho_{\text{hematite}} \cdot f_{\text{hematite}} + V_{\text{silica shell}} \cdot \rho_{\text{silica}} \cdot f_{\text{silica}}} \tag{2.25}$$

Where,

$$V_{\text{silica shell}} = (2\tau_{\text{silica}} + d)^3 - d^3 \tag{2.26}$$

d is the edge length of a perfect cube, τ_{silcia} the thickness of a silica shell, f_{hematite} the fraction of remaining hematite and f_{silica} the fraction of remaining silica. For non-etched particles f_{hematite} and f_{silica} are one. ρ_{hematite} is the density of hematite ($5.2 \times 10^3\,\text{kg/m}^3$) and ρ_{silica} the density of silica ($2.0 \times 10^3\,\text{kg/m}^3$). The density of water was assumed to be $1 \times 10^3\,\text{kg/m}^3$. The turnover-number (TON) in molecules per second per cube is calculated by dividing the speed (molecules/second) by the number of cubes. The theoretical degradation time and the TON given in this thesis actually can not be determined with the high accuracy they are given. However, these numbers are used to compare the experiments with each other.

2.6.3 Infrared Spectroscopy

Organic molecules and inorganic materials can absorb light in the infrared by changing their vibrational energy. The wavelengths where absorption occurs are characteristic for the compound. In infrared spectroscopy, just like in UV-Vis spectroscopy, the absorbance is measured for wavelengths usually between 450 and $4000\,\text{cm}^{-1}$. Inorganic compounds or low concentration solutions are usually measures in a solid KBr matrix. The compound or solution is added to KBr powder and pellets are made from the dried powder whereafter the infrared spectrum is recorded [14].

Chapter 3

Experimental

3.1 Chemicals

Name, purity (acronym)	Formula	Supplier
Ethanol, 100 %	C_2H_5OH	Interchema
Hydrochloric acid, 37 wt% in water	HCl	Emsure
Hydrogen peroxide, 35 wt% solution in water, stabilized, p.a.	H_2O_2	Acros Organics
Iron(III) chloride hexahydrate, p.a.	$FeCl_3 \cdot 6\,H_2O$	Sigma-Aldrich
Methylene blue	$C_{16}H_{18}N_3SCl$	J. T. Baker
Polyvinylpyrrolidone, 40 kg/mol (PVP)	$(C_6H_9NO)_n$	Sigma-Aldrich
Potassium bromide, p.a. for IR-spectroscopy	KBr	Fluka
Rhodamine B	$C_{28}H_{31}N_2O_3Cl$	Sigma-Aldrich
Sodium hydroxide, p.a.	NaOH	Emsure
Tetraethyl orthosilicate, puriss $\geq$99.0 % (TEOS)	$Si(OC_2H_5)_4$	Sigma-Aldrich
Tetramethylammonium hydroxide, 25 wt% in water (TMAH)	$(CH_3)_4NOH$	Fluka

All chemicals were used as received from the supplier and the water used during the syntheses was purified with a Synergy Millipore water purification system (Millipore water).

3.2 Synthesis of Hematite Cubes

Hematite cubes were synthesized following an adjusted method of Sugimoto *et al.* [4, 5, 37], from iron(III) chloride hexahydrate ($FeCl_3 \cdot 6\,H_2O$) and sodium hydroxide (NaOH).

First, 20 g of NaOH was dissolved in Millipore water and transferred quantitatively to a 100 mL volumetric flask, where the volume was brought to 100 mL. The sodium hydroxide solution became warm upon dissociation of NaOH. 50 g of $FeCl_3 \cdot 6\,H_2O$ was dissolved in 100 mL water (measured with a graduated cylinder). The iron(III) chloride hexahydrate solutions were placed in an ultrasound bath for 20 minutes to ensure complete solvation.

In approximately 20 seconds the sodium hydroxide solution was added to the iron chloride solution, while stirred vigorously. Upon addition, a dark brown gel/slurry was formed and the solution was stirred for another ten minutes. After removal of the stirring bar the gel was placed in an oven (Memmert Type UE300) at 100 °C for eight days. After these eight days the cubes were washed several times to remove the acid, the non-perfectly formed small cubes and the possibly remaining needles. The needles are formed in the beginning of the reaction and assemble during the reaction into cubes [35, 36]. The formed cubes were stored in Millipore water.

3.3 Coating of Cubes with Stöber Silica

The hematite cubes were coated with silica according to method of Graf, based on the Stöber method [6, 7, 28].

7 g of 40 kg/mol polyvinylpyrrolidone (PVP) was adsorbed to 1 g of hematite cubes, dispersed in Millipore water, in a total volume of about 200 mL. The cubes were stirred overnight at 300–400 rpm with a magnetic stirring bar. The centrifuge tube in which they were stirred was covered with aluminium foil since it has been suggested that PVP is light sensitive [7].

The PVP coated hematite cubes were subsequently washed twice by centrifugation and redispersion in ethanol to remove the excess PVP and to transfer the cubes to ethanol for the silica coating. The cubes were redispersed in 150–200 mL ethanol. The total volume has to be known, and therefore the ethanol was measured in a graduated cylinder.

For the silica-coating-reaction two stock solutions were prepared. The first is the catalyst for the silica reaction, namely a 1 wt% tetramethylammonium hydroxide (TMAH) solution in water. The other is a solution of 20 g 40 kg/mol PVP in 100 mL ethanol. The PVP mixture was stirred until all the PVP was dissolved and was then placed in an ultrasound bath for 20 minutes.

The silica coating was performed in a 1 L two-neck round-bottom flask (4)[1]. The flask was placed in an ultrasound bath (5) (Branson 8210, cooled), which prevents the cubes to coalesce during the Stöber synthesis. The total reaction volume was 500 mL. First, about 200 mL of ethanol was poured into the flask, depending on the amount of solvent wherein the cubes were redispersed. Thereafter, 66 mL of Millipore water and 10 mL of 1 wt% TMAH were added. Then the ultrasound bath was switched on and the cubes were added. In 45 minutes 10 mL tetraethyl orthosilicate (TEOS), diluted with 10 mL of ethanol, was added with a peristaltic pump (1) (Gilson minipuls 3 or Gilson minipuls evolution), using a tube (3) to the flask. During the whole reaction the mixture was stirred mechanically and ultrasonicated. After the TEOS was added the 20 g PVP solution was added to prevent the particles sticking together. The ultrasound bath was switched on as long as possible, but at least three times 99 minutes. The mixture was stirred during sonication and overnight with an overhead stirrer (2). After the synthesis the cubes were washed with ethanol by centrifugation and redispersion in clean ethanol. The next figure shows a picture of the silica coating set-up.

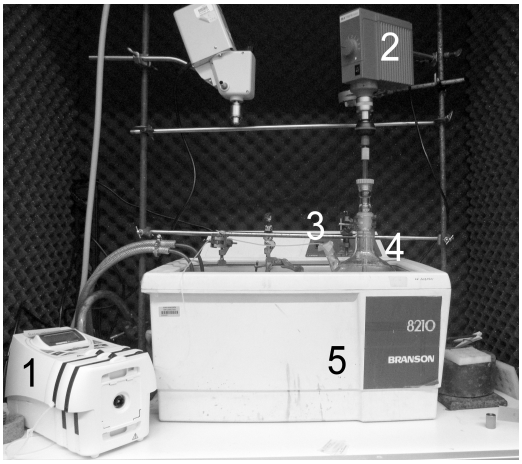

Figure 3.1: Set-up of the silica coating. From the peristaltic pump (1) there is a tube (3) to the round-bottom flask (4) at the right side in the ultrasound bath (5). The mixture in the flask is stirred with an overhead stirrer (2).

3.4 Etching of Hematite

Once the hematite is coated with silica, the hematite inside the particles can be etched to obtain a higher surface area. A higher surface area results in an increased amount of accessible iron ions for the Fenton reaction.

[1] The numbers between brackets correspond to the numbers in figure 3.1

For the etching process, 6 or 12 M hydrochloric acid (HCl) was added to the silica coated hematite cubes portion wise. The reaction was performed in water.

Examples of the final cubes, depending on the HCl concentration and the duration of the etching, are depicted in figure 3.2. Longer etching times and higher concentrations of HCl result in a smaller hematite core.

In figure 3.2, the upper row shows TEM pictures of the cubes and the bottom row shows the color of the dispersion. The cubes in 3.2a were not subjected to etching, the cubes in figure 3.2c were etched over a longer time than the cubes in the middle (3.2b). When the hematite core becomes smaller the color changes from red to orange.

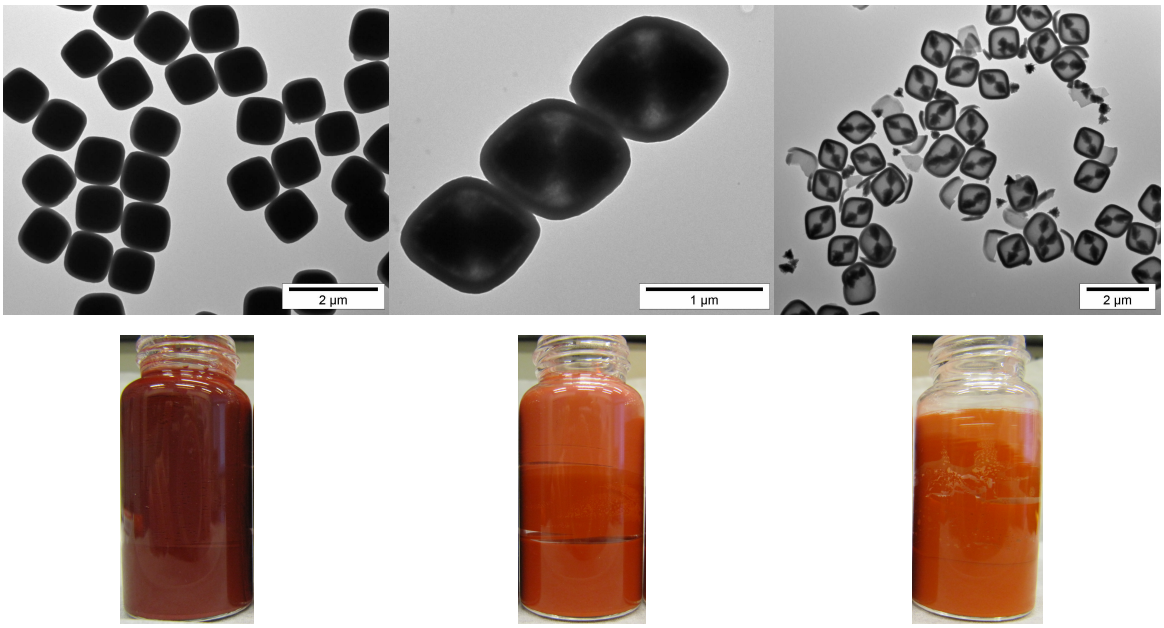

Figure 3.2: The silica coated cubes to the left are not etched, the cubes to the right are etched over a longer time than the cubes in the middle. The hematite core becomes smaller (top) and the color of the particles changes (bottom).

3.5 Surface Protected Water Etching of Silica

Besides etching of hematite, the silica layer can also be etched to make it more porous. The silica layer was etched by surface-protected water etching [47, 48].

A 100 mL three-neck round-bottom flask was used for the etching procedure. The flask was etched overnight with a saturated KOH solution in ethanol prior the reaction.

308.07 mg 40 kg/mol PVP was dissolved in 20 mL of Millipore water (measured with a graduated cylinder). This solution was sonicated for 15 minutes to be sure that the PVP was completely dissolved. The mixture was heated in the flask to 85 °C while refluxing. When the mixture reached 85 °C, 10 mL (10.09 g of 1.28 wt%) of dispersion was added with a Finn pipette (two times 5 mL). The total amount of particles was 129 mg.

Samples were taken after 1, 5, 15, 30, 60 and 120 minutes and were cooled immediately after extraction. The samples with an extracted volume of 1 mL were washed ten times with approximately 1.5 mL ethanol and stored in ethanol, the samples with an extracted volume of 9 mL were washed six times with approximately 10 mL Millipore water and also stored in Millipore water.

3.6 Substrates

Mica plates of around 4 by 2 cm were used as substrates for the cubes. Mica is a mineral which is heat resistant and, when cleaved, atomically flat.

3.6.1 Coating of Substrates

Cubes dispersed in either water or ethanol were deposited on the substrates with a Pasteur pipette, until a large drop was formed, see figure 3.3a and 3.3b. The surface tension of water is higher with respect to the surface tension of ethanol. Therefore, more water could be brought onto the mica plates than in the case of ethanol.

Twice a large drop of cubes was deposited onto the substrates, otherwise not enough cubes would be present to perform the degradation reaction. Figure 3.3a shows the wet first deposition, figure 3.3b shows the second wet deposition. The last two pictures show the dried substrates, 3.3c before the heat treatment in the oven and 3.3d after the heat treatment (see section 3.6.2).

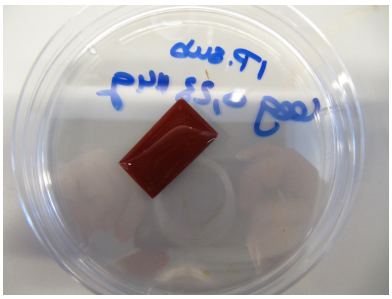

(a) First deposition

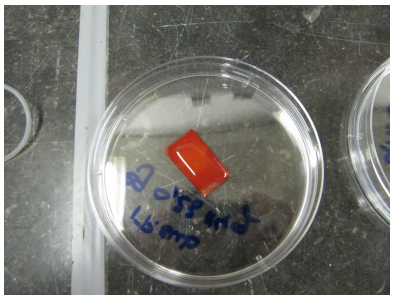

(b) Second deposition, after the first one dried.

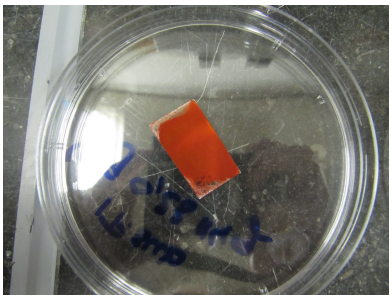

(c) Second depostion after drying.

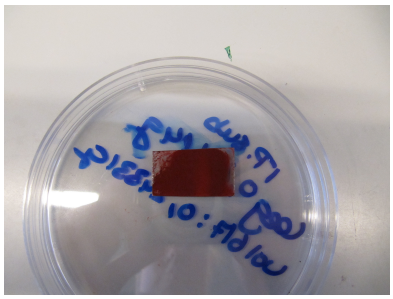

(d) After the heat treatment in the oven.

Figure 3.3: A substrate during the process of deposition with silica coated hematite cubes.

To be able to attach a rope to the substrate to hang the substrate in the reaction mixture, most substrates were not completely covered with cubes, see section 3.7.2. One part of the substrate was therefore taped to a petri dish as is depicted in figure 3.4 and the normal coating procedure was followed. The coated substrate was heated in the oven without the tape.

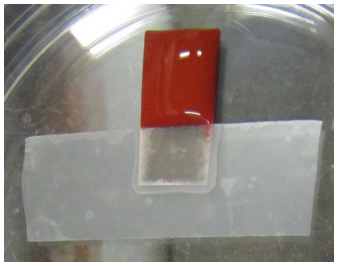

Figure 3.4: Partial coating of a mica substrate.

3.6.2 Heat Treatment

The coated substrates have to undergo a heat treatment, to prevent the cubes to release from the substrate too easily. Figure 4.36 in section 4.3.1 shows TEM pictures of the supernatant of the reactions mixtures from the substrates containing the released cubes and shows why the heat treatment is necessary.

The heat treatments were performed in a calcination oven (Nabertherm P330). The oven heats up to 450 °C in 10 hours where it remains for 3 hours. The oven then cools down to approximately 45 °C in 10 hours. This procedure was followed, unless stated otherwise.

3.7 Preparation of Reaction Mixtures

The reaction mixtures for the catalytic evaluation of the cubes were prepared in 20 mL glass vials. First, 5 mL of methylene blue (unless stated otherwise) (4.39×10^{-4} M) or rhodamine B (1.82×10^{-4} M) was brought in the vial. Second, the cubes were added, typically 1 mL of 1 wt% dispersion in water or a with cubes coated mica substrate. Finally 5 mL of 35 wt% H_2O_2 and the total volume was then brought to 20 mL with Millipore water. The solutions were stirred during the reaction (usually between one and two weeks).

3.7.1 Reaction Mixtures with Dispersed Cubes

The dispersed cubes were stirred magnetically during the reaction and the lids of the vials were screwed loosely to circumvent most evaporation whilst allowing the produced gases to escape.

3.7.2 Reaction Mixtures with Cubes on Substrates

For the substrates two different set-ups were used. The first one is magnetically stirred (in figure 3.5) and the top of the vial is covered with parafilm with a cut for the rope to circumvent evaporation and to let the gases escape. The typical substrate used in this set-up is shown in figure 3.7. For the second set-up, a substrate completely covered (one side) with particles is placed flat on the bottom of a 100 mL vial and is slowly stirred with an overhead stirrer, see figure 3.6. In this set-up it is certain that all the cubes are in the reaction mixture in contrast to the first set-up. Also the chance for cubes to detach from the substrate is lower, because in the first case the stirring bar touches the substrate occasionally. The substrate in this case is a square and completely coated on one side which is lying upwards in the vial. On top of the bottle there is a lid with a hole slightly larger than the stirrer, for the same reason as the loose lid and the parafilm.

Figure 3.5: Set-up for hanging substrates and magnetically stirring. (20 nL vial)

Figure 3.6: Set-up for stirring with overhead stirrer. (100 mL vial)

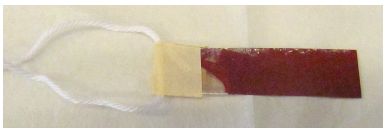

Figure 3.7: Example of substrate which is hanged in the reaction mixture.

3.8 Analytical Techniques

In this section the used analytical techniques for both the syntheses and the catalytic reactions are described.

3.8.1 Microscopy

3.8.1.1 Optical Microscopy

For the visualization of particles with an optical microscope, a Nikon eclipse Ti inverse optical microscope, with a 100x Nikon oil immersion objective and an InfinityX CCD camera was used. Small drops (~20 µL) were placed on a microscope slide. This technique was for instance used to observe the extent of hematite etching.

3.8.1.2 TEM

TEM images were taken with a Philips TECNAI10 or TECNAI12, which have a maximum acceleration voltage of 100 kV and 120 kV, respectively. Copper TEM grids were covered with particles by placing a small drop of sample on it. The grids were dried under a heating lamp, unless hydrogen peroxide was present in the liquid. Hydrogen peroxide affects the grid when heated and therefore these grids were dried without a lamp.

3.8.1.3 SEM

To visualize the substrates with scanning electron microscopy, a Philips XLFEG30 was used with a maximum acceleration speed of 10 kV. A carbon sticker was placed on a SEM stub and the mica substrate with cubes was placed on top. The stubs were sputter coated with a platinum layer of 6 nm.

3.8.2 Measuring pH

The pH was measured with a Hanna instruments pH210 microprocessor pH meter. The pH meter was calibrated with two buffers of pH 4 and pH 7.

3.8.3 UV-Vis Spectroscopy

For the reaction, two types of organic molecules were used, methylene blue and rhodamine b. Both are dyes due to their conjugated π-system, so degradation of the dye molecules can be observed by the naked eye by decolorization. The organic molecules are also suitable for UV-Vis measurements, due to absorption in the visible range. All spectra were recorded on a Perkin-Elmer Lambda35 UV/VIS spectrometer from 700–200 nm. Hellma 110-QS quartz cuvets with a path length of 10 mm were used.

To obtain a suitable sample for the UV-Vis measurements reaction mixtures were centrifuged to remove the cubes. The cubes have to be removed from the solution because they absorb and scatter light, which makes the measurements unreliable. Other methods to remove the cubes were also tried however all the other methods had disadvantages. Filtration of the reaction mixture was attempted with filters with 100 nm size filter holes, unfortunately the filters absorbed some of the dye. The cubes can also be sedimented in the cuvets, however the cleaning of the cuvets is tedious and the reaction does not stop during the recording of the spectra. To conclude, the only way to remove the cubes and avert them from the cuvet is centrifugation of the reaction solution.

3.8.3.1 Overlap of Peaks

The spectra of the used organic molecules and H_2O_2 overlap in the UV part. However, this is not a problem, because H_2O_2 does not absorb in the visible range, see figure 3.8.

Hydrogen peroxide could be removed from solution by making use of manganese oxide (MnO_2). MnO_2 acts as a catalyst for the dissociation of hydrogen peroxide into water and oxygen: $2\,H_2O_2 \longrightarrow O_2 + 2\,H_2O$. However, the solution containing dye decolors and evaporates during the reaction. Therefore, MnO_2

can not be used to remove the H_2O_2 and it remains in the samples which are measured with UV-Vis spectroscopy.

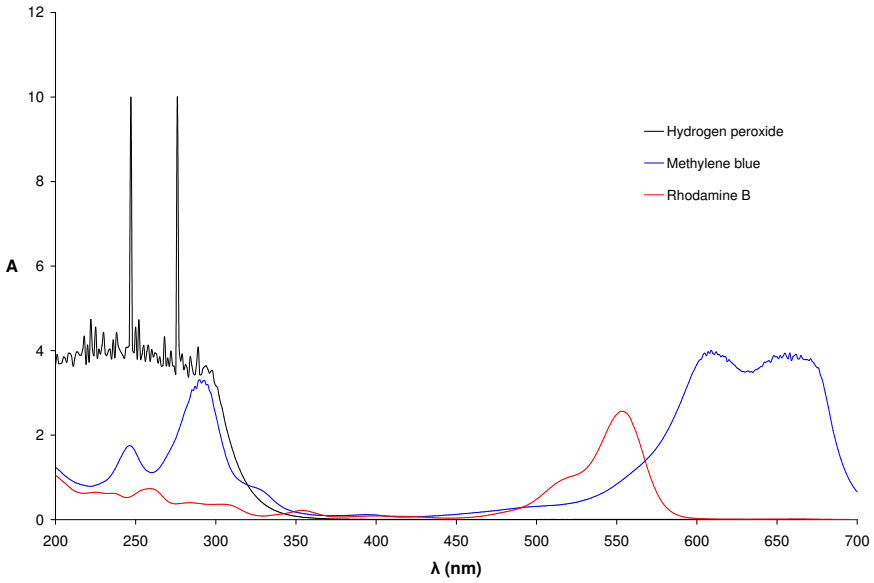

Figure 3.8: The spectra of hydrogen peroxide and the organic dyes only overlap in de UV region of the spectrum. However, in the visible region the absorbance of hydrogen peroxide is zero and the peaks of methylene blue and rhodamine b in the visible region can be used.

3.8.3.2 Methylene blue

(a) Methylene blue dissolved in water.

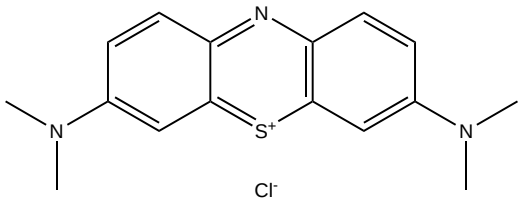

(b) Structural formula

Figure 3.9: Methylene blue

Methylene blue (color in water and structure in figure 3.9) has two absorption peaks in the visible part of the UV-Vis range, at 609 nm and 668 nm, see figure 3.10. The maximum of the peak at 668 nm is concentration dependent and shifts towards lower wavelength with decreasing absorbance and thus concentration. Therefore, the peak at 609 nm was used to monitor the concentration methylene blue over time. The concentration dependence of the peak at 668 nm can be seen in figure 3.13. The molar extinction coefficient for the peak at 609 nm was determined to be 34 419 $M^{-1}cm^{-1}$.

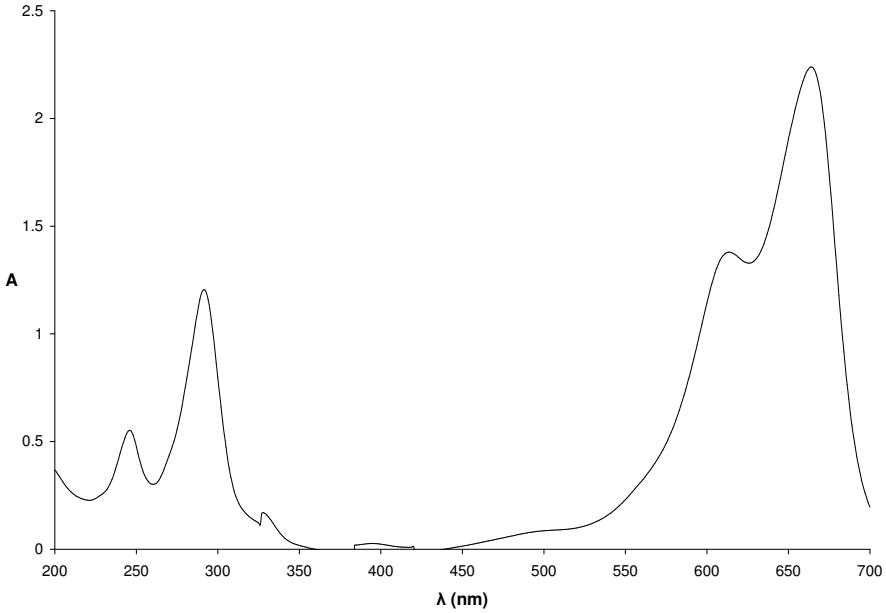

Figure 3.10: UV-Vis spectrum of methylene blue.

3.8.3.3 Rhodamine B

(a) Rhodamine B dissolved in water.

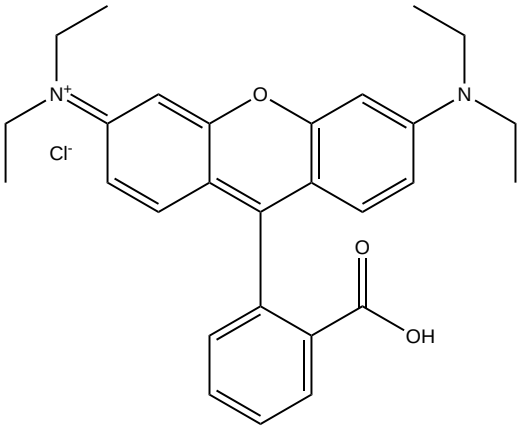

(b) Structural formula

Figure 3.11: Rhodamine B

Rhodamine B (figure 3.11) also has two absorption peaks in the visible range, one at ~520 nm and the other at 554 nm, see figure 3.12. The peak at 554 nm is used to monitor the concentration change over time. The molar extinction coefficient was determined to be 101 426 $M^{-1}cm^{-1}$.

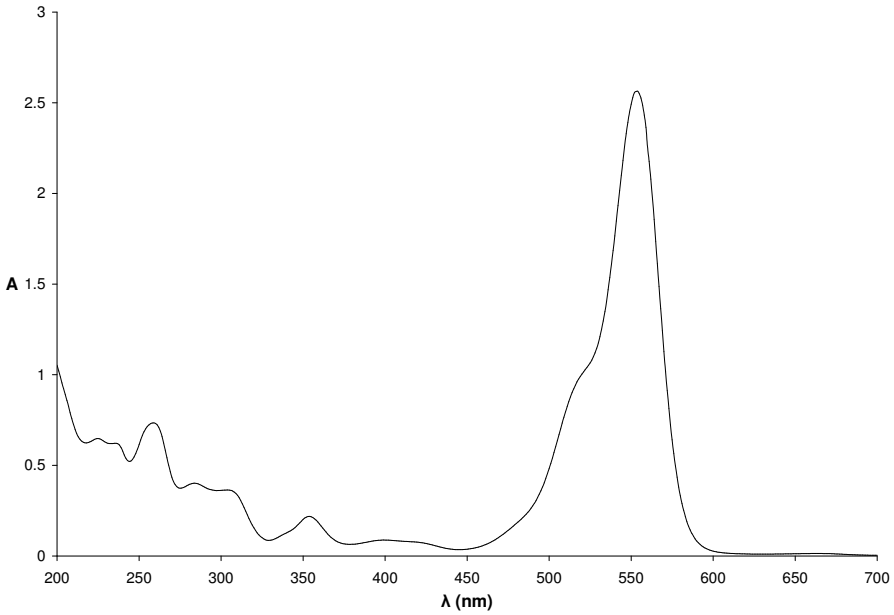

Figure 3.12: UV-Vis spectrum of Rhodamine B.

3.8.3.4 Data Processing

In the figure 3.13 the UV-Vis spectra shown are taken from the reaction mixtures as described in table 4.5, as an example of the acquired data for each set of experiments. As can be seen, this looks rather complicated, due to the amount of spectra the analysis gives. Therefore in chapter 4. Results only the absorbance at 609 nm and 554 nm are reported versus time for methylende blue and rhodamine b respectively. The absorbances are normalized to the absorbance at the beginning of the reaction ($t = 0$).

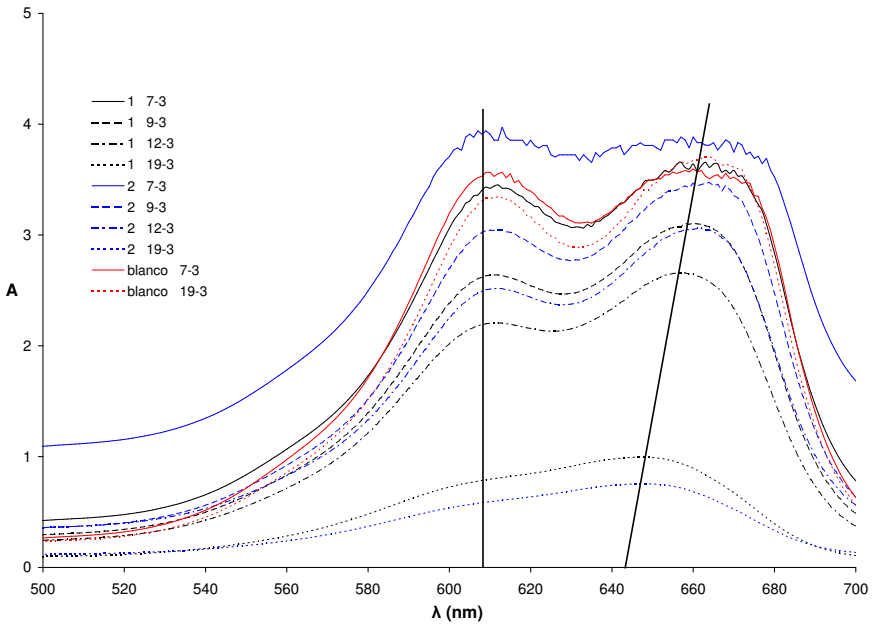

Figure 3.13: Part of the spectra from the catalytic evaluation of bare hematite cubes. The absorbance for 1 (black) and 2 (blue) decreases much more than for the blanco (red spectra). In section 4.2.1.2 the results are discussed. The lines through the maxima of the absorption peaks are drawn for clarity of the concentration dependency of the absorption at 668 nm.

3.8.4 Infrared Spectroscopy

Infrared spectroscopy is a useful technique for the determination of the relative amounts of hematite and silica in the reaction mixtures. During the reaction, Fe^{3+} is converted to Fe^{2+} as described in section 2.1, which probably results in hematite dissolution. This subsequently leads to a decrease of hematite inside the cubes. IR-spectroscopy was used to determine the occurrence of this possible reaction.

Infrared spectroscopy was also used to determine the extent of silica and hematite etching in section 4.1.6.4 and 4.1.6.6. When silica is etched hematite was used as an internal standard and when hematite was etched silica was used as internal standard.

Potassium bromide (KBr) was used as medium to measure the spectra of the colloidal particles. KBr has the advantage that lower energies can be measured and lower concentrations are needed than when using an ATR crystal. Plastic vials were filled with 250 mg of KBr and dispersion or supernatant from the reaction mixture was added. The vials were places overnight in a oven at 100 °C to let the solvent eveporate. KBr pellets from the dried powder were prepared and the spectra were recorded on a Perkin-Elmer Frontier FT-IR/FIR spectrometer.

The peak of hematite is around 550 cm^{-1} [15] and the peak of silica is known to be around 1100 cm^{-1} [51, 52]. In figure 3.14 a spectrum of silica coated hematite cubes is given the silica and hematite peaks are indicated. On the left of the spectrum the large OH band can be seen from not completely evaporated water and probably also from hydroxyl groups present on the surfaces of both silica [44] and hematite [15].

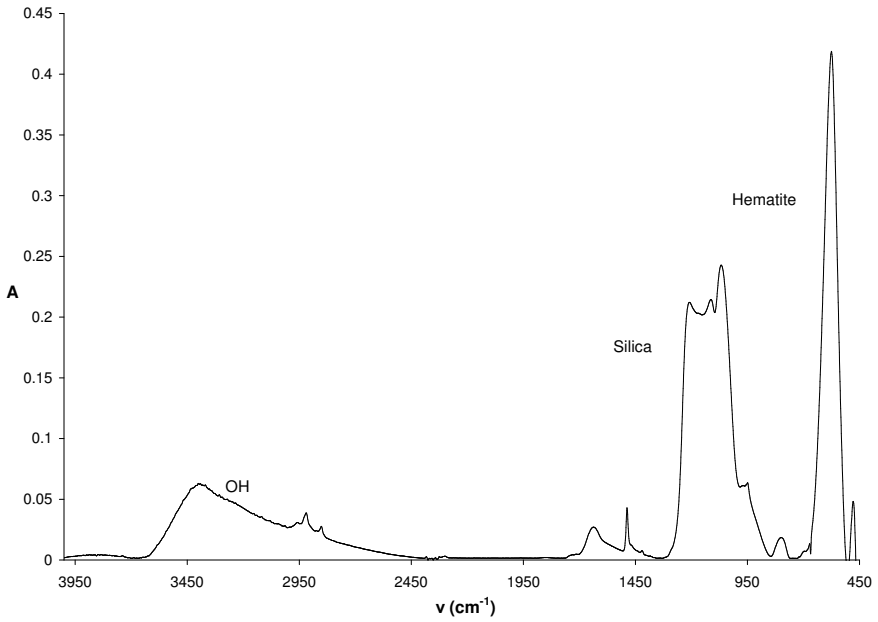

Figure 3.14: Infrared spectrum of silica coated hematite particles. The peak of hematite can be found around 550 cm^{-1} and the peak of silica around 1100 cm^{-1}. Around 2500–3500 cm^{-1} a large band of OH can be seen. The peaks are indicated in the spectrum.

3.8.5 Nitrogen Physisorption

Iron is used as a catalyst in the research, so a high surface area is advantageous due to an increased accessibility of iron. Nitrogen physisorption measurements were performed on a Micromeritics TriStar 3000 V6.08 A, in the group of Inorganic Chemistry & Catalysis at Utrecht University to determine the surface area and the pore sizes.

The synthesized particles were dried in a sample concentrator under nitrogen gas around 70 °C for one or two days. Before measuring the isotherms the samples were dried again overnight at 180 °C with a Micromeritics Smartprep. The results were analyzed by theories discussed in section 2.2.

Chapter 4

Results

4.1 Used and Synthesized Particles

The following cubes were synthesized and/or used in this thesis. Descriptions of the particles which have been silica coated, hematite etched or silica etched come directly after the corresponding hematite synthesis. Also the characterizations of the particles are described in this section. The given sizes of the particles are the edge lengths. The amount of added NaOH solution was determined by the difference in weight of the volumetric flask before and after addition and the density of the solution [37]. In table 4.1 the sizes of the hematite particles are summarized, together with the calculated excess of Fe^{3+} with the formula described in equation 2.15.

As expected the size of the hematite cubes is larger for a higher excess of Fe^{3+} ions during the precipitation reaction. Generally the polydispersity of the obtained particles is higher for smaller particles. The shape of the smaller particles is also less cubic like than for the larger particles.

Table 4.1: Properties of hematite cubes syntheses. The cubes HC4_s1 were very irregularly shaped and contained needles, the given polydispersity is only for the cubic particles. The cubes HC5_s1 were too small to use and were very polydisperse in size and in shape. HC2_s2 still contained needles and needles were present on the surfaces of the cubes.

Cubes	$FeCl_3 \cdot 6\,H_2O$ (g)	NaOH (g)	Fe_x^{3+} (mol)	Size (nm)	Polydispersity (%)
HC1_s1	50.01	20.16	0.018	584	10
HC2_s1	50.07	20.30	0.017	328	11
HC3_s1	50.01	20.15	0.018	465	11
HC4_s1	50.05	20.14	0.019	812	10
HC5_s1	50.02	20.38	0.016	252	18
HC1_s2	50.39	20.14	0.020	920	7
HC2_s2	51.26	20.15	0.022	1587	5
HC3_s2	50.55	20.15	0.020	1028	7
HC4_s2	50.96	20.23	0.022	1181	4
HC5_s2	50.53	20.18	0.019	932	5

Table 4.2: Properties of performed silica coatings. The size of the hematite seed particles, the final size, the polydispersity and the thickness of the silica shell are give. For $SiO_2$13_HC1_s2 three silica coating procedures were performed to obtain the final particles of 1070 nm.

Cubes	Size seed particles (nm)	Final size (nm)	Polydispersity (%)	Thickness silica shell (nm)
SiO_2_HC1_s1	584	743	6	80
SiO_2_HC1_s2	920	1093	6	85
$SiO_2$13_HC1_s2	920	1070	8	75
SiO_2_HC2_s2	1587	1784	6	100
St.HC02_03bII	374	431	12	30

4.1.1 HC1_s1

4.1.1.1 Hematite

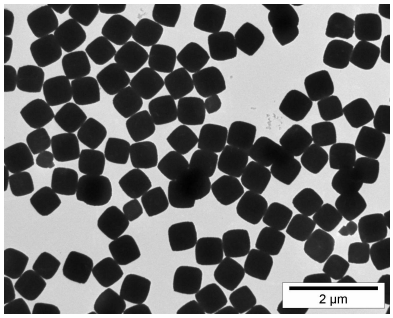

Figure 4.1: HC1_s1

The size of the particles was 584 nm with a polydispersity of 10 %. For the synthesis 50.01 g $FeCl_3 \cdot 6\,H_2O$ was used and 20.16 g NaOH. The sodium hydroxide was dissolved in 100 mL Millipore water and 99.5 mL of this solution was added.

4.1.1.2 Silica Coating

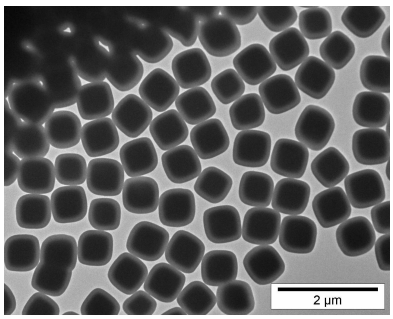

Figure 4.2: SiO_2_HC1_s1

1 g of hematite particles was coated with silica. The final particles had a size of 743 nm, with a polydispersity of 6 %. The thickness of the silica shell was 79 nm. These particles were used in section 4.2.3 and 4.3.2 for catalytic activity tests, together with the hematite etched particles described in the next section.

4.1.1.3 Hematite Etching

A part of the silica coated particles was etched with HCl in two batches. Two times 25 mL of silica coated cubes from the previous section, with a concentration of 1.3 wt% in ethanol were transferred to 10 mL Millipore water. 8 mL of 12 M hydrochloric acid was added in portions over one and a half hour. After a total of three hours stirring, the solutions were diluted with water and transferred to ethanol. Before the particles were used in the experiments they were again transferred to Millipore water. The obtained particles were used in section 4.2.3 and 4.3.2.

The contrast of the hematite in the TEM images is still high, however some of the hematite is etched away, because the color of the particles changed. Infrared spectroscopy was performed on these particles

to determine the amount of remaining hematite. For the particles in figure 4.3a 52 % of the hematite core remained and for the particles in figure 4.3b 53 % hematite remained.

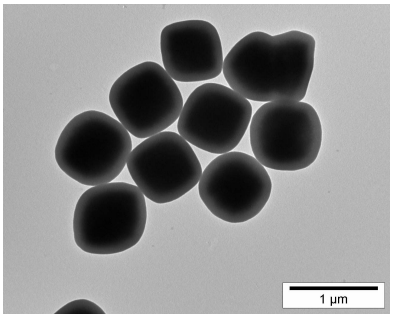

(a) SiO_2_HC1_s1_1, 52 % hematite is left.

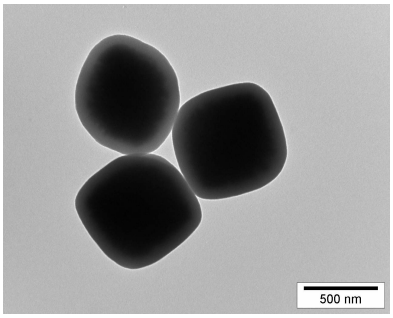

(b) SiO_2_HC1_s1_2, 53 % hematite is left.

Figure 4.3: The particles in both pictures are hematite etched. The difference between the hematite etched particles and the non-etched particles may not be well visible. However, the color of the particles changed during the etching process, which indicates that a part of the hematite was removed.

4.1.2 HC2_s1

4.1.2.1 Hematite

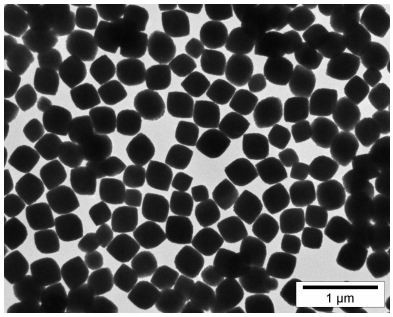

Figure 4.4: HC2_s1

The size of the particles was 328 nm with a polydispersity of 11 %. For the synthesis 50.07 g $FeCl_3 \cdot 6\,H_2O$ was used and 20.30 g NaOH. The sodium hydroxide was dissolved in 100 mL Millipore water and 99.3 mL of this solution was added.

4.1.3 HC3_s1

4.1.3.1 Hematite

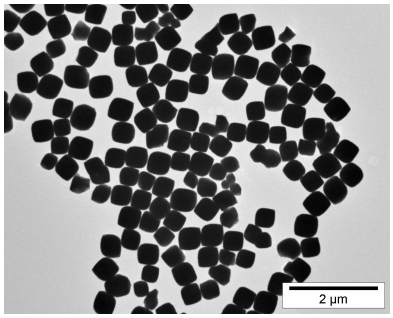

Figure 4.5: HC3_s1

The size of the particles was 465 nm with a polydispersity of 11 %. For the synthesis 50.01 g $FeCl_3 \cdot 6\,H_2O$ was used and 20.15 g NaOH. The sodium hydroxide was dissolved in 100 mL Millipore water and 99.4 mL of this solution was added.

4.1.4 HC4_s1

4.1.4.1 Hematite

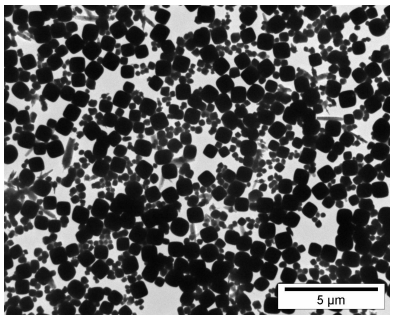

Figure 4.6: HC4_s1

This synthesis was unsuccessful, because many large needles were formed. The size of the particles was 812 nm with a polydispersity of 10 %. However only 35 normal cubes were measured. The needles were not taken into account for this size and polydispersity. For the synthesis 50.05 g $FeCl_3 \cdot 6\,H_2O$ was used and 20.14 g NaOH. The sodium hydroxide was dissolved in 100 mL Millipore water and 99.1 mL of this solution was added. A reason that very polydisperse particles were formed is that the NaOH solution was turbid and probably not well dissolved before it was added to the FeCl solution.

4.1.5 HC5_s1

4.1.5.1 Hematite

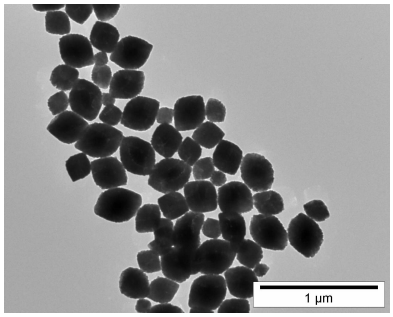

Figure 4.7: HC5_s1

The size of the particles was 252 nm with a polydispersity of 18 %. For the synthesis 50.02 g $FeCl_3 \cdot 6\,H_2O$ was used and 20.38 g NaOH. The sodium hydroxide was dissolved in 100 mL Millipore water and 99.5 mL of this solution was added. These particles are very small and very polydisperse, due to the small excess of Fe^{3+} ions.

4.1.6 HC1_s2

4.1.6.1 Hematite

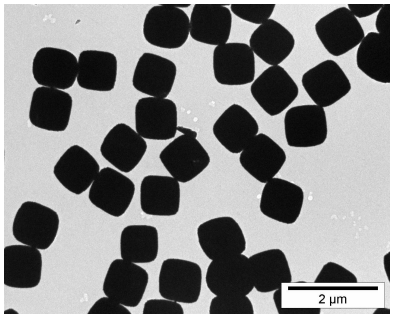

Figure 4.8: HC1_s2

The size of the particles was 920 nm with a polydispersity of 7 %. For the synthesis 50.39 g $FeCl_3 \cdot 6\,H_2O$ was used and 20.14 g NaOH. The sodium hydroxide was dissolved in 100 mL Millipore water and 99.0 mL of this solution was added.

4.1.6.2 Hematite Etching of Bare Cubes

For nitrogen physisorption measurements bare hematite particles were also examined, because Stöber silica has a high surface area and the change of surface area of solely the hematite core after etching with HCl is liked to be known. The surface area of Stöber silica is approximately 515 m^2/g [42] and of cubic hematite particles is expected to be only 2.8 m^2/g [53]. The nitrogen-physisorption results are shown in section 4.5.

15 mL of 8.4 wt% dispersion was brought into a centrifuge tube for both set of particles obtained in figure 4.9. For the particles in figure 4.9a, 50 mL of 12 M hydrochloric acid was added portion wise over

two hours and was stirred for four hours; for the particles in figure 4.9c 80 mL of hydrochloric acid was added in portions over four and was stirred for almost six hours. Both were magnetically stirred during the etching process and were diluted before washing by centrifugation and redispersion with Millipore water. The extent of etching was followed during the reaction with optical microscopy, figures 4.9b and 4.9d are magnifications of a single particle from pictures taken with the optical microscope. The inset in figure 4.9b shows a optical microscope image of a single bare non-etched hematite cube.

The remaining hematite was weighed after drying. For the etched particles in figure 4.9a 25 % of the initial hematite was left and for the particles in figure 4.9c only 1.5 % was left. Some of the hematite was undoubtedly lost during the washing process.

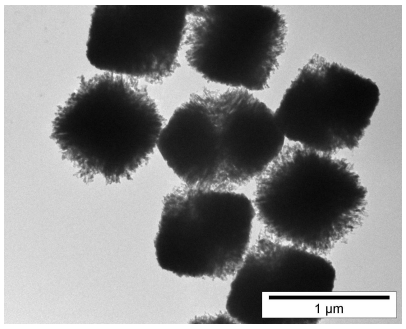

(a) TEM image of hematite etched particles (HC1_s2_e1).

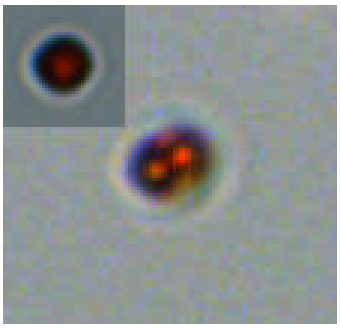

(b) Optical microscope image of a single hetmatite etched particle (HC1_s2_e1). The inset shows a non-etched bare hematite cube (HC1_s2).

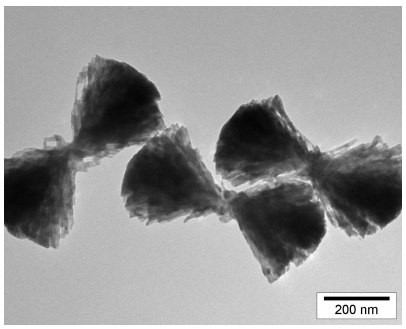

(c) TEM image of hematite etched particles (HC1_s2_e2).

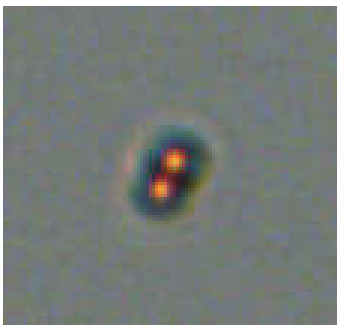

(d) Optical microscope image of a single hematite etched particle (HC1_s2_e2). The particle is more orange, and is smaller than in (b).

Figure 4.9: Bare hematite cubes etched with HCl for nitrogen physisorption measurements. The etching of the particles can also be followed with optical microscopy, which is much faster and easier than transmission electron microscopy. The particles is figures (a) and (b) are etched for four hours, the particles in figures (c) and (d) were etched for six hours. The inset in figure (b) is a non-ethed bare hematite cube. This cube is also darker and more red of color than the particles etched by hydrochloric acid.

4.1.6.3 Silica Coating 1

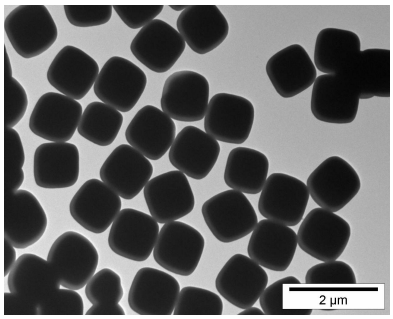

Figure 4.10: SiO_2_HC1_s2

Hematite particles (HC1_s2) were silica coated following the synthesis procedure described in section 3.3. The obtained particles had a size of 1093 nm, with a polydispersity of 6 %. The thickness of the silica shell was 86 nm. These particles were used in catalytic activity measurements in sections 4.3.3, 4.3.4 and 4.3.5.

4.1.6.4 Silica Etching

Silica coated hematite particles from section 4.1.6.3 were silica etched by surface protected water etching as described in section 3.5. In table 4.3 the extracted volumes are given and the temperature of the solution at every extraction. All samples were washed and the samples with the large volumes (after 5, 30 and 120 minutes of etching) were used in catalytic activity measurements in section 4.2.4.

Table 4.3: Temperature of the reaction mixture and extracted volumes during the silica etching of the cubes at given times.

Time (min.)	T (°C)	Volume extracted (mL)
0	69.0	-
1	74.0	1
5	79.8	9
15	84.2	1
30	85.0	9
60	81.9	1
120	84.6	remainder (almost 9 mL)

TEM TEM pictures of the silica etched particles were taken (figure 4.11) and shows the decreasing contrast of the silica shell with increasing etching time. However, the silica shell of some cubes were completely etched as indicated in figure 4.11e. The shape and the surface of the particles has not changed during the etching procedure.

IR spectroscopy Since TEM analysis only gives a qualitative result of the degree of the silica etching, infrared spectroscopy was performed to determine the amount of silica removed. All samples and non-silica etched cubes were analyzed in duplo. In the graph in figure 4.12 it can be seen that about 40 % of the silica was removed by the surface protected water etching after two hours. The points after 5 and 30 minutes etching in figure 4.12 are probably measurement errors, because the amount of remaining silica can not increase during the etching process.

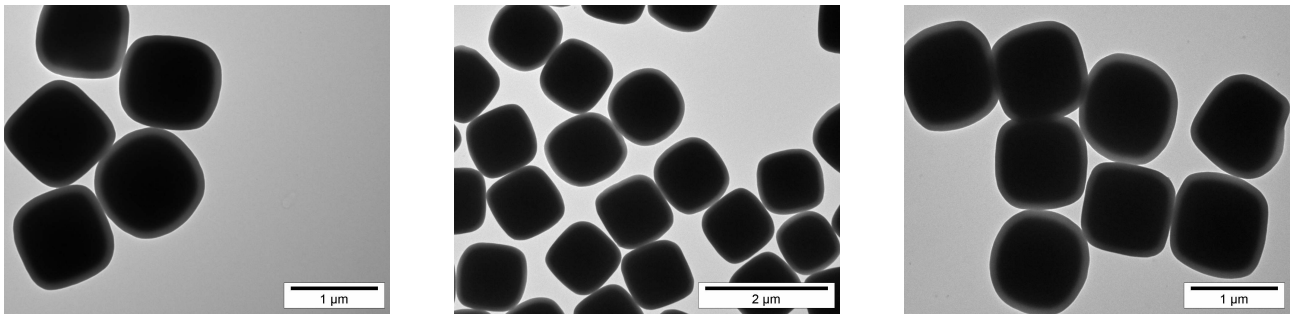

(a) after 1 minute **(b)** after 5 minutes **(c)** after 15 minutes

(d) after 30 minutes **(e)** after 60 minutes **(f)** after 120 minutes

Figure 4.11: TEM pictures of silica etched cubes. The contrast of the silica shell decreases with the etching time, while the shape and the smoothness of the shell is maintained. In (e) there is one bare cube visible, this cube lost his shell completely during the etching process (particle indicated with an arrow).

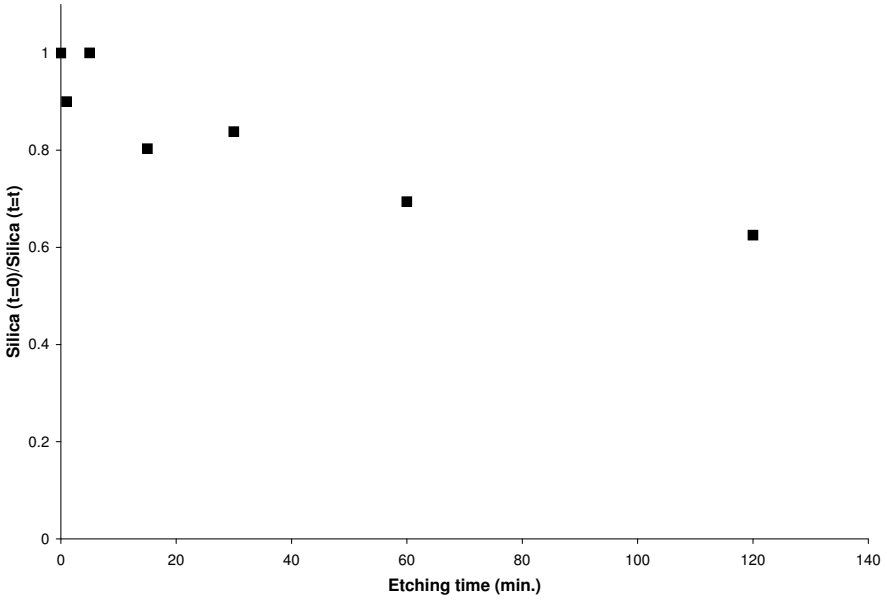

Figure 4.12: Etching of silica analyzed with IR spectroscopy. About 40 % of the silica is etched away after 120 minutes etching time.

4.1.6.5 Silica Coating 2

For nitrogen physisorption measurements a minimum of 20 m^2 of surface is needed. It was calculated that for each measurement approximately 0.5 g of silica coated hematite cubes was needed. Therefore 1.8 g of hematite cubes was coated with silica in a three-step coating procedure. 21.4 g dispersion of bare hematite particles (HC1_s2) with a concentration of 8.4 wt% in water were coated with 10 g of 40 kg/mol PVP overnight. The 1.8 g of particles were then transferred to ethanol by centrifugation and redispersion in ethanol two times.

In a total volume of 1 L in a 2 L two-neck round-bottom flask the first silica coating was performed. 66 mL of Millipore water, 10 mL of 1 wt% TMAH and 10 mL TEOS in 10 mL ethanol were used for the first silica layer. The particles were washed with ethanol and were not coated with PVP for the second coating.

The second coating was performed like the first one, but then with 40 mL Millipore water, 7 mL 1 wt% TMAH and 5 mL of TEOS in 15 mL ethanol. The obtained particles did not grow during the second coating, probably due to a insufficient amounts of reactants (TEOS and water) and/or catalyst (TMAH). Therefore a third coating was performed.

Prior to the third coating the particles were brought to Millipore water to coat the particles overnight with 10 g of 40 kg/mol PVP. After stabilizing the cubes with PVP they were washed twice with ethanol. The third coating was also performed in 1 L total volume in a 2 L flask and the same amounts of reactants were used as in the first coating; 66 mL water, 1 mL 1 wt% TMAH and 10 mL TEOS in 10 mL ethanol. The final particles were washed again with ethanol. One third of the particles was dried directly, the remainder was used for hematite etching, see section 4.1.6.6.

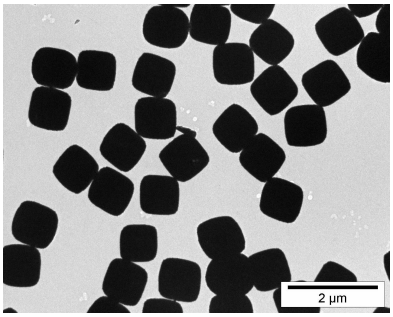

(a) Bare hematite particles (HC1_s2). $d = 920$ nm, pd = 7 %

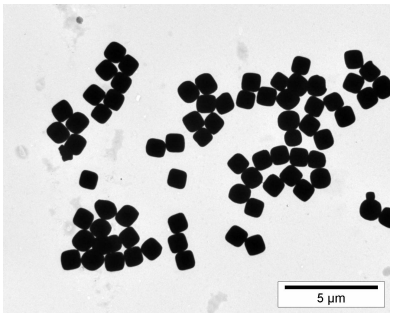

(b) Particles after the first coating. $d = 1013$ nm, pd = 6 %

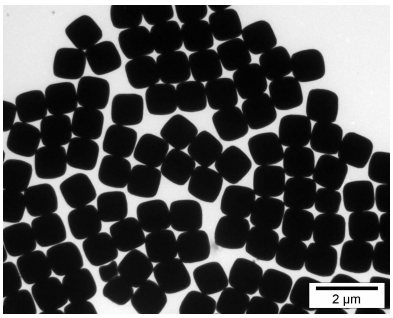

(c) Particles after the second coating. $d = 1003$ nm, pd = 4 %

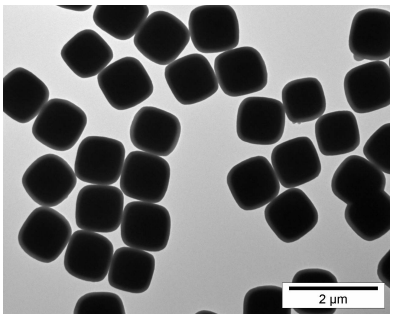

(d) Particles after the third coating, used for the hematite etching in the next section (4.1.6.6). $d = 1070$ nm, pd = 8 %

Figure 4.13: TEM pictures of the particles before, and after each silica coating. The size and polydispersity of each particle set is given below the pictures. The particles in (d) were used for nitrogen physisorption.

The size of the particles after the first coating was 1013 nm with a polydispersity of 6 % (229 particles were measured). After the second coating it turned out that the particles were 1003 nm with a polydispersity of 4 % (215 particles were measured), which is of course impossible. A cause of the smaller particle size can be the focus of the TEM or an inaccurate measurement of the particle size. After the third

coating the size was 1070 nm with a polydispersity of 8 % (22 particles were measured). The thickness of the silica shell was 75 nm. Pictures of the particles are shown in figure 4.13.

The polydispersity of the particles increased after the coating, which is remarkable, because after a silica coating the size distribution should sharpen and the polydispersity should decrease [54].

4.1.6.6 Hematite Etching

Two third of the particles obtained by the silica coating described in section 4.1.6.5 was hematite etched in two batches. Both batches were dispersed in 10 mL Millipore water. The final particles can be seen in figure 4.14. For the particles in figure 4.14b, 15 mL 6 M and 10 mL 12 M hydochloric acid was added portion wise over two and a half hour and the dispersion was stirred for four hours in total. To the particles in figure 4.14c 15 mL 6 M and 15 mL hydrochloric acid was added over four hours and the solution was stirred for five hours in total. Both were diluted to stop the reaction and washed with Millipore water.

On the particles in figure 4.14 nitrogen physisorption measurements were done. The results are presented in section 4.5. Infrared spectroscopy was performed to determine the amount of remaining hematite quantitatively.

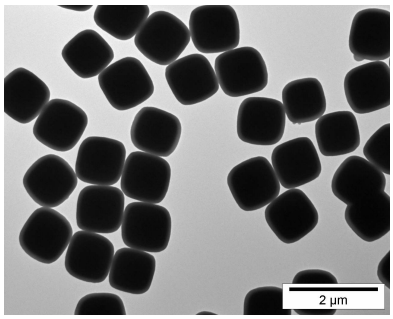

(a) Non-etched particles.

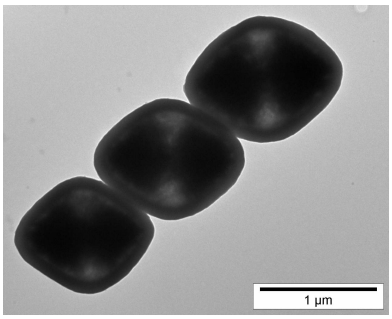

(b) Hematite etched particles I, 19 % hematite is left.

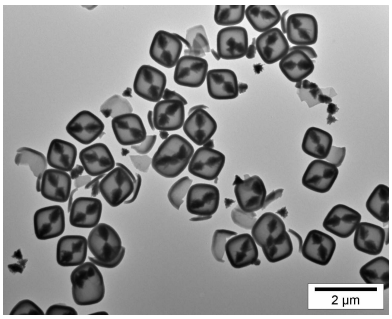

(c) Hematite etched particles II, 4 % hematite is left.

Figure 4.14: The bare hematite particles used were 920 nm, after the silica coating the particles were 1070 nm. The thickness of the silica shell is 75 nm. From left to right the particles are increasingly etched. The silica shells of the particles at the right are broken, which might be due to the overnight stirring with HCl. The numbers of remaining hematite were determined with infrared spectroscopy, see below.

IR IR spectra were taken, with KBr as medium. All spectra were baselinecorrected, the baselines were set to zero and the spectra were normalized to the silica peak of the non-etched particles (ne 1) at 1070.6 cm^{-1}. The normalized absorbances of the hematite were taken at 578.6 cm^{-1}, divided by the silica peak and compared [55].

Figure 4.15 shows the baselinecorrected, zeroed and normalized infrared spectra of the particles shown in figure 4.14. All the measurements were performed in duplo for each set of particles. From the infrared spectra in figure 4.15 can be concluded that for the particles in figure 4.14b approximately 19 % of the hematite core is left and in the case of the particles in 4.14c only 4 % of the hematite remained. Another effect observed in the spectra is a change in the shape of the silica peaks for the etched particles. Where the shape of the spectra for the non-etched particles is plateau-like (solid lines), the dotted lines for the etched particles show a shoulder in the peak. This might be due to a change of the silica shell. The silica shell becomes more porous when etched with hydrochloric acid. This is concluded form the nitrogen physisorption measurements described in section 4.5.

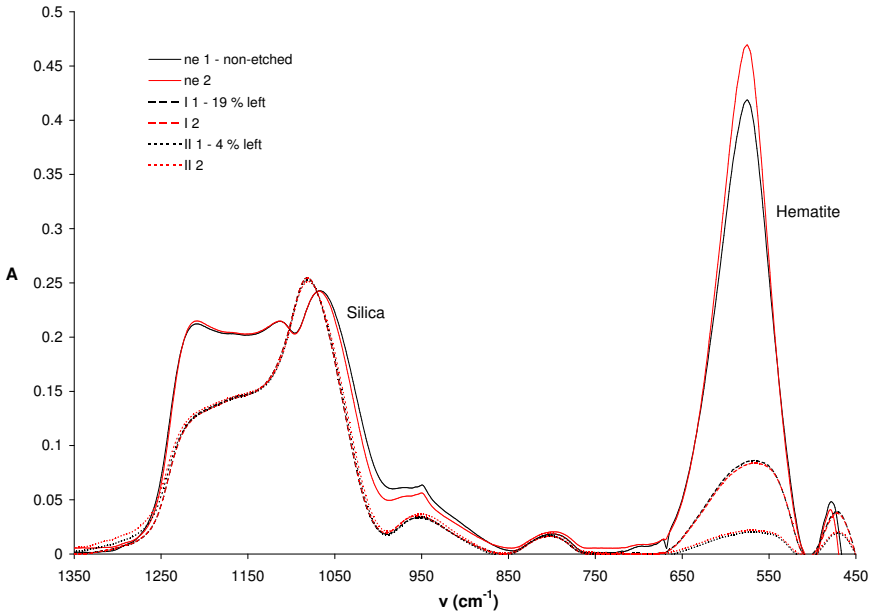

Figure 4.15: Baslinecorrected, zeroed and normalized infrared spectra of the particles in figures 4.14a (ne 1 and ne 2), 4.14b (I 1 and I 2) and 4.14c (II 1 and II 2) (in duplo). The hematite peak decreases with increasing hematite etching. It is also clear that the shape of the silica peak (from 1250 to 1050 cm^{-1}) changes when the particles are etched by hydrochloric acid. The silica peak for the non-etched particles (solid lines) is a kind of plateau, where the silica peak of the etched particles has one distinct peak and a shoulder.

4.1.7 HC2_s2

4.1.7.1 Hematite

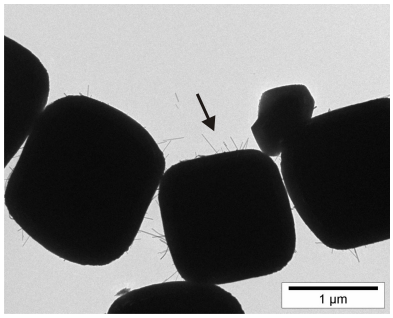

Figure 4.16: HC2_s2

The size of the particles was 1587 nm with a polydispersity of 5 %. For the synthesis 51.26 g $FeCl_3 \cdot 6\,H_2O$ was used and 20.15 g NaOH. The sodium hydroxide was dissolved in 100 mL Millipore water and 99.1 mL of this solution was added. On the surface of the particles needles are visible. The assembly of the needles into the cubes was probably not yet completed, and therefore some needles are left. During the washing process of these particles also a lot of needles were present in the supernatant after the centrifugation.

4.1.7.2 Silica Coating

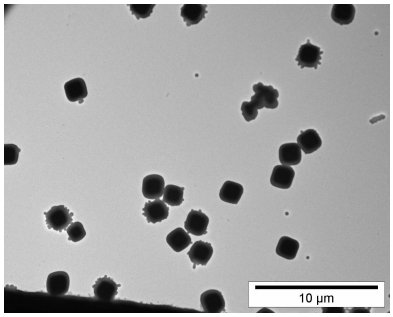

Figure 4.17: SiO_2_HC2_s2

The size of the obtained particles after the silica coating was 1784 nm with a polydispersity of 6 %. However only 25 particles were measured. The thickness of the silica layer was 98 nm. During the silica coating procedure the needles present on the surfaces of the hematite particles were also coated with silica. Therefore the surfaces of the major part of the particles were not smooth. These particles were used is section 4.2.3 and 4.3.2 for catalytic activity tests, together with the hematite etched particles described in the next section.

4.1.7.3 Hematite Etching

These particles were used in section 4.2.3 and 4.3.2 for catalytic activity measurements. These particles were also etched with hydrochloric acid in two batches of 25 mL 0.75 wt% dispersion of the particles as described in the previous section. 8 mL of 12 M HCl was added in portions over one and a half hour and the solutions were stirred for a total of three hours. After the etching, the solutions were diluted and transferred to ethanol. Before the particles were used in experiments the particles were transferred to Millipore water.

From the TEM pictures in figure 4.18 it is not clearly visible that the hematite inside has been etched, however a color change of the particles was observed. This indicates that the etching was successful. Infrared spectroscopy was performed on these particles to determine the amount of remaining hematite. For the particles in figure 4.18a 38 % of the hematite core was left and for the particles in figure 4.18b 39 % hematite remained.

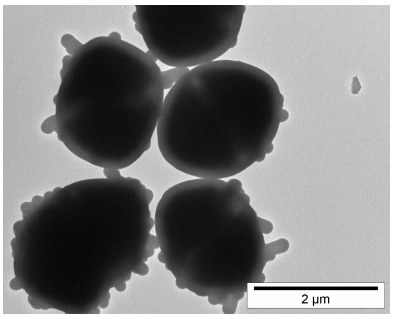

(a) SiO_2_HC2_s2_1, 38 % hematite is left.

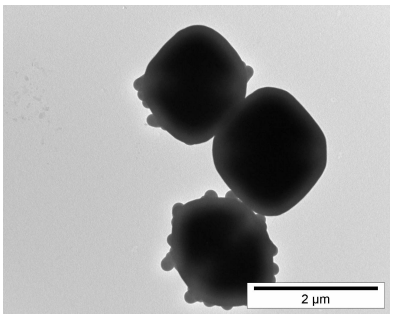

(b) SiO_2_HC2_s2_2, 39 % hematite is left.

Figure 4.18: TEM pictures of partially hematite etched particles. The contrast of the hematite is still high and the etching may not be very well visible, however the color of the dispersion changed during the etching with HCl. The spikes on the surfaces are formed by silica coating the hematite particles and the needles present on the surface.

4.1.8 HC3_s2

4.1.8.1 Hematite

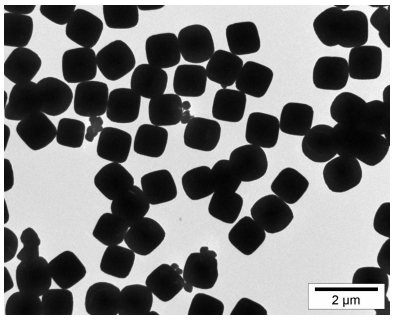

Figure 4.19: HC3_s2

The size of the particles was 1028 nm with a polydispersity of 7 %. For the synthesis 50.55 g $FeCl_3 \cdot 6\,H_2O$ was used and 20.15 g NaOH. The sodium hydroxide was dissolved in 100 mL Millipore water and 99.6 mL of this solution was added.

4.1.9 HC4_s2

4.1.9.1 Hematite

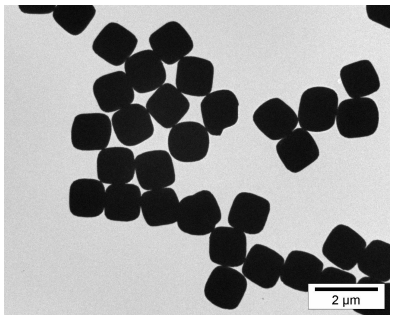

Figure 4.20: HC4_s2

The size of the particles was 1181 nm with a polydispersity of 4 %. For the synthesis 50.96 g $FeCl_3 \cdot 6\,H_2O$ was used and 20.23 g NaOH. The sodium hydroxide was dissolved in 100 mL Millipore water and 99.2 mL of this solution was added.

4.1.10 HC5_s2

4.1.10.1 Hematite

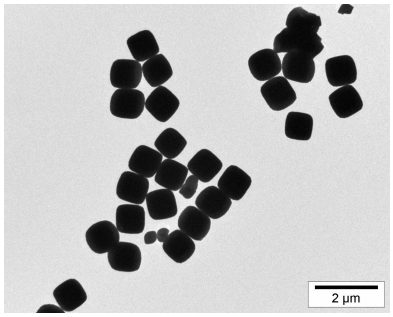

Figure 4.21: HC5_s2

The size of the particles was 932 nm with a polydispersity of 5 %. For the synthesis 50.53 g $FeCl_3 \cdot 6\,H_2O$ was used and 20.18 g NaOH. The sodium hydroxide was dissolved in 100 mL Millipore water and 99.2 mL of this solution was added.

4.1.11 HC02_03bII

4.1.11.1 Hematite

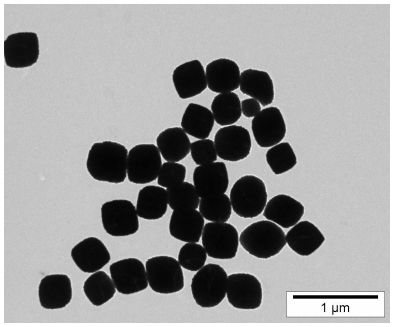

Figure 4.22: HC02_03bII

These particles were synthesized by Sonja Castillo. The size of the particles was 374 nm with a polydispersity of 14 %. These particles were used in section 4.2.1.

4.1.11.2 Silica Coating

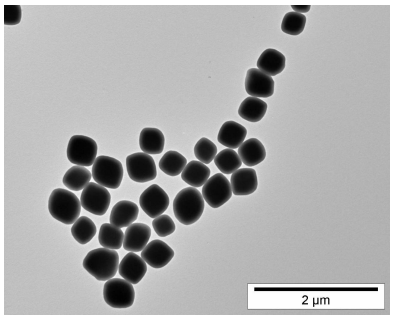

Figure 4.23: St.HC02_03bII

Approximately 1 g of bare hematite particles were coated with silica, the particles obtained were 431 nm with a polydispersity of 12 %. The thickness of the silica layer was 29 nm. These silica coated cubes were used in the experiments in section 4.2.2.

4.1.12 HC02_01c

4.1.12.1 Hematite

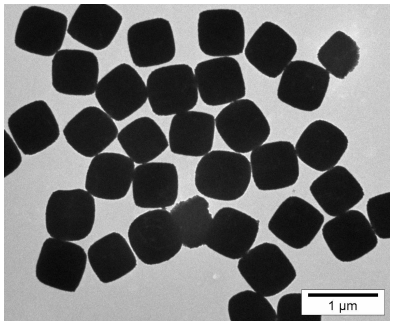

Figure 4.24: HC02_01c

These particles were synthesized by Sonja Castillo. The size of the particles was 663 nm and the polydisperdity was 7 %.

4.1.12.2 Silica Coating

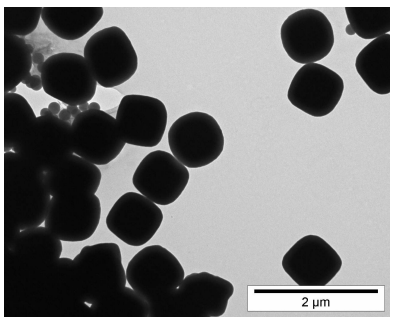

Figure 4.25: St03b2.2

These particles were silica coated by Sonja Castilo and has a size of 813 nm. The polydispersity was 4 %, the thickness of the silica shell was 75 nm. These particles were used in the experiments in section 4.2.2.

4.2 Catalytic Activity of Dispersed Cubes

4.2.1 Bare Hematite Cubes

The degradation of methylene blue by bare hematite cubes was investigated by observing samples by eye and with UV-Vis spectroscopy.

4.2.1.1 Observations by the Eye

To investigate whether the degradation of methylene blue is faster in the presence of iron oxide cubes and hydrogen peroxide than in the presence of only hydrogen peroxide, samples were made as described in table 4.4. Two samples were covered with aluminium foil to investigate the influence of light on the decolorization of the methylene blue.

The suspension of hematite cubes contained around 1.6 wt% of the bare hematite cubes of 374 nm described in section 4.1.11.1, the concentration of the methylene blue in water was approximately 4.3×10^{-4} M and a 35 wt% hydrogen peroxide solution was used.

Table 4.4: Concentration of samples 1 to 6 (from left to right in picture 4.26). The concentration of cubes was 1.6 wt%, the concentration methylene blue was 4.3×10^{-4} M and the concentration hydrogen peroxide was 35 wt%.

Bottle	Cubes (mL)	Methylene blue (mL)	H_2O_2 (mL)	Remarks
1	0.1	0.3	5	
2	0.1	0.5	5	
3	0	0.5	5	
4	0	0.5	10	
5	0	0.5	5	aluminium foil
6	0	0.5	10	aluminium foil

Figure 4.26 shows photos of the samples with methylene blue. From these pictures it can be concluded that the degradation of methylene blue in the presence of hydrogen peroxide and hematite cubes is faster than the degradation by only hydrogen peroxide. Moreover, the degradation of the methylene blue was not observably influenced by light, because samples with aluminium foil show the same decolorization as the corresponding samples without aluminium foil (compare 3 and 5, and 4 and 6). From the pictures can also be concluded that the concentration hydrogen peroxide influences the degradation speed; a higher concentration of hydrogen peroxide gives rise to a higher degradation rate of methylene blue. The influence of light on the reaction in the presence of cubes was not investigated. However, the formation of radicals from hydrogen peroxide is accelerated under the influence of UV-light [56]. The influence of light on this reaction could therefore be determined.

Bottle 7 in figure 4.26e only contains 0.5 mL methylene blue solution in 19.5 mL water. This bottle does not decolor. From figure 4.26e and 4.26f can be seen that the bottles with hematite are completely decolored, while the bottle with the same amount of hydrogen peroxide (number 3) is still blue. Therefore, it can be concluded from this experiment followed by the naked eye that bare hematite cubes speed up the degradation reaction of methylene blue.

(a) day 0

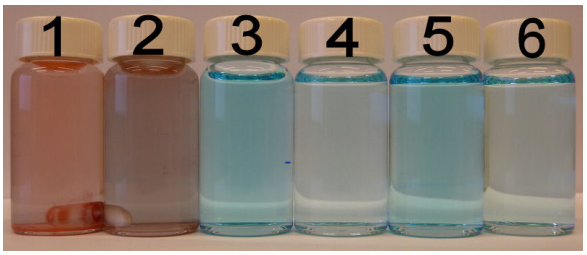

(b) day 12

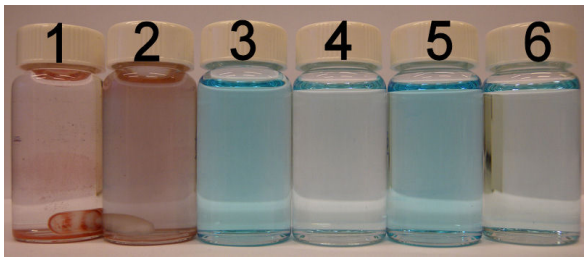

(c) day 15

(d) day 18

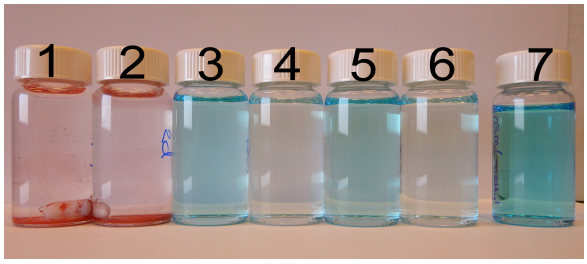

(e) day 22 - The most right bottle in the picture (bottle 7) is a bottle with 0.5mL of methylene blue in water. This bottle does not decolor.

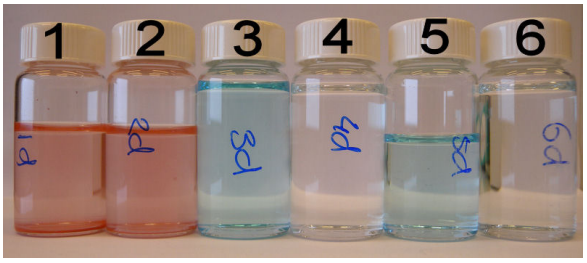

(f) day 43

Figure 4.26: Photos of samples as described in table 4.4. The degradation of methylene blue in the presence of cubes and hydrogen peroxide is faster than in only the presence of hydrogen peroxide. From the difference in color of bottle 2 and 3 this can be clearly seen. These bottles contained the same amount of hydrogen peroxide and methylene blue. In figure (d) and (e) bottle 2 is obviously less blue than bottle 3. No difference in color between bottle 3 and 5 and 4 and 6 was observed which indicates that light has no influence on the degradation of methylene blue in the presence of only hydrogen peroxide. Bottles 4 and 6 are less blue due to a higher concentration of hydrogen peroxide.

4.2.1.2 Degradation Reaction Followed by UV-Vis

For these experiments also the bare hematite cubes described in section 4.1.11.1 were used. The dispersion of cubes had a concentration of 1.6 wt% in water. For each sample 5 mL of methylene blue solution (4.39×10^{-4} M) and 5 mL of 35 wt% hydrogen peroxide was used, each sample was brought to a total volume of 20 mL with Millipore water. The amounts of cubes in sample 1 and 2 are listed in table 4.5.

Table 4.5: Amounts of cubes (weight of dispersion added), methylene blue and hydrogen peroxide used for each sample.

Sample	Cubes (g)	Methylene blue (mL)	H_2O_2 (mL)
blanco	-	5	5
1	0.26	5	5
2	1.01	5	5

The degradation of methylene blue in the presence of hematite cubes can conviently be followed by UV-Vis spectroscopy. Moreover, the catalytic influence of the cubes on the degradation can be quantified using UV-Vis spectroscopy. In the next figure it can be seen that the degradation of methylene blue proceeds much faster in the case where besides hydrogen peroxide also hematite cubes are present. The black squares in figure 4.27 represent the experiment without hematite cubes and almost do not descend over time, where the red triangles and the blue diamonds do.

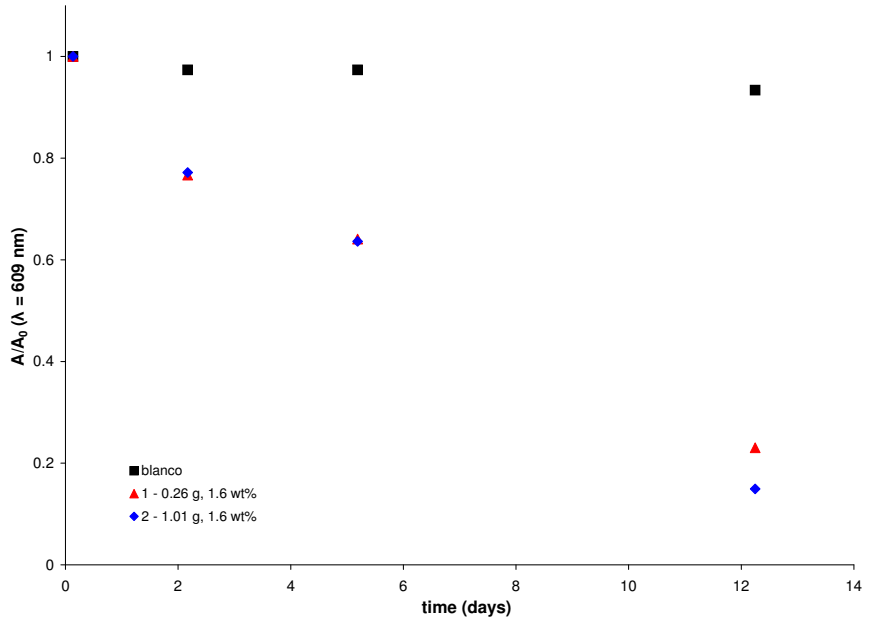

Figure 4.27: Normalized absorbance versus time. The black points indicate the blank experiment without cubes. The absorbance for the reactions with cubes decreases much faster than the absorbance for the reaction without cubes. Therefore, it can be concluded that the colloidal hematite particles accelerate the degradation reaction of methylene blue.

Although for sample 2 nearly four times more cubes were used than for sample 1, the reaction speed for the former is not much higher than for the latter. In table 4.6 the absolute reaction speeds of the degradation reaction are given, calculated by the difference in absorbance between the last (after twelve days) and first measurement point assuming a linear decay. In the second last column the theoretical degradation time is given, which indicates the time in which all color would be disappeared. However, fragments without any aborbance at 609 nm could still be present by then. The turn-over-number is given in the last column, which indicate the number of molecules converted per cube per second. Hydrogen peroxide decomposes during the reaction and therefore its concentration decreases. If this influences the reaction speed in this case and the following cases is not known and should be investigated.

Table 4.6: Reaction speeds for bare hematite cubes (described in section 4.1.11.1). The reaction speeds between sample 1 and 2 are small, although sample 2 contained nearly four times more cubes.

Sample	Speed $\left(\frac{\Delta A}{\Delta t}\right)$	Speed (molecules/day)	Speed (molecules/s)	Theoretical degradation time (days)	TON $\left(\frac{\text{molecules}}{s \cdot \text{cube}}\right)$
blanco	0.02	7.5×10^{15}	8.7×10^{10}	217	
1	0.22	8.4×10^{16}	9.7×10^{11}	19	63
2	0.28	1.1×10^{17}	1.2×10^{12}	15	80

4.2.2 Silica Coated Hematite Cubes

For the next two sets of experiments, the two types of silica coated cubes described in section 4.1.11.2 (430 nm) and 4.1.12.2 (810 nm) were used. They are referred to small and large cubes respectively. The dispersion of the small cubes contained 1.04 wt% and the dispersion of large cubes 0.81 wt% of cubes.

4.2.2.1 Methylene blue

These reactions were performed with methylene blue as organic molecule. 4 mL of methylene blue solution (4.39×10^{-4} M) was added and 5 mL of 35 wt% hydrogen peroxide. The amount of added cubes are given in table 4.7.

Table 4.7: Amount of cubes, methylene blue solution and hydrogen peroxide added to the reaction mixtures.

Sample	Small cubes (mL)	Large cubes (mL)	Methylene blue (mL)	H_2O_2 (mL)
blanco	-	-	4	5
1	1	-	4	5
2	2	-	4	5
3	-	1	4	5
4	-	2	4	5

UV-Vis In figure 4.28 the absorbance relative to the initial absorbance measured over time for the samples as described in table 4.7 is depicted. Again the reaction rate for the mixtures with cubes is higher than for the mixture without cubes. From this it can be concluded that also silica coated cubes are able to catalyze the degradation reaction. Sample 1 from these experiments can be compared with sample 2 from the previous section. Both contain approximately the same amount of the same type of cubes, where the cubes from the previous section were bare these cubes are silica coated.

The silica coated cubes converted 50 molecules per cube per second and the bare cubes 80 molecules per cube per second. However, the initial amount of methylene blue was not the same in both cases, which might influence the reaction speed. The reaction rates were also calculated over a different period of time, which makes the results also hard to compare, because the reaction rate probably drops with increasing reaction time due to the decreasing concentration of hydrogen peroxide.

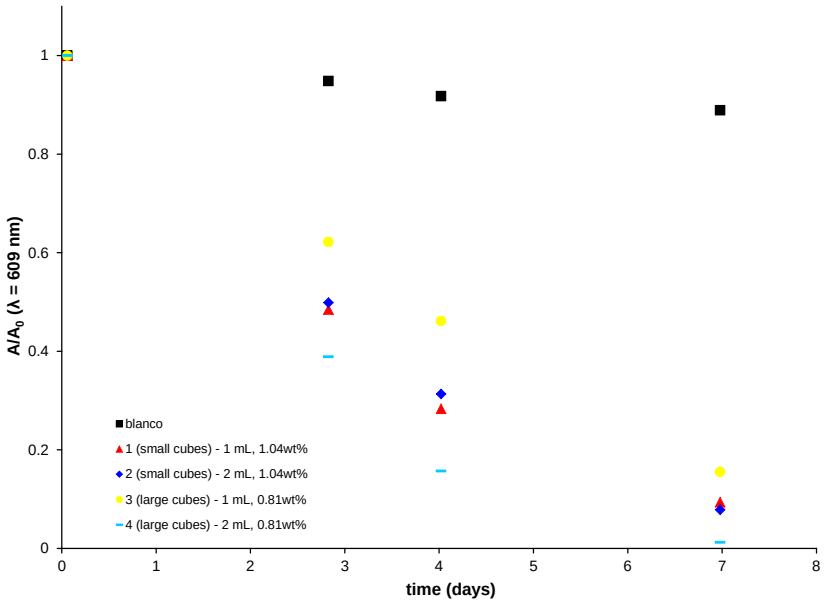

Figure 4.28: Decrease of absorbance by methylene blue over time by both different sizes and amounts of silica coated hematite cubes. All silica coated cubes catalyze the degradation reaction, which can be concluded from the difference in slope for the samples with cubes and the blanco. However, there is no large difference between the different sizes and different amounts of cubes.

In table 4.8 the calculated speeds for each reaction are given between the start of the reaction and after seven days. All samples have similar rates. The rates are difficult to compare, because the samples

contain different numbers of cubes and the cubes have different sizes whereby the total accessible surface area for the reaction is different. The speeds for 2 mL samples are slightly higher in both cases, although more experiments should be performed to clarify this effect.

Table 4.8: Reaction speeds for the degradation of methylene blue by the silica coated hematite cubes listed in table 4.7. The reaction speeds for samples 2 and 4 are slightly higher than for the samples with the same, but less cubes.

Sample	Speed $\left(\frac{\Delta A}{\Delta t}\right)$	Speed (molecules/day)	Speed (molecules/s)	Theoretical degradation time (days)	TON $\left(\frac{\text{molecules}}{s \cdot \text{cube}}\right)$
blanco	0.05	2.0×10^{16}	2.3×10^{11}	65	
1	0.36	1.4×10^{17}	1.6×10^{12}	10	50
2	0.38	1.5×10^{17}	1.7×10^{12}	9	27
3	0.34	1.3×10^{17}	1.5×10^{12}	10	374
4	0.37	1.4×10^{17}	1.6×10^{12}	9	201

4.2.2.2 Rhodamine B

These reactions were performed with rhodamine B as organic molecule. 5 mL of rhodamine B stock solution (1.82×10^{-4} M) was added and 5 mL 35 wt% H_2O_2. The amount of added cubes for each sample is given in table 4.9. The dispersion of the small cubes contained 1.04 wt% and the dispersion of large cubes 0.81 wt% of cubes.

Table 4.9: Amount of cubes, rhodamine B solution and hydrogen peroxide added to the reaction mixtures.

Sample	Small cubes (mL)	Large cubes (mL)	Rhodamine B (mL)	H_2O_2 (mL)
blanco	-	-	5	5
1	1	-	5	5
2	2	-	5	5
3	-	1	5	5
4	-	2	5	5

UV-Vis Figure 4.29 illustrates that the absorbance by rhodamine B decreases faster when the reaction mixtures contains cubes. In table 4.10 the calculated reactions rates between the start of the reaction and day six assuming a linear decrease. The reaction rates for the samples containing methylene blue are slightly higher than for the samples containing rhodamine B. The theoretical degradation times are however approximately the same. The start concentrations of the dye molecules were not the same in both cases, the used concentration methylene blue was higher than the used concentration of rhodamine B.

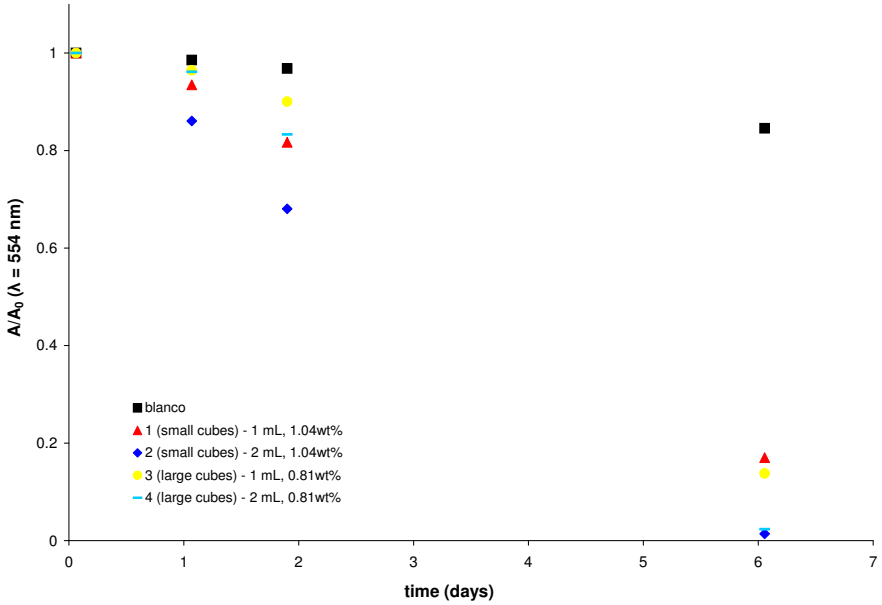

Figure 4.29: Decrease of absorbance due to the degradation of rhodamine B by silica coated hematite cubes. The samples correspond to the samples described in table 4.9.

Table 4.10: Reaction speeds of the degradation of rhodamine B by silica coated hematite cubes.

Sample	Speed $\left(\frac{\Delta A}{\Delta t}\right)$	Speed (molecules/day)	Speed (molecules/s)	Theoretical degradation time (days)	TON $\left(\frac{\text{molecules}}{s \cdot \text{cube}}\right)$
blanco	0.08	1.1×10^{16}	1.2×10^{11}	56	
1	0.43	5.6×10^{16}	6.5×10^{11}	11	20
2	0.51	6.7×10^{16}	7.7×10^{11}	9	12
3	0.45	5.8×10^{16}	6.8×10^{11}	10	167
4	0.51	6.6×10^{16}	7.7×10^{11}	9	95

In the last two experiments the same silica coated cubes were used with two different organic molecules. Both experiments show that also the silica coated cubes are able to speed up the degradation reaction of organic molecules (both methylene blue and rhodamine B), despite their shell. As stated before the reaction speeds between these silica coated particles and the bare particles are hard to compare, because of a different amount methylene blue used for the degradation reaction. Later in this thesis, in section 4.2.4 the bare hematite particles will be compared with silica coated particles for which the same amount of dye was used.

4.2.3 Silica Coated and Hematite Etched Cubes

In the next table the cubes are given which were applied in the following experiments. Samples 1, 2 and 3 contained silica coated cubes of ~750 nm, samples 4, 5, and 6 contained silica coated cubes of ~1800 nm. Samples 2, 3, 5, and 6 contained partially hematite etched particles, the cubes in samples 1 and 4 were not hematite etched. The numbers of the TEM pictures of the particles are given in the following table and can be found in section 4.1.1 and section 4.1.7.

For the reaction mixtures 5 mL of dispersion was used with the concentrations as given in table 4.11. 5 mL of methylene blue stock solution (4.39×10^{-4} M) was used and 5 mL of 35 wt% H_2O_2.

Table 4.11: Specifications of the samples and cubes used for the catalytic activity measurements of the hematite etched cubes. The cubes in sample 1 and 4 are not etched by hydrochloric acid, the rest of the particles are etched.

Sample	Figure	Cubes	Size (nm)	Concentration dispersion (wt%)
1	4.2	SiO_2_HC1_s1	743	0.74
2	4.3a	SiO_2_HC1_s1_1	743	0.64
3	4.3b	SiO_2_HC1_s1_2	743	0.64
4	4.17	SiO_2_HC2_s2	1784	0.75
5	4.18a	SiO_2_HC2_s2_1	1784	0.30
6	4.18b	SiO_2_HC2_s2_2	1784	0.35

4.2.3.1 UV-Vis data

In figure 4.30 it can be seen that also these cubes can be used as a catalyst in the conversion of organic dyes. For sample 1 the third measurement is left out, because the liquid in the cuvet contained some cubes and so the spectrum is unreliable due to scattering and absorption of the cubes present.

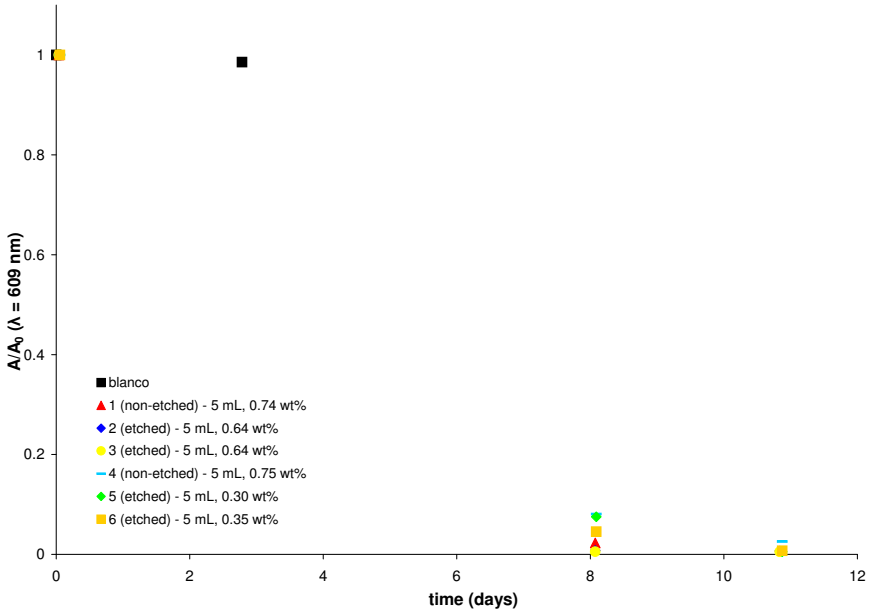

Figure 4.30: Decrease in absorbance of methylene blue. The samples correspond to the samples described in table 4.11.

Reaction speeds are calculated between the point at day zero and day eight, because the absorbance at the later measurements is too low. For the blanco the difference between day zero and day three was calculated. Although samples 1 and 4 have a relatively high amount of cubes in the reaction (table 4.11), the reaction speeds are comparable or even lower than the reaction speeds for the etched cubes 2, 3, 5 and 6, see table 4.12. However, the difference in reaction speed is less clear for the large cubes in samples 4, 5 and 6.

The higher reaction speeds could be caused by the fact that the cubes in 2, 3, 5 and 6 are hematite etched and have an increased surface area of iron oxide available. However, to determine the precise amount of cubes present in the mixtures the amount of remaining hematite has to be determined. Infrared spectroscopy was performed on the reaction mixtures at the beginning of the reaction from which the amount of remaining hematite can be determined from. The results are described in section 4.2.3.3.

Table 4.12: Reaction speeds of the mixtures with hematite etched and not hematite etched particles. The reaction speed for samples 2 and 3 are slightly higher than for sample 1, which contained non-etched particles. The differences between samples 4, 5 and 6 are very small.

Sample	Speed $\left(\frac{\Delta A}{\Delta t}\right)$	Speed (molecules/day)	Speed (molecules/s)	Theoretical degradation time (days)	TON $\left(\frac{\text{molecules}}{s \cdot \text{cube}}\right)$
blanco	0.02	6.9×10^{15}	8.0×10^{10}	237	
1	0.36	1.4×10^{17}	1.6×10^{12}	12	63
2	0.47	1.8×10^{17}	2.1×10^{12}	9	63
3	0.47	1.8×10^{17}	2.1×10^{12}	9	64
4	0.42	1.6×10^{17}	1.8×10^{12}	10	1190
5	0.42	1.6×10^{17}	1.9×10^{12}	10	1390
6	0.44	1.7×10^{17}	1.9×10^{12}	10	1269

4.2.3.2 TEM

TEM images were made of the particles in each reaction mixture to see the condition of the particles during the reaction. From figure 4.31 it can be seen that almost all the silica shells around the hematite cubes are broken or damaged. In the following sections TEM pictures of the cubes in the reaction mixtures will also be shown. The cause and the effect of the breaking will be discussed in section 4.4.

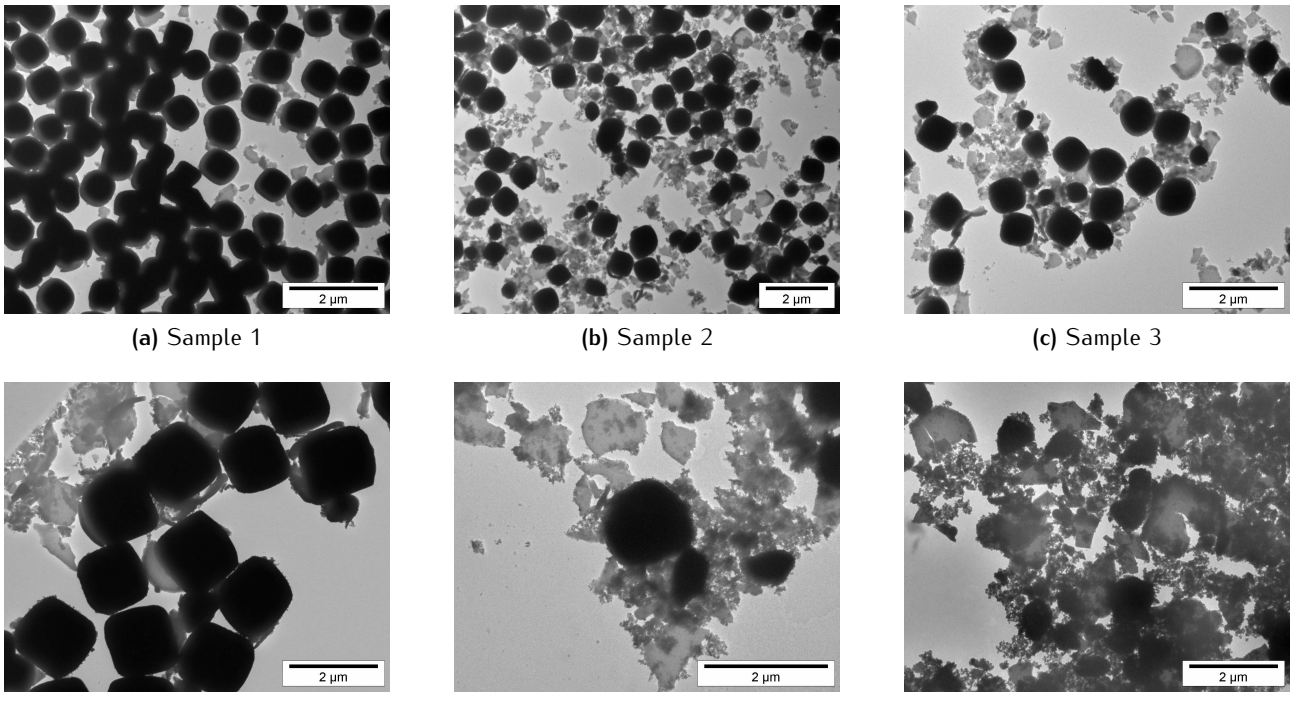

(a) Sample 1 **(b)** Sample 2 **(c)** Sample 3

(d) Sample 4 **(e)** Sample 5 **(f)** Sample 6

Figure 4.31: TEM pictures of cubes from the supernatants of the reactions mixtures as described in table 4.11, after 16 days of reaction. In all cases the silica shells were broken.

Because the silica shells of these cubes were damaged, the breakage of the same cubes was monitored over time in new reaction mixtures. The concentration of cubes in the experiment above was higher (5 mL ~1 wt%) than normal (1 mL ~1 wt%) and therefore reaction mixtures with 1 mL and 5 mL dispersion were prepared. Only the non-hematite etched particles were used, because there was no significant difference between the etched and the non-etched particles. The concentration of the dispersion containing the SiO_2_HC1_s1 cubes was 0.81 wt% and the concentration of the dispersion containing the SiO_2_HC2_s2 cubes was 0.75 wt%. The TEM pictures can be found in appendix A. No significant difference in breaking of the silica shell was observed between the different amounts of cubes. The silica shells do not break

instantaneously after the reaction has started. After a few days of reaction broken silica shells were observed and after a longer period more silica shells are broken.

4.2.3.3 IR spectroscopy

Infrared spectroscopy was used in this case to determine the dissolution of iron during the degradation reaction. During the Fenton reaction the oxidation states of the iron ions at the surface of the particles changes. It could be the case that the iron ions go into solution during the degradation reaction, also because of the acidic environment. Dissolved oxides will not show up in the infrared spectra and therefore this technique was used to determine the amount of the non-dissolved and so remaining amount of hematite. Figure 4.32 shows the IR spectra of 1 mL reaction mixture in about 250 mg KBr. All the measurements were performed in duplo. The first aspect to notice is the change in shape of the silica peak around 1100 cm^{-1} after fourteen days of reaction. The peaks are more stretched than at the start of the reaction. The peak ratios between the highest silica peak (around 1100 cm^{-1}) and the hematite peak (around 550 cm^{-1}) were calculated for the measurements at the start of the reaction and after fourteen days (table 4.13). From the spectra taken at the beginning of the reaction also the amount of remaining hematite after etching with hydrochloric acid was determined in the same way as described in section 4.1.6.6.

Table 4.13: In this table the ratios between the silica and the hematite peaks on the first day of the reaction and after two weeks are given. The ratios are larger after fourteen days which could indicate that the hematite partially dissolved.

Sample	Day 0 A (silica)/A (hematite)	Day 15 A (silica)/A (hematite)
1	1.04	1.10
2	1.95	1.96
3	1.92	1.93
4	0.58	0.72
5	1.50	2.05
6	1.46	1.98

It can be concluded from the peak ratios of hematite and silica is that the ratios between silica and hematite are slightly increased. This could indicate the dissolution of hematite during the degradation reaction. However, more experiments should be performed to investigate the dissolution of hematite. With Atomic Absorption Spectroscopy (AAS) the supernatant of the reaction mixtures could be investigated on the presence of iron ions.

Also the peak ratio increased more for the large cubes, albeit a small difference. The hematite cores were not etched, so far can be seen with TEM, see figure 4.31. The silica shell of the big cubes (4, 5 and 6) is about 100 nm and the shell of the smaller cubes (1, 2 and 3) is about 80 nm. So the thicker silica shell of the large cubes does not prevent the solvation of iron better than the thin layer. Because the smaller cubes have a relatively larger surface area compared to the bigger cubes more solvation of iron ions would be expected, but this is certainly not the case.

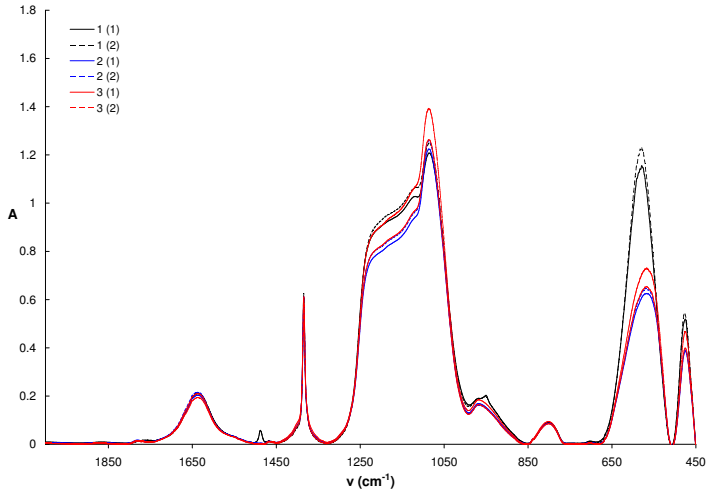

(a) Day zero, samples (1), (2) and (3)

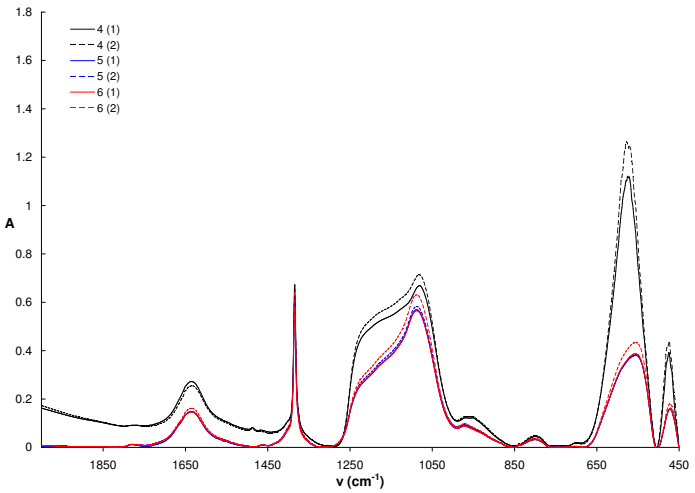

(b) Day zero, samples (4), (5) and (6)

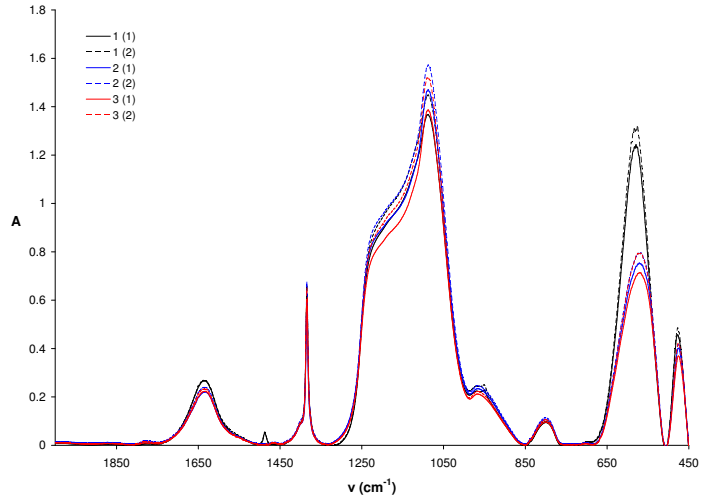

(c) Day fourteen, smaples (1), (2) and (3)

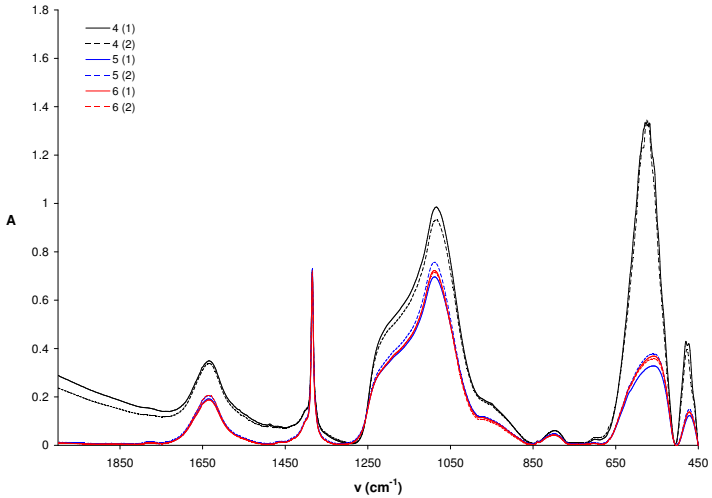

(d) Day fourteen, smaples (4), (5) and (6)

Figure 4.32: IR spectra (in duplo) on day zero (figure (a) and (b)) and after fourteen days (figure (c) and (d)). The numbers in the graphs correspond to the samples as described in table 4.11 and the numbers between brackets correspond to the duplo number. The difference of the peak ratio are not well visible from the graphs. The calculated numbers are shown in table 4.13.

4.2.3.4 pH measurements

Another method to investigate if the iron oxide has dissolved is by measuring the pH. Dissolved iron ions make the solution acidic by repulsion of hydrogen atoms of the water, forming complexes with iron, as described on page 18 [41].

pH measurements were done with diluted reaction mixture, because less sample was needed. 1 mL of the reaction mixture, without cubes, was taken and diluted to a total volume of 10 mL.

Table 4.14: pH of diluted reaction mixture after zero and seventeen days of reaction, after 2 and 5 minutes equilibrating.

Sample	Day 0		Day 17	
	2 min.	5 min.	2 min.	5 min.
blanco	6.27	6.06		
1	5.98	6.00	5.66	5.50
2	6.37	6.22	5.18	5.03
3	6.11	5.88	4.88	4.71
4	6.18	6.06	5.68	5.66
5	6.30	6.11	5.38	5.31
6	6.35	6.15	5.39	5.15
blanco (not diluted)	3.33	3.30		

Also the pH of a 5 mL methylene blue and 5 mL 35 wt% H_2O_2 in 10 mL of Millipore water was measured. This solution was more acidic and had a pH of 3.33 after 2 minutes and 3.30 after 5 minutes. At the end of the reaction the pH of the diluted liquids (without cubes) was slightly lower than in the beginning. This could also indicate that some of the iron dissolved during the reaction. This low pH is beneficial for the Fenton reaction which has the highest reaction rate a low pH [11, 16].

The real pH could also be calculated, however due to the high dilution factor this would not be very accurate. However, the pH of the reaction mixtures containing the cubes will be probably below 3.3, because of the presence of the aqua acid. Because the measured supernatants of the reaction mixtures were diluted the difference between the non-diluted mixtures was even larger.

4.2.4 Silica Etched Hematite Cubes

This section discusses the results of the catalytic activity tests of the silica etched cubes (~1100 nm) from section 4.1.6.4. The amount of remaining silica and the number of cubes in the reaction mixtures are given in table 4.15. The reaction mixtures were again prepared with 5 mL of 4.39×10^{-4} M and 5 mL 35 wt% H_2O_2 in a total reaction volume of 20 mL.

Table 4.15: The amount of remaining silica after etching and number of cubes in each reaction mixture. The first number from the sample names in the first colums is the etching time of the silica cubes.

Sample	Fraction remaining silica	Concentration (wt%)	Added dispersion (mL)	Number of cubes
5 min. (1)	1.00	0.33	2	1.3×10^9
5 min. (2)	1.00	0.33	4	2.5×10^9
30 min. (1)	0.84	0.40	2	1.6×10^9
30 min. (2)	0.84	0.40	4	3.3×10^9
120 min. (1)	0.63	0.27	2	1.1×10^9
120 min. (2)	0.63	0.27	4	2.3×10^9

4.2.4.1 UV-Vis

The next graph (figure 4.33) shows the degradation of methylene blue over time by cubes whereof the silica shell is etched by surface protected water etching. The silica etched particles also catalyze the degradation reaction, however the rate of degradation is not higher for the longer etched particles. From the figure and table 4.16 it can be seen that the sample with the highest number of cubes degrades the methylene blue fastest. Therefore the speed depends on the number of cubes rather than on the extent of etching of the silica shell.

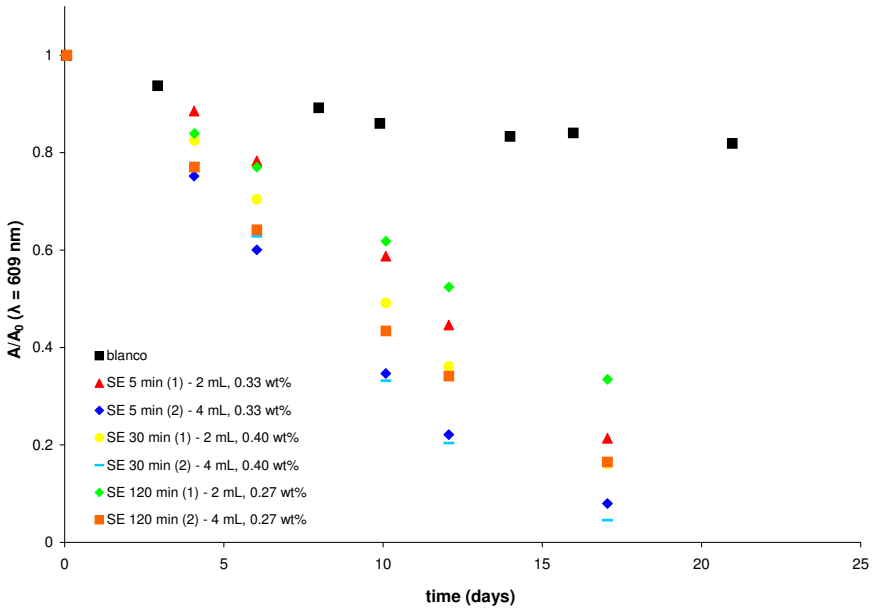

Figure 4.33: Decreased absorption over time of the reactions with silica etched cubes. The blanco decreases slowly, whilst the relative absorption decreases faster when the cubes are present. Due to the normalization of the UV-Vis data it can not be seen from this graph, however 30 min. (2) is the fastest while 5 min. (1) is the slowest.

In table 4.16 the calculated reaction rates are give. The reaction rates were calculated between the beginning of the reaction and at day ten of the reaction, assuming a linear decrease.

Table 4.16: Reaction speeds for the silica etched cubes.

Sample	Speed $\left(\frac{\Delta A}{\Delta t}\right)$	Speed (molecules/day)	Speed (molecules/s)	Theoretical degradation time (days)	TON $\left(\frac{\text{molecules}}{s \cdot \text{cube}}\right)$
blanco	0.05	2.1×10^{16}	2.4×10^{11}	78	
5 min. (1)	0.14	5.4×10^{16}	6.3×10^{11}	30	494
5 min. (2)	0.23	8.9×10^{16}	1.0×10^{12}	18	402
30 min. (1)	0.18	6.9×10^{16}	8.0×10^{11}	24	487
30 min. (2)	0.24	9.1×10^{16}	1.1×10^{12}	18	323
120 min. (1)	0.14	5.5×10^{16}	6.3×10^{11}	30	557
120 min. (2)	0.21	8.0×10^{16}	9.3×10^{11}	20	409

30 min. (2) has the highest reaction rate while 5 min. (1) has the lowest. This corresponds to the larger amount of cubes present in the former sample. Although 120 min. (1) had less cubes (1.1×10^{-9} cubes) than 5 min. (1) (1.3×10^{-9} cubes) their reaction rates are equal. There might be a little advantage due to the silica etching of sample 120 min. (1), since the reaction rate should be lower than for 5 min. (1). However, more experiments have to be performed and further no clear conclusion can be drawn regarding the etching time of the particles. The etching time could also be increased to make the silica shell more porous and increase the reaction rate.

These reaction mixtures contained slightly less cubes than the reaction mixtures with the bare cubes from section 4.2.1.2. However, the reaction rates are in the same order of around 10^{12} molecules per second. This indicates that the silica shell does not inhibit catalysis although most of the silica shells break during the reaction.

In figure 4.34 the turn-over-frequency per cube is plotted against the total amount of cubes present in the reaction mixture. Strikingly the more cubes present, the less molecules they convert per second. This could denote a struggle for methylene blue between the cubes. Therefore more experiments with different and higher concentrations of methylene blue should be performed to investigate this effect.

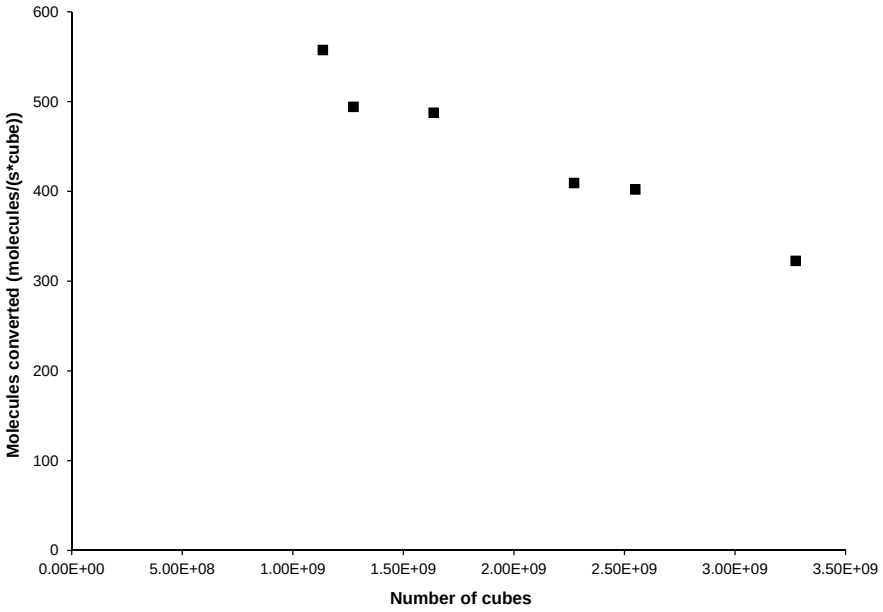

Figure 4.34: The reaction speed per cube versus the number of cubes. The reaction speed per cube decreases with increasing number of cubes present in the reaction mixture.

4.2.4.2 TEM

The aim of silica etching is to make the silica layer more porous. Rendering it more accessible to large molecules one could expect that the pressure inside the silica etched cubes would not become as high as is the non-etched cubes. However, the silica etching did not prevent the shells from breaking, as can be seen in figure 4.35. For the particles which have been etched for two hours no less shells are broken during the degradation reaction than for the five minutes etched particles. The arrows in the pictures indicate some of the bare hematite particles.

From nitrogen physisorption measurement can be concluded that the silica shells become more porous during surface protected water etching. In appendix B.8, B.9 and B.10 the isotherms and pore size distributions for silica etched particles are shown. For more severely etched particles the pores are larger and also the total pore volume per gram of particles becomes larger. Although these particles are different particles than the particles used in these catalytic activity measurements, it can be concluded from the measurements that the surface protected water etching increases the porosity and the pore size.

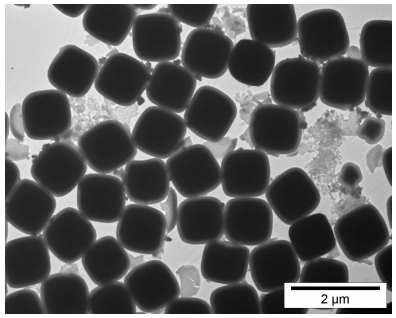

(a) 5 min. (1)

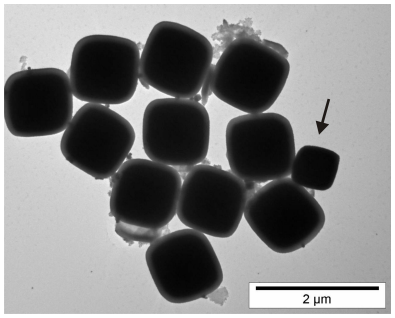

(b) 5 min. (1)

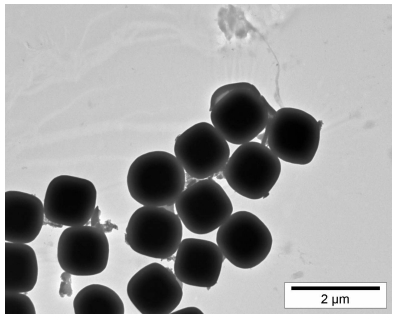

(c) 5 min. (2)

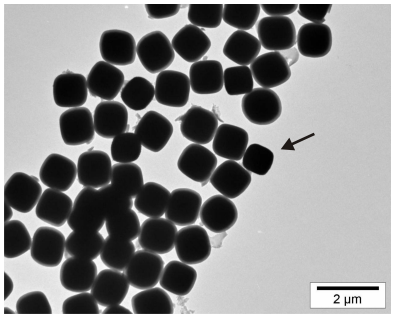

(d) 5 min. (2)

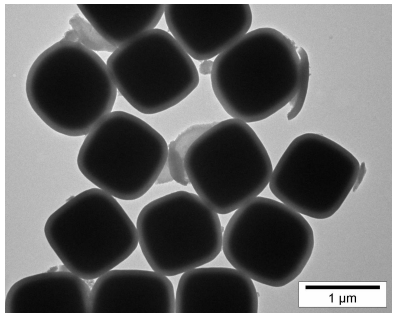

(e) 30 min. (1)

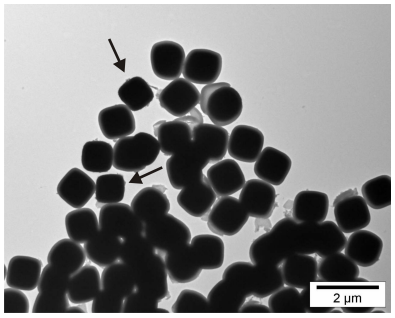

(f) 30 min. (1)

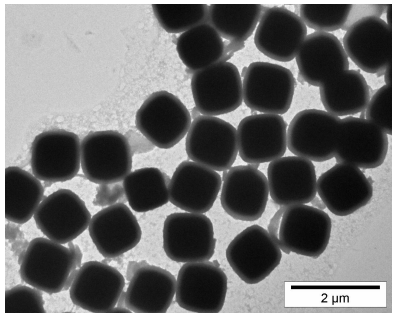

(g) 30 min. (2)

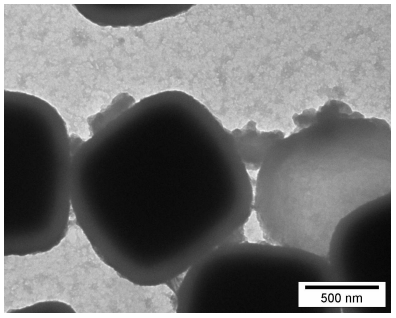

(h) 30 min. (2)

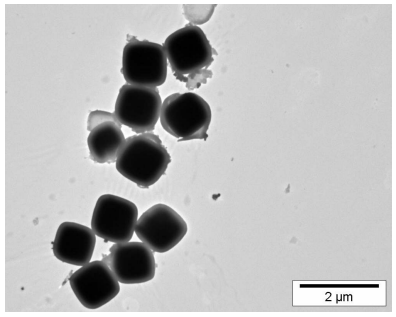

(i) 120 min. (1)

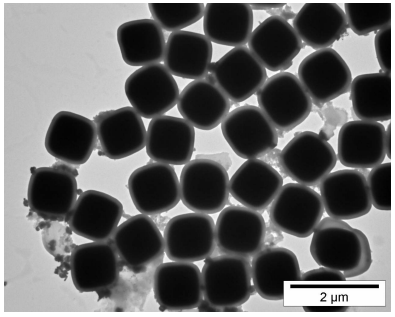

(j) 120 min. (1)

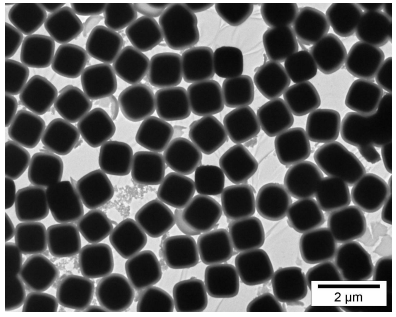

(k) 120 min. (2)

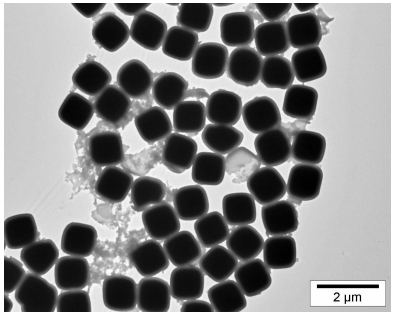

(l) 120 min. (2)

Figure 4.35: Of each reaction mixture two TEM pictures of the supernatant are shown. It is clear from every picture that large amounts of silica shells and bare hematite cubes are present. Some of the bare hematite particles are indicated in the pictures with arrows. Silica etching did not prevent the breaking of the silica shell during the decomposition reaction.

4.3 Substrates

In this section, the results of the activity measurements and some general results of the substrates with cubes are described. On all substrates a layer of cubes was deposited twice and were heat treated at 450 °C as described in Chapter 3. Experimental, unless stated otherwise.

4.3.1 General Results

The reaction mixture of the non-heat treated substrates contain a lot more cubes than the liquid of the heat treated substrates. Therefore, the heat treatment ensures the cubes to stick better on the substrate during the reaction. TEM pictures were taken, from the liquid of the bottom on the reaction bottle, after one or two and 30 days. In figure 4.36e it seems that the silica shell is affected by the reaction, because the contrast of the silica decreased and does not look as thick and firm as before.

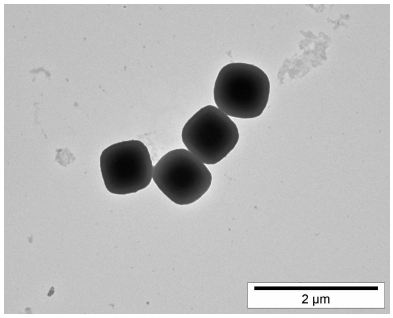

(a) Heat treated, after 1 day of reaction.

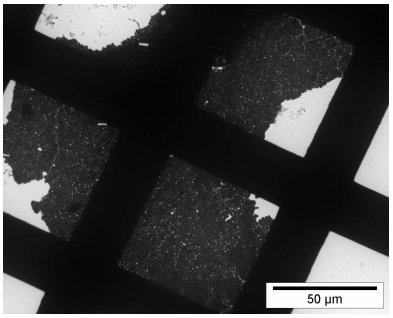

(b) No heat treatment, after 2 days of reaction.

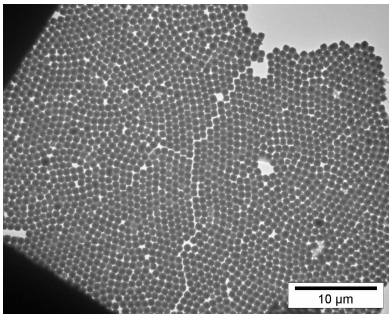

(c) No heat treatment, after 2 days of reaction.

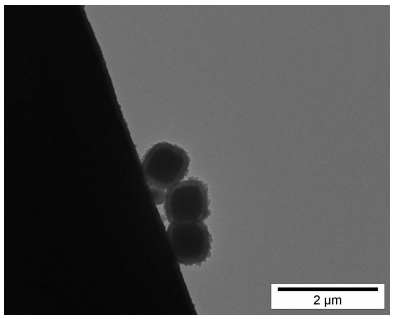

(d) Heat treated, after 30 days of reaction.

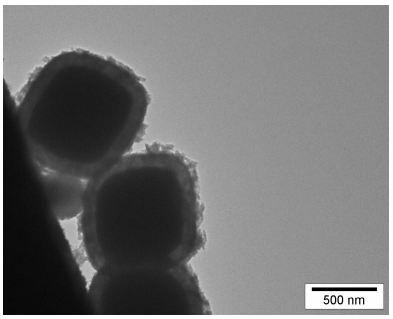

(e) Zoom in of (d), the contrast of the silica shell decreased.

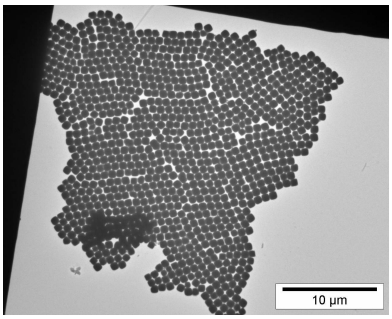

(f) No heat treatment, after 30 days of reaction.

Figure 4.36: TEM images of the supernatant of the reaction mixtures with heated and non-heated substrates.

Usually the cubes formed ordered structures on the mica substrates. In figure 4.37 SEM images are shown of substrates after they had been in the oven. The first picture shows a substrate that has one dried deposition of silica coated hematite cubes in water and underwent heat treatment once. The layer out of focus lies directly on the mica surface and the part in focus shows a multi-layer packing. The second picture shows another piece of the same substrate after another deposition and heat treatment cycle, these substrates were not used in activity measurements. The cubes are self-assembled into densely packed multi-layer structures on the mica platelets showing local, but no long range order. The formed structures are promising to form a closed-packed membrane from these particles in future work. The cubes deposited on the mica are silica coated cubes of 743 nm, described in section 4.1.1.2. The cubes were not hematite nor silica etched.

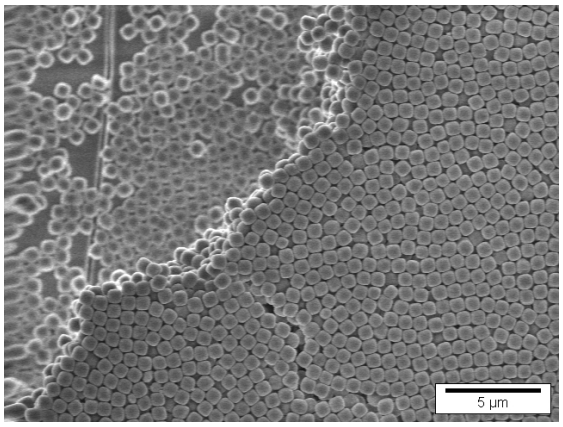

(a) Substrate after one coating and one heat treatment.

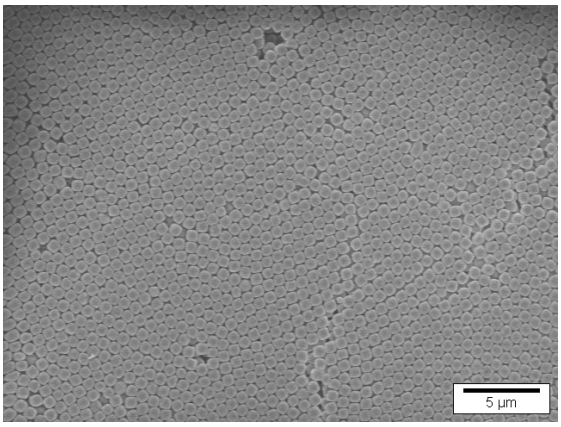

(b) Substrate after two coatings and two heat treatments.

Figure 4.37: (a) one deposition once in the oven and (b) two deposition two times in the oven. Densely packed structures with local order are formed by self-assembly of silica coated hematite cubes upon drying. The structures were formed after depositions of silica coated hematite cubes dispersed in water on mica.

4.3.2 Activity of Heat Treated Substrates

In these experiments, the same cubes were used as in section 4.2.3, and are recalled in table 4.17. In this table also the total weight of dried particles present on each substrate is given. The blanco was the reaction mixture of methylene blue and hydrogen peroxide with merely an empty mica substrate. This substrate was placed in the reaction mixture in the same way as the coated substrates. The substrates were placed in mixture of 5 mL 4.39×10^{-4} M methylene blue, 5 mL 35 wt% H_2O_2 and 10 mL Millipore water as shown in figure 3.5, by hanging them in the mixture.

Table 4.17: Used cubes on substrates for the degradation of methylene blue. The cubes in samples 2, 3, 5 and 6 are hematite etched. The sizes of the cubes are given and the total weight of dried particles on the substrate.

Sample	Figure	Cubes	Size (nm)	Weight dried cubes (mg)
1	4.2	SiO_2_HC1_s1	743	11
2	4.3a	SiO_2_HC1_s1_1	743	10
3	4.3b	SiO_2_HC1_s1_2	743	11
4	4.17	SiO_2_HC2_s2	1784	13
5	4.18a	SiO_2_HC2_s2_1	1784	5
6	4.18b	SiO_2_HC2_s2_2	1784	7

4.3.2.1 UV-Vis

In the following graph in figure 4.38 the decrease in absorbance of methylene blue by the degradation of silica coated hematite cubes on substrates is depicted. In the presence of the substrates with cubes the degradation is faster, but not as fast as for the dispersed cubes shown in the previous sections. This might be due to the fact that not all the cubes are in the reaction mixture during the whole reaction, because the liquid level drops when samples to measure with UV-Vis spectroscopy are taken. Also the substrates can not be placed on the bottom because the vials are magnetically stirred. Interestingly, the absorbance for the blanco increased over time, because the sample concentrated by evaporation. The samples could evaporate more easily because they were covered by parafilm with a hole in stead of a lid. In table 4.18 the corresponding reaction rates are given and as mentioned the reaction speed for the blanco is negative. Furthermore, all the reaction speeds are quite low, probably due to the immobilization of the particles. Moreover, like in the blanco sample the samples containing cubes could evaporate, increasing

the apparent concentration. The reaction rates were calculated between the start of the reaction and day ten of the reaction, assuming a linear decrease.

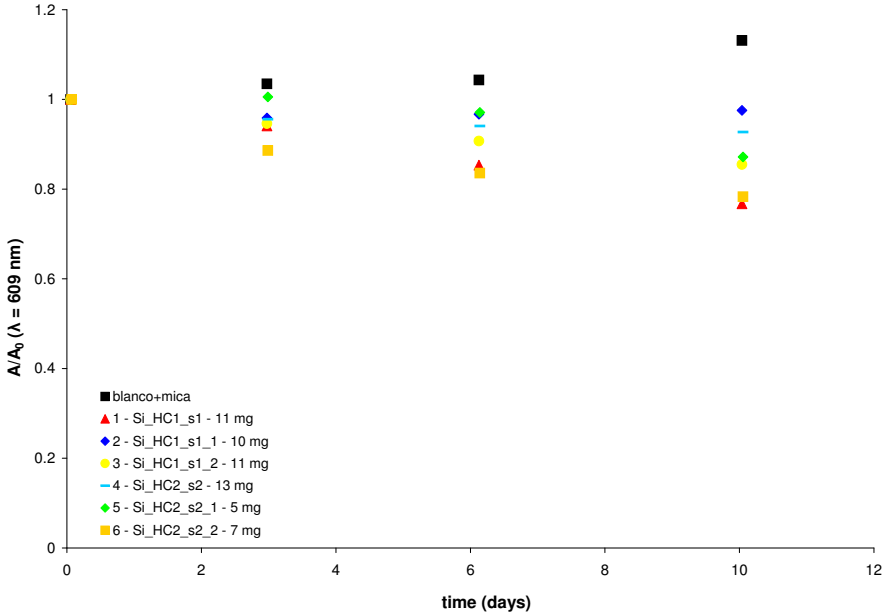

Figure 4.38: Decrease in absorbance by silica coated hematite cubes on substrates. For the blank experiment a non-coated mica plate was added to the normally used blanco.

Table 4.18: Reaction speeds of silica coated and hematite etched cubes on substrates. The samples correspond to the samples in table 4.17.

Sample	Speed $\left(\frac{\Delta A}{\Delta t}\right)$	Speed (molecules/day)	Speed (molecules/s)	Theoretical degradation time (days)	TON $\left(\frac{\text{molecules}}{s \cdot \text{cube}}\right)$
blanco + mica	-0.05	-1.9×10^{16}	-2.2×10^{11}	-85	
1	0.09	3.4×10^{16}	3.9×10^{11}	48	51
2	0.01	3.5×10^{15}	4.1×10^{10}	459	4
3	0.05	2.1×10^{16}	2.4×10^{11}	78	22
4	0.03	1.1×10^{16}	1.2×10^{11}	153	222
5	0.05	1.9×10^{16}	2.1×10^{11}	88	454
6	0.08	3.2×10^{16}	3.7×10^{11}	51	629

4.3.2.2 TEM

Some of the particles were released from the substrate during the reaction and dispersed into the supernatant. These particles were imaged with transmission electron microscopy. As can be seen in figure 4.39, the silica shells are less broken than in the case of the dispersed cubes in figures 4.31 and 4.35. In the TEM pictures also some mica flakes are visible, which broke off the mica plates by the stirring bar touching the mica plates. In figure 4.39b the mica flakes are indicated.

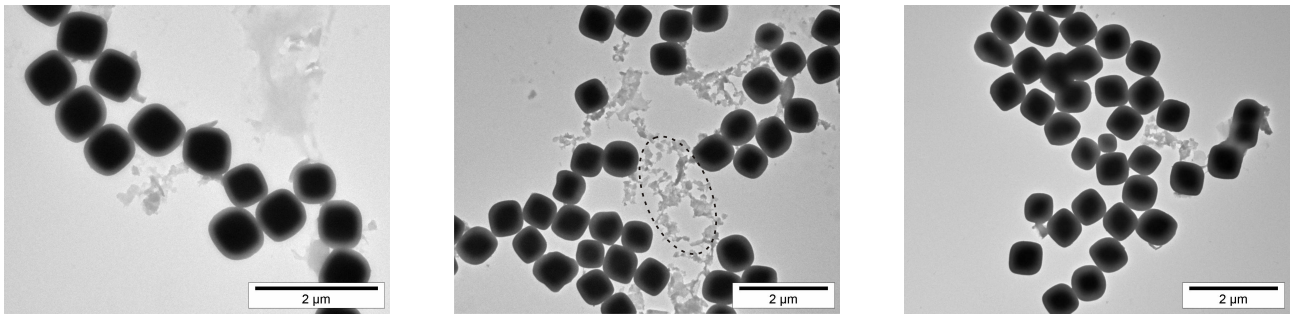

(a) Sample 1 **(b)** Sample 2, containing mica flakes **(c)** Sample 3

(d) Sample 4 **(e)** Sample 5 **(f)** Sample 6

Figure 4.39: TEM images of the particles present in the supernatant after ten days of reaction with hydrogen peroxide and methylene blue. These particles detached from the substrate during the reaction.

4.3.2.3 SEM

The substrates were imaged with scanning electron microscopy after ten days of reaction. The substrates were dried and a small piece was cut off and placed on a SEM stub. In the SEM images in figure 4.40 only a few broken cubes, as indicated in figure 4.40f at the substrates were observed.

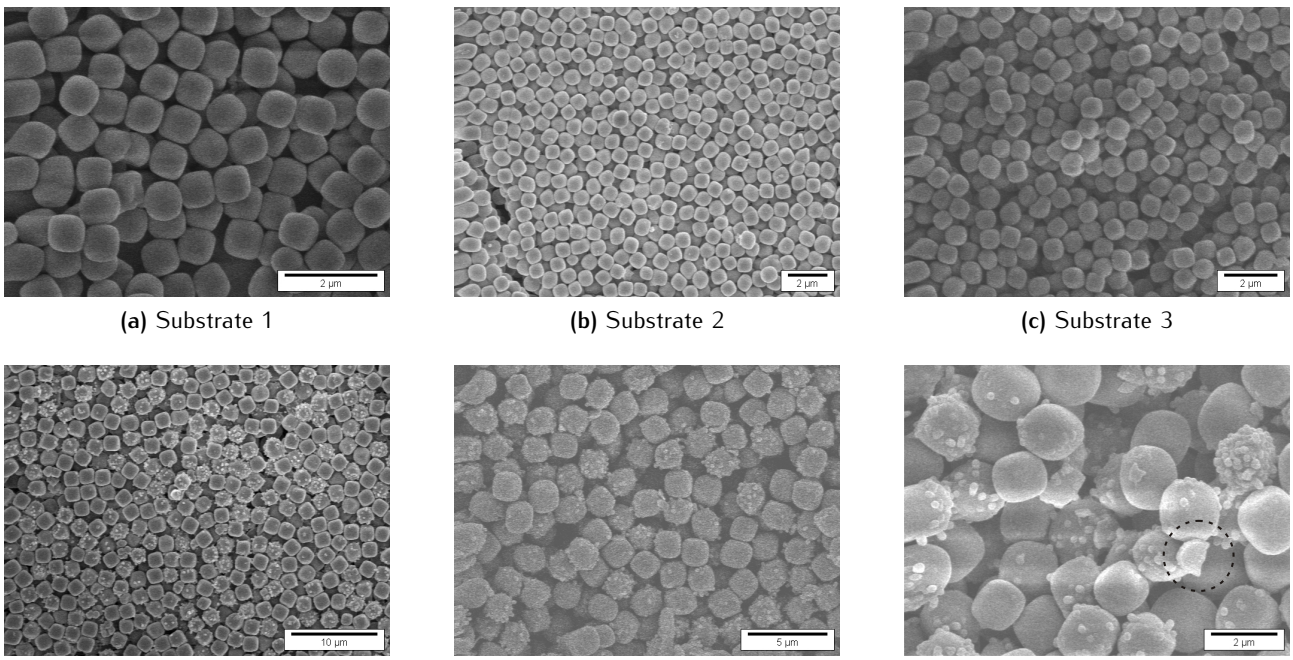

(a) Substrate 1 **(b)** Substrate 2 **(c)** Substrate 3

(d) Substrate 4 **(e)** Substrate 5 **(f)** Substrate 6

Figure 4.40: SEM images of the substrates. The reaction was stopped after ten days, whereafter the parts of the substrate were imaged. In (f) one broken silica shell is indicated.

In appendix C the TEM pictures of the dispersed cubes (see also figure 4.31 in section 4.2.3.2), the TEM pictures of the cubes in the supernatant of the substrates and the SEM pictures of the substrates (see above) are placed next to each other. It can be seen that the dispersed cubes are more damaged than the cubes that are dispersed into the liquid from the substrate after they have been in the oven at 450 °C.

4.3.3 Activity of Substrates Heated to Different Temperatures

Onto all substrates used in this section silica coated hematite cubes of approximately 1100 nm described in section 4.1.6.3 were deposited. The cubes were not silica nor hematite etched. The substrates were all heated to a different temperatures, ranging from 200 °C to 450 °C as listed below and were placed in mixture of 5 mL 4.39×10^{-4} M methylene blue, 5 mL 35 wt% H_2O_2 and 10 mL Millipore water.

Table 4.19: Heat treatment temperatures of the substrates and the weight of cubes on each substrate.

Substrate	Temperature (°C)	Weight dried cubes (mg)
1	200	29
2	250	28
3	300	31
4	350	17
5	400	24
6	450	24

4.3.3.1 UV-Vis

In the next figure the decrease of absorbance by methylene blue in the presence of silica coated cubes on substrates elevated to different temperatures is shown. The reaction rates are shown in table 4.20 and were calculated between the start of the reaction and day eight for the blanco, the blanco+mica and mixture 1, and between the start and day six for the other reaction mixtures. Roughly, it can be said that the reaction rate decreases with increasing heating temperature of the substrate. The increase of reaction speed for lower temperature can be caused by the fact that more cubes are released from the substrate and might deliver most of the activity. By coincidence less cubes were initially present on the substrates for the substrates treated at higher temperatures. In figure 4.42 the percentage of remaining particles is plotted against the heating temperature of the substrates. When the substrates are heated to higher temperatures less cubes are released into the reaction mixture. Again due to evaporation the absorbance of the blanco+mica increased over time. The degradation rates for these substrates are higher than for the substrates in section 4.3.2 because more cubes were initially present on the substrates. Overall the speed for these substrate was relatively high, probably caused by the dispersion of most of the cubes into the reaction mixture.

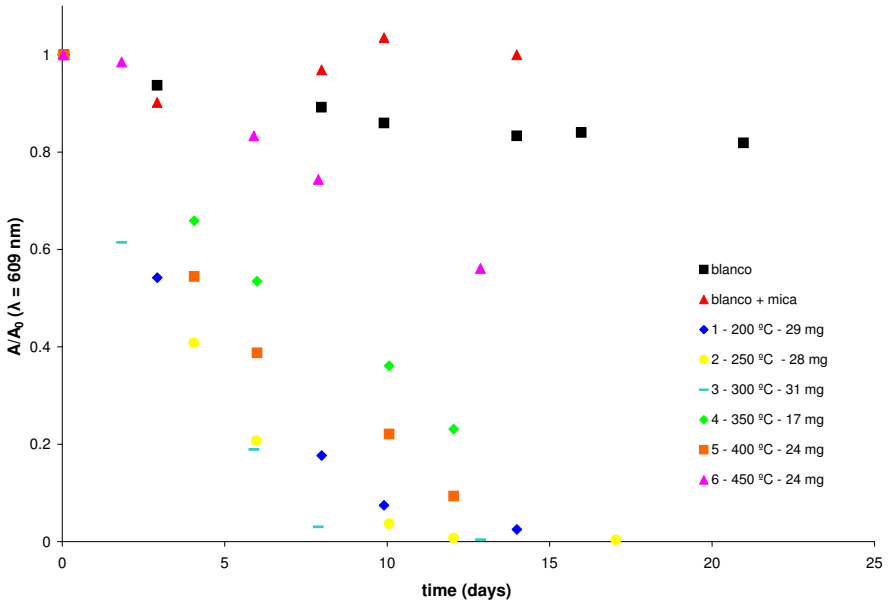

Figure 4.41: Decrease of absorbance of methylene blue. The degradation of methylene blue is slightly slower by substrates elevated to higher temperatures.

Table 4.20: Reaction speeds for the substrates heated to different temperatures.

Sample	Speed $\left(\frac{\Delta A}{\Delta t}\right)$	Speed (molecules/day)	Speed (molecules/s)	Theoretical degradation time (days)	TON $\left(\frac{\text{molecules}}{s \cdot \text{cube}}\right)$
blanco	0.05	2.0×10^{16}	2.3×10^{11}	82	
blanco+mica	0.02	5.8×10^{15}	6.7×10^{10}	282	
1 (200 ℃)	0.38	1.4×10^{17}	1.7×10^{12}	11	296
2 (250 ℃)	0.50	1.9×10^{17}	2.2×10^{12}	9	409
3 (300 ℃)	0.49	1.9×10^{17}	2.2×10^{12}	9	367
4 (350 ℃)	0.28	1.1×10^{17}	1.2×10^{12}	15	367
5 (400 ℃)	0.35	1.4×10^{17}	1.6×10^{12}	12	336
6 (450 ℃)	0.09	3.5×10^{16}	4.0×10^{11}	47	87

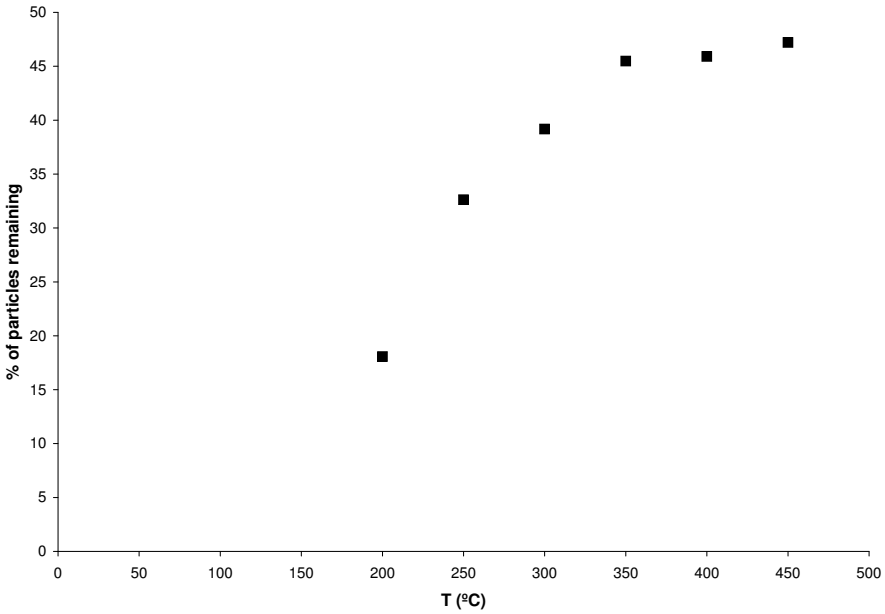

Figure 4.42: Percentage of the cubes that remained on the substrate versus the temperature of the heat treatment before the reaction. The higher the temperature was during the heat treatment, the more cubes stayed on the substrate. The graph levels to a more or less constant number of around 45 %.

4.3.3.2 TEM

In figure 4.43 TEM images are shown of the cubes in the supernatant of the reaction mixtures which were released from the substrates. The cubes seem all less damaged than the cubes in the reactions without substrates. However, it is difficult to quantify whether the cubes elevated to 200 ℃ are more broken than the cubes heated to for instance 450 ℃. In these pictures also mica flakes are visible as indicated in figure 4.43d.

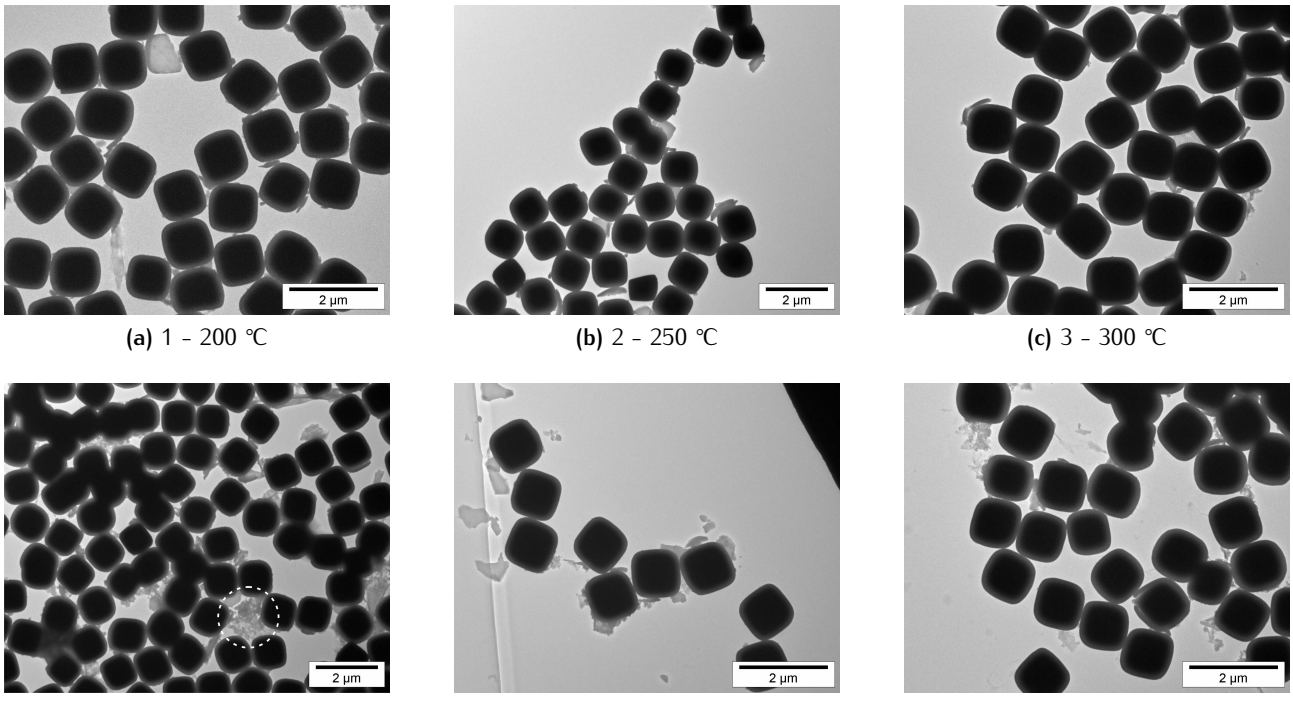

(a) 1 - 200 ℃ **(b)** 2 - 250 ℃ **(c)** 3 - 300 ℃

(d) 4 - 350 ℃ **(e)** 5 - 400 ℃ **(f)** 6 - 450 ℃

Figure 4.43: TEM pictures of cubes in the supernatant. Some of the silica shells are broken and also mica flakes are present in the supernatant as indicated in figure (d).

4.3.4 Activity of Reused Substrates

For these substrates also the cubes described in section 4.1.6.3 were used. Two substrates with a deposition of cubes were used: substrate 1 was heated to 400 °C and substrate 2 was heated to 450 °C. The substrates were placed in mixture of 5 mL 4.39×10^{-4} M methylene blue, 5 mL 35 wt% H_2O_2 and 10 mL Millipore water.

4.3.4.1 UV-Vis

The substrates were tested twice in a fresh reaction mixture, to examine how many cubes were released from the substrate during the first and the second reaction and to determine the activity during the second reaction. The results are shown in figure 4.44 for the first and the second test. During the first reaction 21 % of the cubes was released from substrate 1 and 16 % of substrate 2. During the second reaction these percentages were 51 and 59 % respectively of the remaining cubes. Overall, during the two reactions 61 % of the cubes disappeared from substrate 1 and 66 % from substrate 2. These numbers were determined by weighing the substrates before and after each reaction.

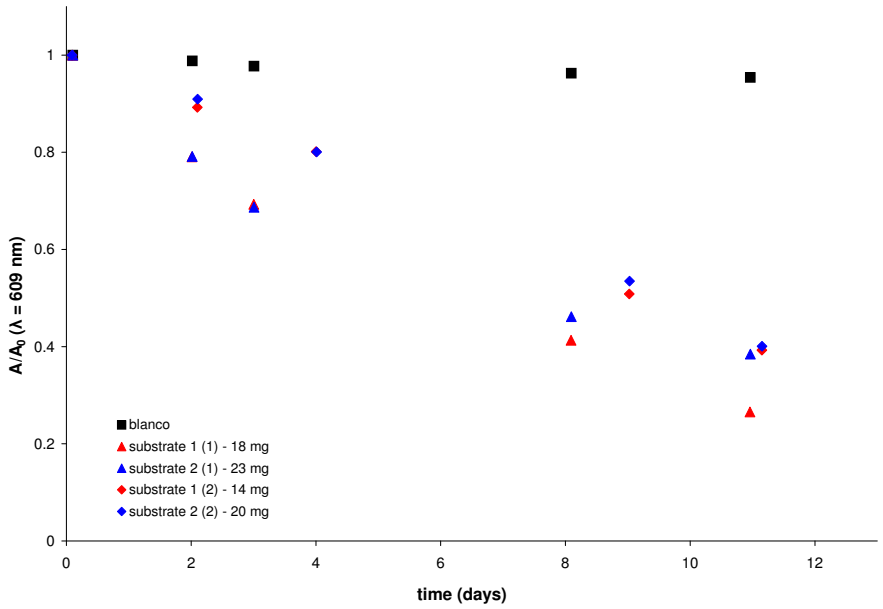

Figure 4.44: Decrease in absorbance by methylene blue by the first and second use of two substrates. The triangles indicate the first use and the diamonds the second use.

Approximately the amount of cubes disappeared in reaction 1 was used in dispersed form to determine if the dispersed cubes deliver most of the activity. These results are shown in figure 4.45. 350 µL 1.16 wt% of the same silica coated cubes was used is a total reaction volume of 20 mL. The reaction mixture contained 5 mL 4.3×10^{-4} M methylene blue and 5 mL 35 wt% H_2O_2.

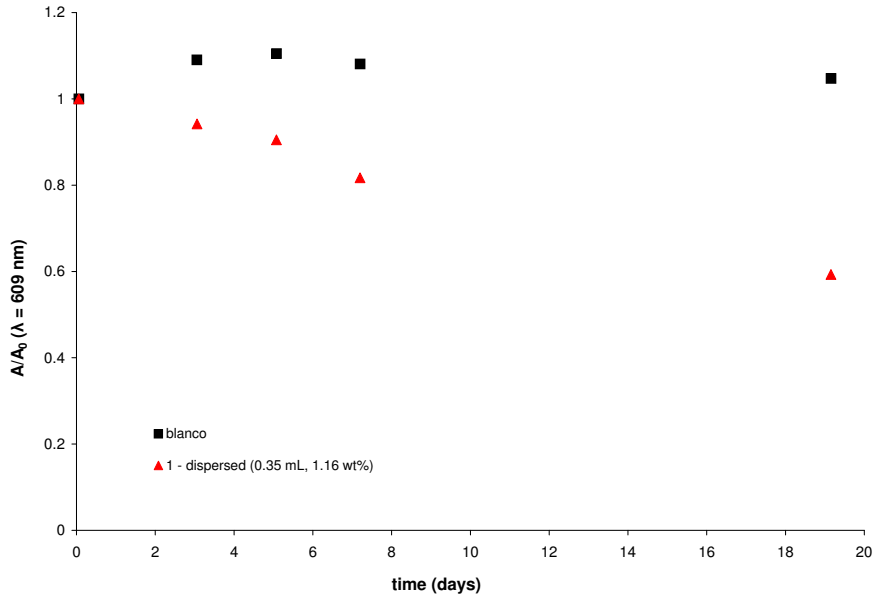

Figure 4.45: Decrease in absorbance by a small amount of dispersed cubes dispersed cubes. The degradation rate is lower than for the substrates used above. This indicates that not only the dispersed cubes in the reactions with substrates contribute to the reaction.

In table 4.21 the reaction speeds for the substrates and the dispersed cubes from the two previous graphs are calculated. The reaction rate for reaction 1 of the substrates was calculated between the start of the reaction and day ten of the reaction. For substrate 2 the speed was calculated between the start and day eleven, for the dispersed cubes the rate was calculated between day zero and day seven, assuming a linear decrease.

Table 4.21: Reaction speeds of the reused substrates and small amount of dispersed cubes. The rate of the second blanco in this table in probably negative due to evaporation of the solvent.

Sample	Speed $\left(\frac{\Delta A}{\Delta t}\right)$	Speed (molecules/day)	Speed (molecules/s)	Theoretical degradation time (days)	TON $\left(\frac{\text{molecules}}{s \cdot \text{cube}}\right)$
blanco	0.016	6.2×10^{15}	7.2×10^{10}	261	
substrate 1 (1)	0.250	9.6×10^{16}	1.1×10^{12}	17	314
substrate 2 (1)	0.205	7.8×10^{16}	9.1×10^{11}	21	199
substrate 1 (2)	0.195	7.5×10^{16}	8.6×10^{11}	22	308
substrate 2 (2)	0.191	7.3×10^{16}	8.5×10^{11}	22	220
blanco	-0.038	-1.5×10^{16}	-1.7×10^{11}	-98	
1 - dispersed	0.094	3.6×10^{16}	4.2×10^{11}	39	528

From these rates can it be concluded that the substrates catalyzed the degradation better in the first reaction than in the second and that the degradation is not mainly performed by the dispersed cubes. The reaction rate for the small amount of dispersed cubes is namely very low with respect to the substrates.

The conversion of molecules per second for the reused substrates is comparable with the reaction rate of the silica etched cubes used in dispersed form in section 4.2.4. However, less cubes were present in the reaction with the dispersed cubes than present on these substrates. These experiment show therefore also that the reaction is faster in the presence of dispersed cubes.

4.3.5 Activity of Substrates in a Set-up with an Overhead Stirrer

For the coating of these substrates again the cubes described in section 4.1.6.3 were applied. Substrate 1 was heated at 400 °C and substrate 2 at 450 °C. These substrates were placed on the bottom of two

100 mL vials and the reaction mixtures were stirred with an overhead stirrer, the side of the substrate with the deposited cubes was up. In this case all the cubes were in the reaction mixture during the whole reaction, but the reaction volumes were five times as large as in the other cases. 25 mL 4.39×10^{-4} M methylene blue solutions and 25 mL 35 wt% hydrogen peroxide was used for each reaction mixture.

In figure 4.46 the degradation of methylene blue by these substrates is shown over 40 days. The degradation is quite slow but still faster than the blank experiment. During this reaction 38 % of the cubes was released from substrate 1 and 19 % was released from substrate 2 during the reaction. These numbers were also determined by weighing the substrates before and after the reaction.

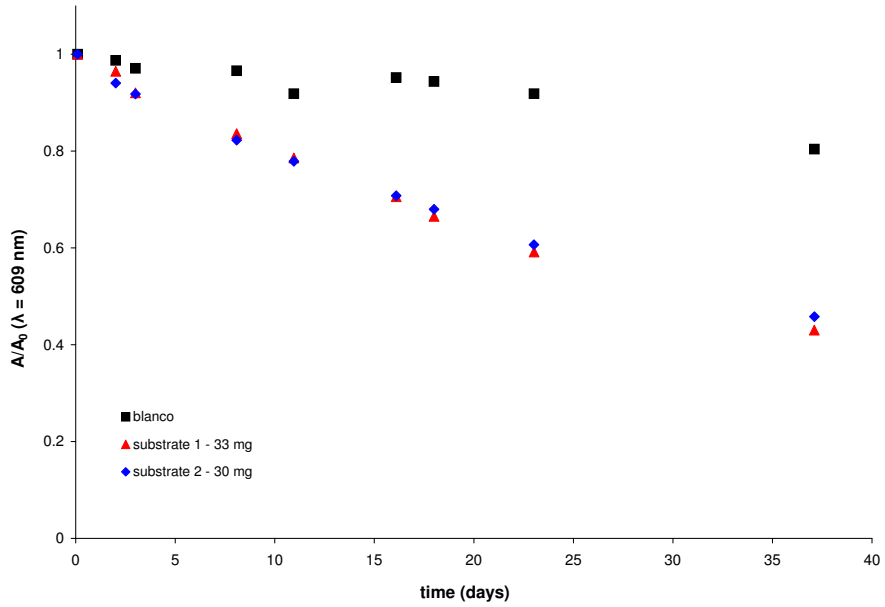

Figure 4.46: Decrease in absorbance by substrates used in the set-up using an overhead stirrer. For these substrates it takes much longer to decolor the reaction mixture, because of the large total amount of methylene blue molecules present in the reaction mixtures.

The calculated reaction rates are given in table 4.22 and were calculated between day zero of the reaction and day sixteen. The reaction rates are very low and equal for both substrates, due to the little amount of cubes present on the substrates compared to the large total amount of methylene blue in the reaction mixture. Nevertheless, the reaction rate for the substrates were higher than for the blank experiment. However, one should note that the blanco was covered with parafilm and the reaction with the substrates with a lid with a small hole in it. Probably more evaporation could take place from the blanco. This causes also the high theoretical degradation time for the blanco and the incidental increase in absorbance.

Table 4.22: Reaction speeds of the activity test using substrates in the set-up using an overhead stirrer.

Sample	Speed $\left(\frac{\Delta A}{\Delta t}\right)$	Speed (molecules/day)	Speed (molecules/s)	Theoretical degradation time (days)	TON $\left(\frac{\text{molecules}}{s \cdot \text{cube}}\right)$
blanco	0.01	2.2×10^{16}	2.6×10^{11}	1464	
1	0.07	1.3×10^{17}	1.5×10^{12}	251	233
2	0.07	1.3×10^{17}	1.5×10^{12}	244	267

4.4 Breaking of Silica Shells

In many cases where the particles were dispersed during the reaction the silica shells broke. To investigate whether the hydrogen peroxide alone caused the breaking of the silica shell, 1 mL 1.2 wt% silica coated hematite particles were magnetically stirred with 5 mL 35 wt% H_2O_2 and 14 mL Millipore H_2O in a 20 mL

vial. TEM grids were made after two hours and one, five, seven and fourteen days. The pictures are shown in figure 4.47. Broken silica shells are present, however clearly less than in the reaction with organic molecules present.

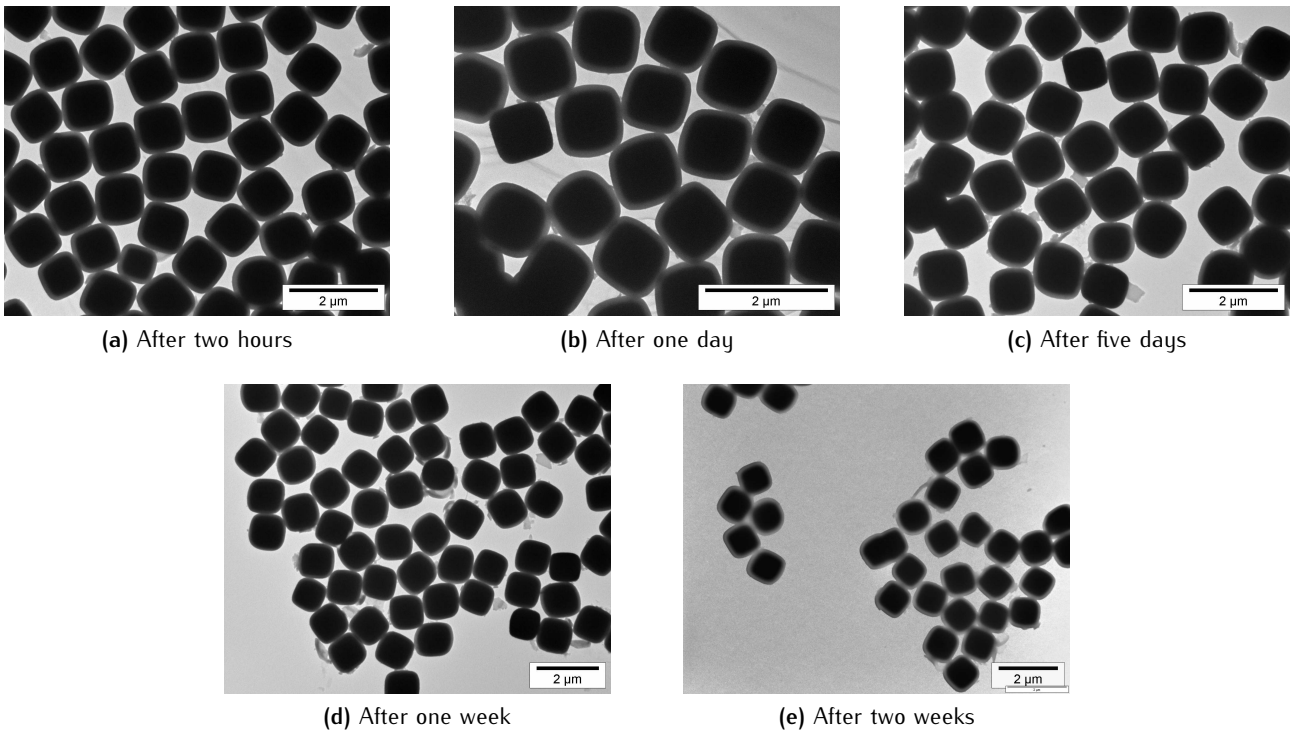

(a) After two hours **(b)** After one day **(c)** After five days

(d) After one week **(e)** After two weeks

Figure 4.47: Breaking of the silica shell in the presence of only water and hydrogen peroxide. The shells are less broken than in the case of dispersed cubes reacting with methylene blue and hydrogen peroxide.

Silica coated particles were also stored in water for longer periods of time, and were viewed with TEM. The silica shells were not affected by the storage in water. The breaking of the silica shells is therefore caused by the degradation reaction in the presence of organic molecules. A explanation for the breaking is that the osmotic pressure inside the silica box rises due to the products formed out of hydrogen peroxide in the Fenton reaction. With an increasing osmotic pressure the more solvent is going into the silica cube, which could cause the breaking. The reaction between the hematite surface and hydrogen peroxide, generating hydroxyl radicals, is probably not the only cause of the broken silica shells since more silica shells break in the presence or methylene blue. In the degradation reaction between the organic molecules and the radicals probably more gas is produced in the reaction mixture (not necessarily inside the silica box). This gas formation could also be a cause of the broken silica shells.

4.5 Nitrogen Physisorption

Nitrogen physisorptopn measurements were performed on the bare hematite and silica coated particles etched by hydrochloric acid. These particles are described in section 4.1.6.2 (bare particles) and 4.1.6.6 (silica coated particles).

All the measured isotherms and determined pore size distributions are also given in appendix B. The results of the hematite etched (bare and silica coated) particles will be discussed in this section. The data can be found in appendices B.1, B.2, B.3 B.4, B.5, B.6 and B.7. In this appendix the results for the silica etched particles can also be found.

4.5.1 Isotherms

4.5.1.1 Bare Hematite Etched Particles

The bare hematite etched particles, etched with hydrochloric acid, from section 4.1.6.2, were measured with nitrogen physisorption to determine the effect of etching. In figure 4.48 the measured isotherms are shown and TEM images of the particles are shown as inset.

The first conclusion drawn from these isotherms is the kind of isotherm obtained following the IUPAC classifications in section 2.2.3.1. The isotherms have the shape of type II, showing no hysteresis and some have the shape of type IV, showing little hysteresis. However, the isotherms do not start at zero at a very low pressure and therefore it can be concluded that micropores are present.

In contrast to the isotherms in figures 4.48b and 4.48c the isotherm in figure 4.48a does not show hysteresis. The non-etched bare hematite cubes therefore contain no mesopores. These mesopores arise thereby upon etching by hydrochloric acid.

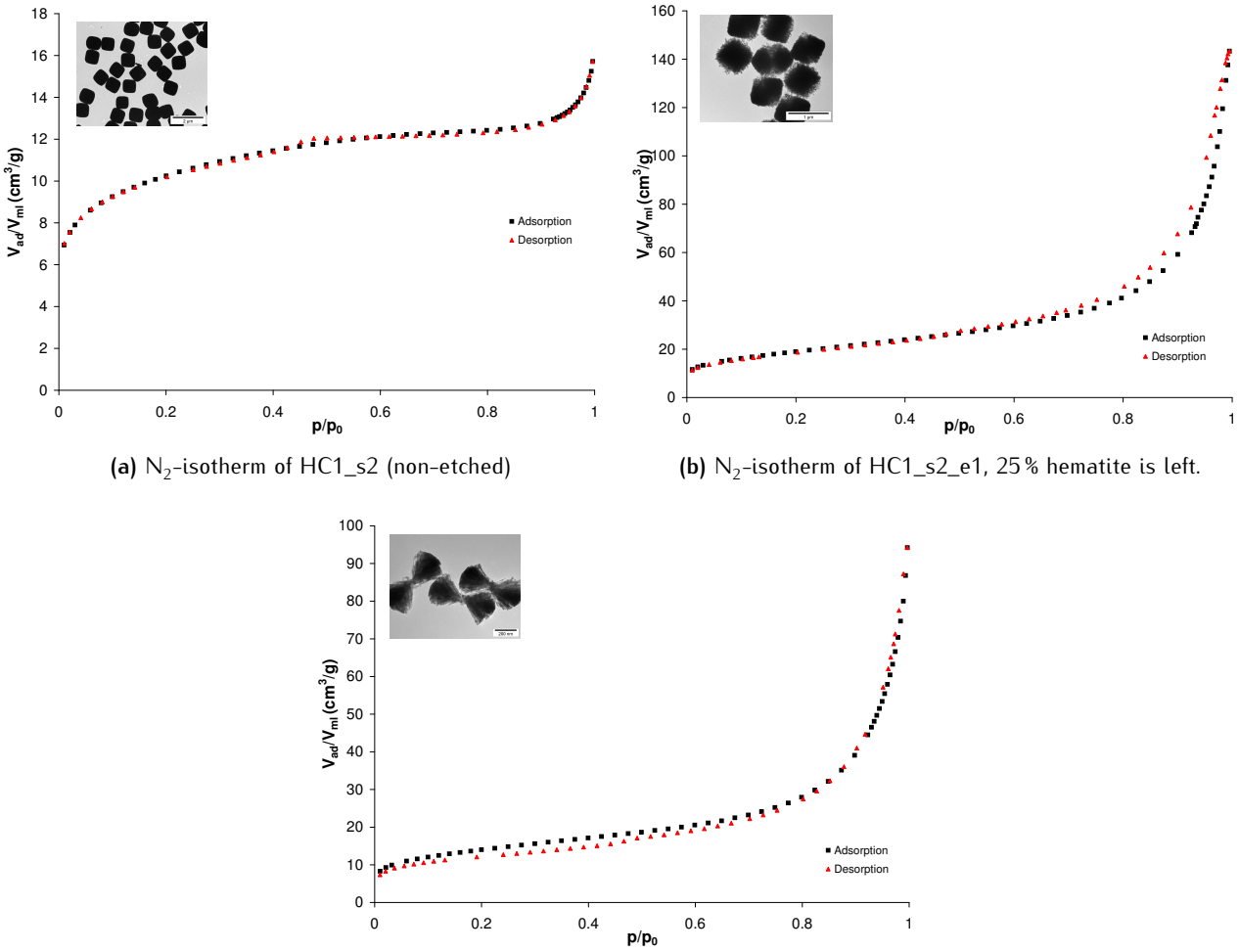

(a) N_2-isotherm of HC1_s2 (non-etched)

(b) N_2-isotherm of HC1_s2_e1, 25 % hematite is left.

(c) N_2-isotherm of HC1_s2_e2, 1.5 % hematite is left.

Figure 4.48: Nitrogen Physisorption isotherms of the hematite etched particles.

4.5.1.2 Silica Coated and Hematite Etched Particles

Also silica coated hematite cubes etched by hydrochloric acid were measured with nitrogen physisorption. The used particles are described in section 4.1.6.6, apart from the hollow silica shell which were also measured. These silica shells had the same shell thickness as the filled particles.

For the silica coated cubes the same behavior in the isotherms is observed. However, the isotherms start at a higher value of adsorbed amount therefore, more micropores are present. The isotherms are shown in figure 4.49 and the insets show TEM images of the measured particles.

The behavior of the desorption isotherm in figure 4.49a is strange, because of the fast desorption. This could be caused by blocking of the pores, probably by remaining PVP. Because these particles were also not etched with HCl PVP still could be present from the silica coating procedure. The isotherm from figure 4.49b shows a little hysteresis which indicate the presence of mesopores. This is in agreement with the etched bare hematite particles from figure 4.48b, which contain approximately the same amount of hematite and also show hysteresis. The isotherms for the particles with a little or no hematite remaining in figures 4.49c and 4.49d show no hysteresis.

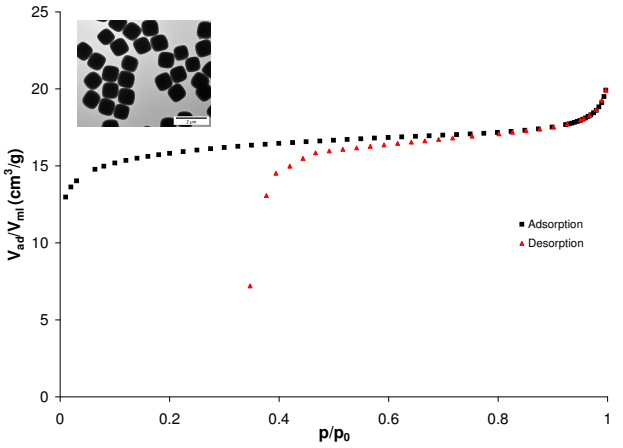

(a) Isotherm of non-hematite-etched cubes (Si13_HC1_s2). The desorption isotherm drops very fast at a value of $p/p_0 = 0.4$ which means that the pores empty very fast at that point. However, this behavior is a bit uncommon.

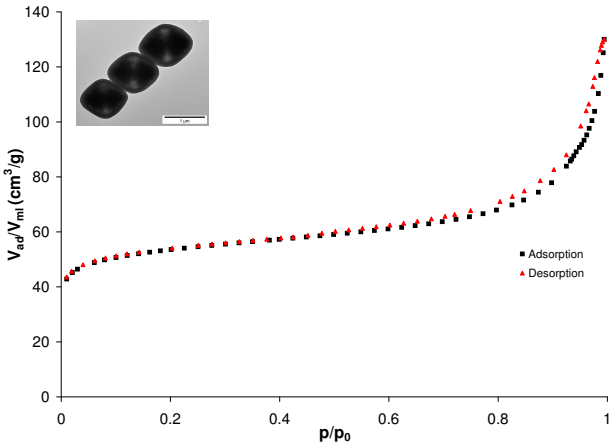

(b) Isotherm of etched I cubes, 19 % hematite is left.

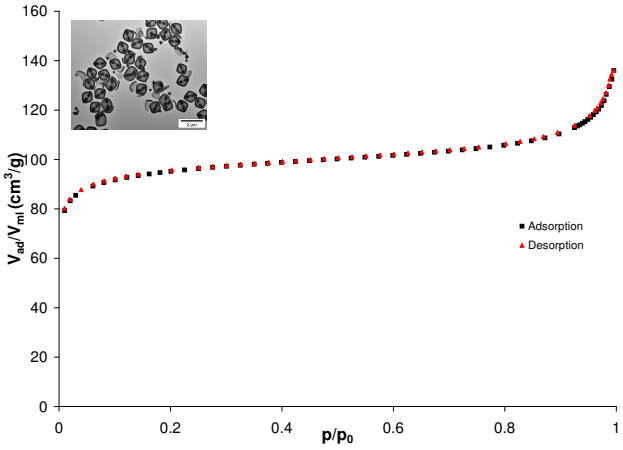

(c) Isotherm of etched II cubes.

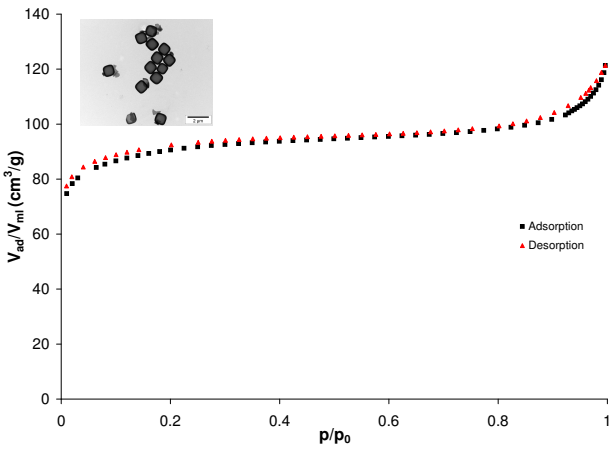

(d) Isotherm of hollow silica shells, 4 % hematite is left.

Figure 4.49: Nitrogen physisorption isotherms of the silica coated and hematite etched particles.

4.5.2 Surface Areas and Pore Volumes

From the isotherms in figures 4.48 and 4.49 the BET-surface and the micropore volume and the total pore volume are derived. The specific surface area is derived by fitting the BET-isotherm for the first part of the adsorption isotherm. The micropore volume is determined by the t-plot method and the total pore volume can be determined from the pore size distribution.

In table 4.23 the determined numbers for the surface area, the t-plot micropore volume and the total pore volume are given per gram and per particle. The number of particles per gram were determined from infrared spectroscopy (silica coated particles) or by weighing the before and after etching with HCl (bare particles).In figures 4.50, 4.51 and 4.52 these values per particle are plotted.

Table 4.23: BET-surface area (per gram and per particle), the t-plot micropore volume (per gram and per particle) and the total pore volume (per gram and per particle) for the hematite etched cubes.

Sample	Remaining hematite	BET (m^2/g)	BET (m^2/cube)	t-plot micropre vol. (cm^3/g)	t-plot micropre vol. (cm^3/cube)	Total pore vol. (cm^3/g)	Total pore vol. (cm^3/cube)
HC1_s2_ne	1	35	1.4×10^{-10}	0.007	2.7×10^{-14}	0.024	1.0×10^{-13}
HC1_s2_e1	0.25	68	7.0×10^{-11}	0.002	2.5×10^{-15}	0.222	2.3×10^{-13}
HC1_s2_e2	0.01	50	3.1×10^{-12}	0.003	1.9×10^{-16}	0.146	9.0×10^{-15}
Si13_HC1_s2_ne	1	51	2.5×10^{-10}	0.019	9.3×10^{-14}	0.031	1.5×10^{-13}
Si13_HC1_s2_I	0.19	175	2.9×10^{-10}	0.056	9.3×10^{-14}	0.201	3.3×10^{-13}
Si13_HC1_s2_II	0.05	308	3.3×10^{-10}	0.116	1.3×10^{-13}	0.210	2.3×10^{-13}
Si13_HC1_s2_hollow	0	294	2.9×10^{-10}	0.105	1.0×10^{-13}	0.188	1.8×10^{-13}

From the table above and figure 4.50 it can be seen that the surface area per particle for the silica coated particles is higher than for the bare particles. This is straightforward, because the Stöber silica is very porous. The surface area per particle for the bare particles decreases upon increased etching where the surface area for the silica coated particles stays relatively constant. Note that the silica shells of the hollow and almost hollow particles are partially broken which could cause an increased surface area. Although the surface area for the bare etched particles decreases after etching the area for the particles with 25 % remaining hematite is only twice as small as for the non-etched particle. Probably a maximum in the surface area per particle can be found between 100 % and 25 % remaining hematite.

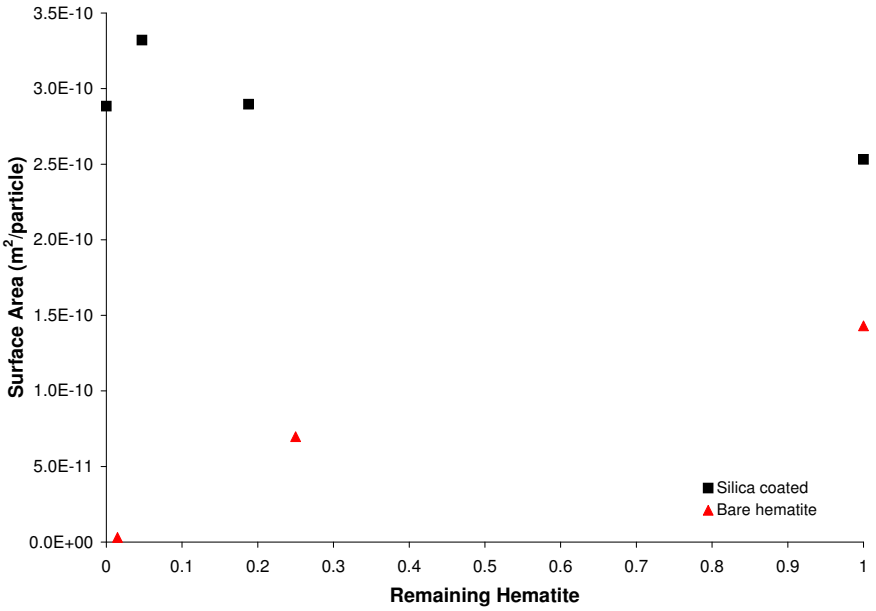

Figure 4.50: BET-surface area per particle for the bare and silica coated particles. The surface area for the silica coated particles is higher than for the bare particles, because of the high surface area and porous silica shell. At the right side of the graph (remaining hematite = 1), the hematite core is not etched.

From figure 4.51 it can be seen that the micropore volume for the hollow and almost completely etched silica coated particles is increased compared to the filled particles. This could indicate that the porosity of the silica increases upon etching with hydrochloric acid.

Most pores in the three-step silica layer are micropores. According to Ayral *et al.* [42] Stöber silica should contain pores between 1 and 20 nm. From these physisorption measurement larger pores upto 20 nm were not found. To investigate whether one-step silica coating have larger pores physisoprtion measurement have to be performed on such particles.

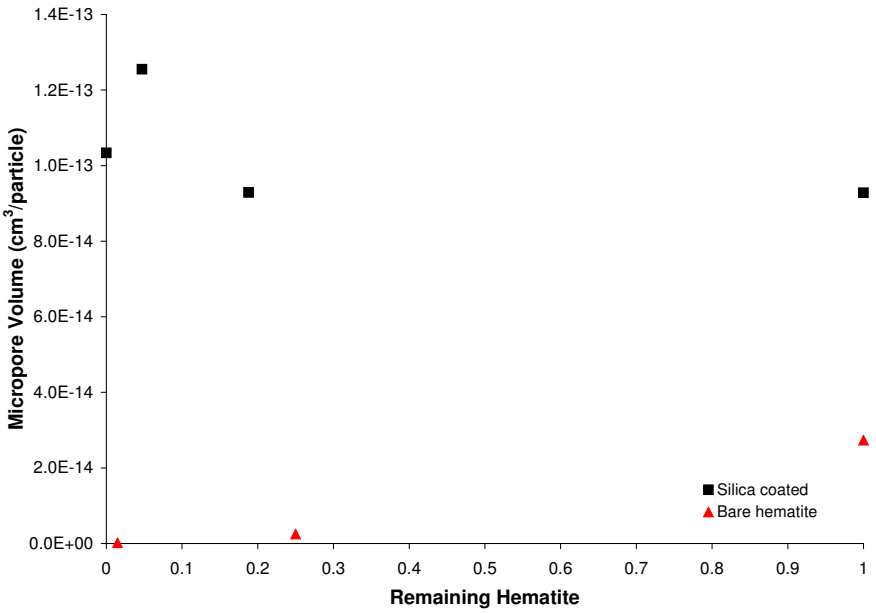

Figure 4.51: t-plot micropore volume per particle for the bare and silica coated particles. The pore volume for the silica coated particles is higher, due to the porous silica shell. At the right side of the graph (remaining hematite = 1), the hematite core is not etched.

The total pore volume of the particles with around 20 % of remaining hematite of both the bare and silica coated particles is increased in comparison with the non-etched particles. This is due to the presence of mesopores, which can also be seen from the isotherms showing hysteresis.

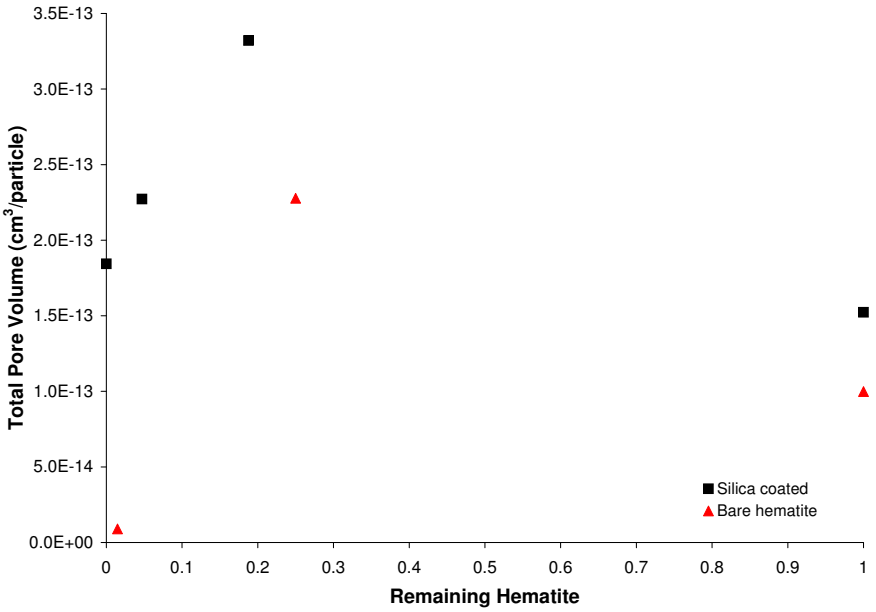

Figure 4.52: Total pore volume per particle for the bare and silica coated hematite particles. At the right side of the graph (remaining hematite = 1), the hematite core is not etched.

Non complete etching of the hematite core increases the porosity of the hematite and probably a maximum in surface area can be found. However, more physisorption measurements would have to be performed to determine this maximum.

Chapter 5

Discussion

It is clear that the hematite particles, either bare, coated with silica or immobilized on a substrates are able to catalyze the degradation reaction of organic molecules in a Fenton-like way. However, to make a fair comparison between all the different reactions the absorbance should be determined at the same point for each reaction. Furthermore, the number of cubes and the concentration of organic molecule should be equal in every experiment. Moreover, the reaction rates were not all calculated according to the same period of time. In the case of the experiments with the substrates the number of cubes per volume increased when liquid was removed for the UV-Vis measurements. In the case of the dispersed cubes it did not, because the cubes were removed with the liquid. These make it difficult to compare the reactions rates found from the experiments.

The evaporation of most samples was also not controlled and therefore there is an error in the measured aborbance. The amount of remaining dye was determined by UV-Vis spectroscopy at one particular wavelength. Therefore, the degradation of organic molecules was not completely finished at zero absorbance and it is unknown when the degradation process is finished.

The colloidal particles are able to accelerate the catalytic degradation reaction of organic molecules. However, the rate is much lower than reported in literature by Lee *et al.* for the Fenton-like reaction in the presence of hematite [13]. The difference could arise from the organic molecules used, the used form and amount of hematite or the used concentrations of organic molecule and hydrogen peroxide. Lee *et al.* used phenol as model organic molecule which probably has a different degradation pathway.

In the nitrogen physisorption isotherms of the silica coated particles almost no hystheresis is present which means that there are no mesopores present in the silica layer. From the pore size distributions it also can be concluded that no mesopores are present in the Stöber silica. According to literature, one-step-base-catalyzed silica should have pores between 1 and 20 nm [42]. Mesopores are larger than 2 nm and silica should have many mesopores, which were not observed in these physisorption measurements. The pores could be blocked by PVP-molecules used during the Stöber synthesis. However, the PVP should partially disappear during the etching procedure with HCl. The PVP is probably only partially dissolved because the measurement of the non-etched particles has a defect at the desorption curve. The nitrogen molecules diffuse slowly out of the pores when they are blocked by the PVP. The lack of pores can be caused by the multiple step synthesis. The pores formed can be filled with silica in the second and third synthesis. To determine the pore size in single step coated particles physisorption measurements should be performed on such particles.

The silica shells are less broken when only hydrogen peroxide is added to the cubes than in the presence of organic dye and hydrogen peroxide. When the hydrogen peroxide enters the particles it can be converted into hydroxyl radicals at the hematite surface. The osmotic pressure inside the silica shell is then probably raised thereby, possibly causing the observed breaking. The hematite surface is better accessible when the silica breaks, which also makes the comparison difficult between the dispersed and immobilized particles. The silica coated particles are namely not entirely coated anymore after a few days of reaction.

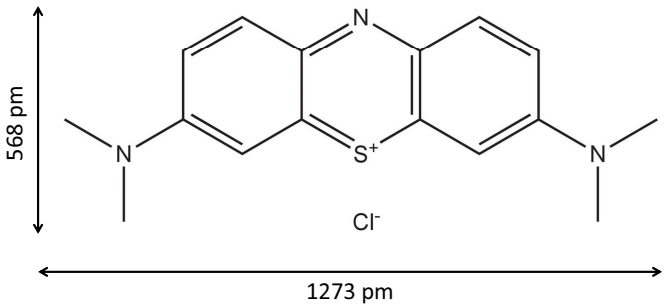

Figure 5.1: Actual sizes of a methylene blue molecule.

However, the question remains whether the organic molecules enter the non damaged silica shells. In the article by Ayral *et al.* [42] is stated that the pores are between 1 and 20 nm, but the nitrogen physisorption measurements performed on the particles described in this thesis do not confirm this. From these measurements the presence of mesopores could not be proven. The largest dimension of methylene blue is slightly larger than 1 nm and therefore it can be stated that the molecules do not fit inside the pores of the triple silica coated particles. The actual sizes of the molecule are given in figure 5.1. The pore size of the used particles in the catalytic activity measurements is not determined with physisorption measurements.

Chapter 6

Conclusion

Silica coated hematite cubes were successfully synthesized and were used in catalytic activity tests for the degradation of organic dyes in combination with hydrogen peroxide. We have demonstrated that the hematite cubes accelerate the degradation of methylene blue, even when they are coated with Stöber silica. The reaction rate for all the reactions is around 10^{12} molecules per second converted in the reaction mixture, which is much lower than reported in literature for this reaction in the presence of hematite [13]. The activity of the colloidal cube-like particles was tested for dispersed particles and for immobilized particles on mica substrates. The degradation rate was higher in the case of dispersed particles. In the case of the immobilized particles probably not all the particles took place in the reaction, because of multi-layer stacking. To immobilize silica coated hematite particles a drop of particles dispersed in water were deposited on mica substrates. Upon drying and after a heat treatment at 450 °C these particles formed densely packed multi-layer structures with local order.

UV-Vis spectroscopy proved to be a useful technique to follow and quantify the amount of methylene blue and rhodamine B during the reaction. The pH of the reaction mixture of hydrogen peroxide and methylene blue without cubes was determined to be in the proper range for the Fenton reaction. Surface protected water etching of the silica shells of the particles was performed and the amount of left silica was determined with infrared spectroscopy. Although the etching was successful, the more porous shells were not beneficial to the reaction rate.

From the nitrogen physisorption measurements it can be concluded that the porosity of the hematite increases upon etching with hydrochloric acid. For the bare hematite particles the surface area per particle was decreased after etching 75 % of the hematite core. However, a maximum in the surface area probably can be found between 25 % and 100 % of remaining hematite. The increased surface area per particle for the silica coated and hematite etched particles is therefore probably caused by an increase in surface area of the Stöber silica layer during etching with hydrochloric acid. The shape of the silica peak in the infrared spectrum changes upon etching with hydrochloric acid and infrared spectroscopy is a useful technique to determine the amount of remaining hematite and the extent of silica etching.

During the catalytic degradation reaction the cubes which have had a heat treatment in the oven at 450 °C and were immobilized on mica substrates did not break as much as the non-treated dispersed cubes. The breaking is mostly caused by the reaction with an organic molecule present. The cubes in the presence of only hydrogen peroxide did not break as much as the cubes in the reaction with organic molecules did and the silica coated cubes stored in water were stable. The heat treatment of the substrates ensured also that the cubes remained better on the substrate.

Chapter 7

Outlook

The reaction speed in these experiments depends on the amount of cubes and therefore there can be a lack of methylene blue for the cubes. A possible experiment is to use much more methylene blue and dilute the reaction mixture before taking a UV-Vis spectrum. Another option is to search for an organic molecule with a lower molar extinction coefficient, because the concentration of organic molecule can be higher to get a proper absorbance with UV-Vis spectroscopy.

Smaller molecules can be used as reactant, to see whether the size of the molecules limits the reaction speed. The smaller molecules may enter the pores of the silica shell an might be degraded faster. The four next molecules in figure 7.1 are some options, because they absorb light in the visible range, which is necessary for UV-Vis spectroscopy and are probably all water soluble due to the chargeable groups.

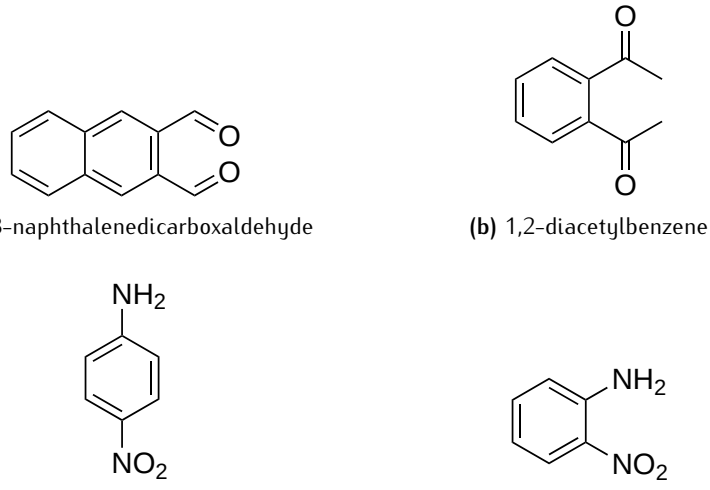

(a) 2,3-naphthalenedicarboxaldehyde **(b)** 1,2-diacetylbenzene

(c) p-nitroaniline **(d)** 2-nitroaniline

Figure 7.1: Options for organic molecules to use in the catalytic activity measurements.

The porosity of the silica shell is increased by surface protected water etching. However, the silica etched particles used in the catalytic activity test did not have a increased reaction rate in contrast to the non-etched particles, also the silica shells broke during the reaction. Therefore, catalytic tests could be performed with more porous silica.

With nitrogen physisorption particles with more than 25 % hematite can be measured, because the surface area probably has a maximum between 25 and 100 % of remaining hematite. Single step silica coated particles can be measured to see the effect of the multi-step synthesis on the surface area and the pore size distribution.

The hydrogen peroxide used was stabilized with an organic phosphorous compound of which is not sure how it influenced the reaction. Although it was stabilized, the hydrogen peroxide did probably degrade over time. Unstabilized hydrogen peroxide could be used to be certain of the absence of any stabilizing agent. The concentration of both stabilized and not stabilized hydrogen peroxide can be determined by titration to know the exact amount of hydrogen peroxide in the reaction mixture.

Another substrate material for the cubes can be used. Mica was used, because it is flat and is heat resistant. However, a different material as substrate could have another effect on the assembly of the cubes.

The dissolution of iron oxide during the reaction was only investigated with infrared spectroscopy. However the liquid of the reaction mixture could also be investigated with Atomic Absorption Spectroscopy (AAS) to determine the concentration of iron ions in the liquid.

A way to prevent the breaking of the cubes should be found to the determine the exact effect of the silica coating on the reaction. Since the heat treatment before the reaction resulted in less broken cubes, silica coated particles could be heated on forehand and can be attempted to redisperse them.

The catalytic degradation reaction of organic molecules in the presence of hematite cubes and hydrogen peroxide is relatively slow. One of the reasons for this can be the fact that the iron ions in the hematite have a charge of 3+. Therefore the start up of the reaction is quite slow since the radicals are produced in the presence of iron(II). To increase the reaction rate one could try to modify the hematite surface. Treatment of the cubes at elevated temperatures in a reducing atmosphere (N_2 and a small amount of H_2) could produce iron(II) ions at the surface. The cubes could also be treated with a solution of chrome(II) to convert the iron(III) ions into iron(II) ions. A too large amount of chrome(II) can however dissolve the particles. Another way to increase the reaction speed is the use of another peroxide; peroxodisulphate ($S_2O_8^{2-}$). The produced radicals are much stronger than the hydroxyl radicals produced in the classical Fenton reaction. However, peroxodisulphate might be able to degrade the organic molecules directly.

Since the formed hydroxyl radicals formed during the Fenton reaction have a very high reduction potential they are able to degrade almost all organic molecules. Therefore, the cubes in combination with hydrogen peroxide could also be effective in killing bacteria.

Hematite is also a promising material in the field of photocatalysis. Where currently titania is used, hematite in combination with solar cells could be able to produce hydrogen gas from water under the influence of light [57].

Only the influence of light on the degradation reaction of methylene blue in the absence of cubes was investigated. However, the formation of radicals out of hydrogen peroxide on the surface of hematite is accelerated by UV-light [56]. Therefore, the degradation reaction of methylene blue by the hematite cubes in the absence of light could be investigated.

Acknowledgments

First of all I like to thank Sonja Castillo and Albert Philipse for their supervision during my masterthesis and to let me combine the two worlds of colloids and catalysis. Sonja, I had a very nice time with you. Your enthusiasm is great, not only for nice results, but also at coffee breaks and borrels. I also enjoyed the moments at the TEM and SEM when we discovered nice structures and all kinds of funny shaped particles in the form of turtles, monsters and dancers (they are hidden, but you can find them).

The Master room at FCC should of course to be mentioned. Daan, Elleke, Fabian, Jenneke, Joen, Pepijn, Rick, Samia, Simone, Suzanne, Vera and Yuri thank you for having nice conversations and the nice atmosphere. I really enjoyed all the moments listening to Dumb Ways to Die (Sonja, thank you for the hint) and our Master room play list for the Friday afternoons. Elleke and Suzanne, I like to thank you in particular. It was nice to have you around during our hours at FCC and afterwards. Rick and Fabian, thank you for searching the internet for all what LaTeX can do!

Bas, although I don't like most of your music, I hope you have enjoyed playing Dancing Queen together with me and Jan Groenewold at the New Year Dinner, however I did.

Further I like to thank Ad Mens and Arjan den Otter from the group of Inorganic Chemistry and Catalysis. Ad Mens for doing all the nitrogen physisorption measurements and Arjan den Otter for his help with the data analysis. Also I would like to thank John Kelly for his suggestions for the modification of the hematite surface to accelerate the reaction rate.

Last but not least I want to thank everyone of FCC for a very nice time!!!

Bibliography

[1] S. C. Glotzer and M. J. Solomon. Anisotropy of Building Blocks and their Assembly into Complex Structures. *Nature materials*, 6(8):557–562, 2007.

[2] D. H. Everett. *Basic Principles of Colloid Science*. The Royal Society of Chemistry, 1988.

[3] H. J. H. Fenton. Oxidation of Tartaric Acid in the presence of Iron. *Journal of the Chemical Society, Transactions*, 65:899–910, 1894.

[4] T. Sugimoto and K. Sakata. Preparation of Monodisperse Pseudocubic α-Fe_2O_3 Particles from Condensed Ferric Hydroxide Gel. *Journal of Colloid and Interface Science*, 152(2):587–590, 1992.

[5] T. Sugimoto, M. M. Khan, and A. Muramatsu. Preparation of Monodisperse Peanut-type α-Fe_2O_3 Particles from Condensed Ferric Hydroxide Gel. *Colloids and Surfaces A: Physicochemical and Engineering Aspects*, 70(2):167–169, 1993.

[6] W. Stöber, A. Fink, and E. Bohn. Controlled Growth of Monodisperse Silica Spheres in the Micron Size Range. *Journal of Colloid and Interface Science*, 26(1):62–69, 1968.

[7] C. Graf, D. L. J. Vossen, A. Imhof, and A. van Blaaderen. A General Method To Coat Colloidal Particles with Silica. *Langmuir*, 19(17):6693–6700, 2003.

[8] F. Haber and J. Weiss. The Catalytic Decomposition of Hydrogen Peroxide by Iron Salts. *Proceedings of the Royal Society A: Mathematical, Physical and Engineering Sciences*, 147(861):332–351, 1934.

[9] W. G. Barb, J. H. Baxendale, P. George, and K. R. Hargrave. Reactions of Ferrous and Ferric Ions with Hydrogen Peroxide Part I.–The Ferrous Ion Reaction. *Transactions of the Faraday Society*, 47:462–500, 1951.

[10] W. G. Barb, J. H. Baxendale, P. George, and K. R. Hargrave. Reactions of Ferrous and Ferric Ions with Hydrogen Peroxide Part II.–The Ferric Ion Reaction. *Transactions of the Faraday Society*, 47:591–616, 1951.

[11] E. Neyens and J. Baeyens. A Review of Classic Fenton's Peroxidation as an Advanced Oxidation Technique. *Journal of Hazardous Materials*, 98(1):33–50, 2003.

[12] P. Bautista, A. F. Mohedano, J. A. Casas, J. A. Zazo, and J. J. Rodriguez. An Overview of the Application of Fenton Oxidation to Industrial Wastewaters Treatment. *Journal of Chemical Technology and Biotechnology*, 83(10):1323–1338, 2008.

[13] S. Lee, J. Oh, and Y. Park. Degradation of Phenol with Fenton-like Treatment by Using Heterogeneous Catalyst (Modified Iron Oxide) and Hydrogen Peroxide. *Bulletin-Korean Chemical Society*, 27(4):489–494, 2006.

[14] D. C. Harris. *Quantitative Chemical Analysis*. WH Freeman, Seventh edition, 2007.

[15] R. M. Cornell and U. Schwertmann. *The Iron Oxides: Structure, Properties, Reactions, Occurrences, and Uses*. VCH, 1996.

[16] S. M. Arnold, W. J. Hickey, and R. F. Harris. Degradation of Atrazine by Fenton's Reagent: Condition Optimization and Product Quantification. *Environmental Science & Technology*, 29(8):2083–2089, 1995.

[17] P. Atkins and J. de Paula. *Physical Chemistry*. Oxford University Press, Ninth edition, 2010.

[18] O. L. J. Gijzeman. *Adsorption, Adsorption Isotherms and Surface Texture*. Utrecht University, 2004.

[19] K. S. W. Sing, D. H. Everett, R. A. W. Haul, L. Moscou, R. A. Pierotti, J. Rouquérol, and T. Siemieniewska. Reporting Physisorption Data for Gas/Solid Systems with Special Reference to the Determination of Surface Area and Porosity. *Pure & Applied Chemistry*, 57(4):603–619, 1985.

[20] K. S. W. Sing. Reporting Physisorption Data for Gas/Sollid Systems with Special Reference on the Determination of Surface Area and Porosity. *Pure & Applied Chemistry*, 54(11):2201–2218, 1982.

[21] I. Langmuir. The Constitution and Fundamental Properties of Solids and Liquids Part I. Solids. *Journal of the American Chemical Society*, 38(11):2221–2295, 1916.

[22] I. Langmuir. The Adsorption of Gases on Plane Surfaces of Glass, Mica and Platinum. *Journal of the American Chemical Society*, 40(9):1361–1403, 1918.

[23] S. Brunauer, P. H. Emmett, and E. Teller. Adsorption of Gases in Multimolecular Layers. *Journal of the American Chemical Society*, 60(2):309–319, 1938.

[24] J. H. de Boer, B. C. Lippens, B. G. Linsen, J. C. P. Broekhoff, A. van den Heuvel, and Th. J. Osinga. The *t*-curve of Multimolecular N_2-adsorption. *Journal of Colloid and Interface Science*, 21(4):405–414, 1966.

[25] D. Harkins and G. Jura. Surfaces of Solids. XIII. A Vapor Adsorption Method for the Determination of the Area of a Solid Without the Assumption of a Molecular Area, and the Areas Occupied by Nitrogen and Other Molecules on the Surface of a Solid. *Journal of the American Chemical Society*, 66(8):1366–1373, 1944.

[26] D. Dollimore and G. R. Heal. An improved method for the calculation of pore size distribution from adsorption data. *Journal of Applied Chemistry*, 14(3):109–114, 1964.

[27] K. Kaneko. Determination of Pore Size and Pore Size Distribution 1. Adsorbents and Catalysts. *Journal of Membrane Science*, 96(94):59–89, 1994.

[28] L. Rossi, S. Sacanna, W. T. M. Irvine, P. M. Chaikin, D. J. Pine, and A. P. Philipse. Cubic Crystals from Cubic Colloids. *Soft Matter*, 7(9):4139–4142, 2011.

[29] Y. Jiao, F. H. Stillinger, and S. Torquato. Optimal Packings of Superdisks and the Role of Symmetry. *Physical Review Letters*, 100(24):245504, 2008.

[30] Y. Jiao, F. H. Stillinger, and S. Torquato. Optimal Packings of Superballs. *Physical Review E*, 79(4):041309–1–041309–12, 2009.

[31] R. D. Batten, F. H. Stillinger, and S. Torquato. Phase Behavior of Colloidal Superballs: Shape Interpolation from Spheres to Cubes. *Physical Review E*, 81(6):061105, 2010.

[32] U. Schwertmann and R. M. Cornell. *Iron Oxides in the Laboratory Preparation and Characterization*. Wiley-VCH, 2000.

[33] L. Pauling and S. B. Hendricks. The Crystal Structures of Hematite and Corundum. *Journal of the American Chemical Society*, 47(3):781–790, 1925.

[34] Hematite mineral. http://en.wikipedia.org/wiki/Hematite.

[35] T. Sugimoto, K. Sakata, and A. Muramatsu. Formation Mechanism of Monodisperse Pseudocubic α-Fe_2O_3 Particles from Condensed Ferric Hydroxide Gel. *Journal of Colloid and Interface Science*, 159(2):372–382, 1993.

[36] G.-S. Park, D. Shindo, Y. Waseda, and T. Sugimoto. Internal Structure Analysis of Monodispersed Pseudocubic Hematite Particles by Electron Microscopy. *Journal of Colloid and Interface Science*, 177(1):198–207, 1996.

[37] S. I. R. Castillo. *Cubic Hematite Colloids with Reproducible Size and Shape: Adjusted Gel-sol Synthesis Method*. Internal report, Van 't Hoff Laboratory for Physical and Colloid Chemistry, Utrecht University, 2012.

[38] T. Sugimoto, A. Muramatsu, K. Sakata, and D. Shindo. Characterization of Hematite Particles of Different Shapes. *Journal of Colloid and Interface Science*, 158(2):420–428, 1993.

[39] T. Sugimoto. Formation of Monodispersed Nano- and Micro-Particles Controlled in Size, Shape, and Internal Structure. *Chemical Engineering & Technology*, 26(3):313–321, 2003.

[40] L. Rossi. *Colloidal Superballs*. PhD thesis, Utrecht University, 2012.

[41] D. Shriver and P. Atkins. *Inorganic Chemistry*. Oxford University Press, Fourth edition, 2006.

[42] A. Ayral, A. Julbe, S. Roualdes, and V. Rouessac. Silica Membranes - Basic Principles. *Periodica Polytechnica Ser. Chem. Eng.*, 50(1):67–79, 2006.

[43] A. van Blaaderen and A. Vrij. Synthesis and Characterization of Monodisperse Colloidal Organo-silica Spheres. *Journal of Colloid and Interface Science*, 156:1–18, 1993.

[44] R. K. Iler. *The Chemistry of Silica Solubility, Polymerzation, Colloid and Surface Properties, and Biochemistry*. John Wiley & Sons, Inc., 1979.

[45] L. Zhang, M. D'Acunzi, M. Kappl, A. Imhof, A. van Blaaderen, H.-J. Butt, R. Graf, and D. Vollmer. Tuning the Mechanical Properties of Silica Microcapsules. *Physical Chemistry Chemical Physics*, 12(47):15392–15398, 2010.

[46] A. Matsuda, Y. Matsuno, M. Tatsumisago, and T. Minami. Changes in Porosity and Amounts of Adsorbed Water in Sol-gel Derived Porous Silica Films with Heat Treatment. *Journal of Sol–Gel Science and Technology*, 20(2):129–134, 2001.

[47] Q. Zhang, T. Zhang, J. Ge, and Y. Yin. Permeable Silica Shell Through Surface-Protected Etching. *Nano Letters*, 8(9):2867–2871, 2008.

[48] Y. Hu, Q. Zhang, J. Goebl, T. Zhang, and Y. Yin. Control over the Permeation of Silica Nanoshells by Surface-Protected Etching with Water. *Physical Chemistry Chemical Physics*, 12(38):11836–11842, 2010.

[49] J. W. Geus. *Lecture slides, Electron Microscopy*. Utrecht University, 2009.

[50] Electron Microscopes. http://da.wikipedia.org/wiki/Elektronmikroskop.

[51] J. S. Falcone, J. L. Bass, P. H. Krumrine, K. Brensinger, and E. R. Schenk. Characterizing the Infrared Bands of Aqueous Soluble Silicates. *The Journal of Physical Chemistry A*, 114(7):2438–46, 2010.

[52] J. Osswald and K. T. Fehr. FTIR Spectroscopic Study on Liquid Silica Solutions and Nanoscale Particle Size Determination. *Journal of Materials Science*, 41(5):1335–1339, 2006.

[53] K. Kandori, Y. Kawashima, and T. Ishikawa. Characterization of Monodispersed Haematite Particles by Gas Adsorption and Fourier-transform Infrared Spectroscopy. *Journal of the Chemical Society, Faraday Transactions*, 87(14):2241–2246, 1991.

[54] A. van Blaaderen, J. van Geest, and A. Vrij. Monodisperse Colloidal Silica Spheres from Tetraalkoxysilanes: Particle Formation and Growth Mechanism. *Journal of Colloid and Interface Science*, 154(2):481–501, 1992.

[55] S. I. R. Castillo. *Surface-protected Water Etching of Silcia*. Internal report, Van 't Hoff Laboratory for Physical and Colloid Chemistry, Utrecht University, 2011.

[56] J. Palacci, S. Sacanna, A. P. Steinberg, D. J. Pine, and P. M. Chaikin. Living Crystals of Light-Activated Colloidal Surfers. *Science*, 339(6122):936–940, 2013.

[57] L. M. Peter. Energetics and Kinetics of Light-Driven Oxygen Evolution at Semiconductor Electrodes: The Example of Hematite. *Journal of Solid State Electrochemistry*, 17:315–326, 2013.

Appendix A

Breaking of Silica Shells

Below the TEM pictures are shown as described in section 4.2.3.2. The pictures show the breaking of silica shells during the degradation reaction of methylene blue. For each sample TEM pictures were taken of the particles after a few hours and three, seven and fourteen days. As it can be seen, the silica shells do not break instantaneously and the amount of broken silica shells increases with increasing reaction time.

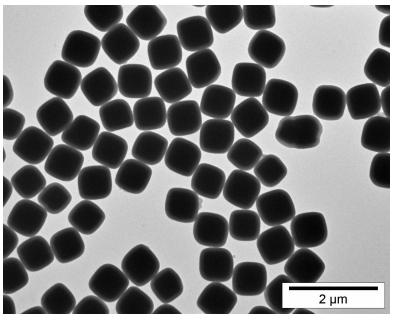

(a) After a few hours

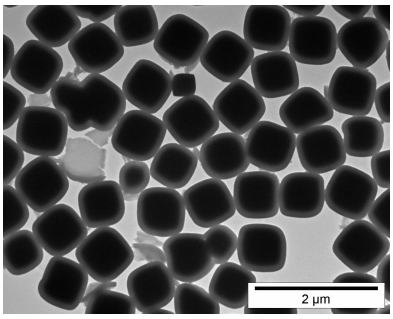

(b) After three days

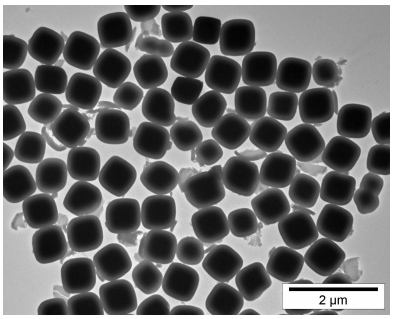

(c) After seven days

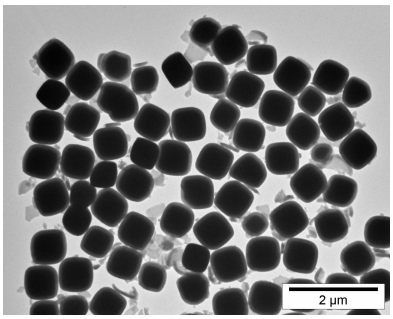

(d) After fourteen days

Figure A.1: 1 mL, 0.81 wt% SiO_2_HC1_s1 (section 4.1.1.2)

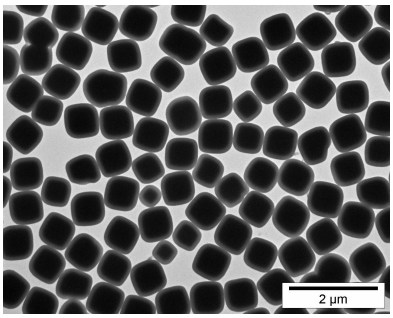

(a) After a few hours

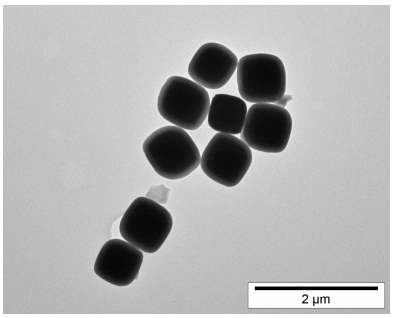

(b) After three days

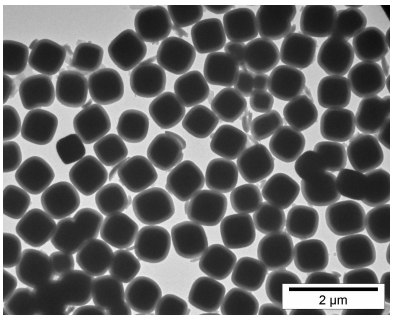

(c) After seven days

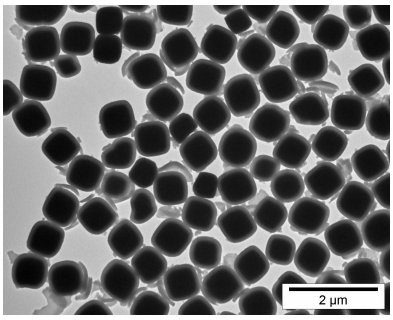

(d) After fourteen days

Figure A.2: 5 mL, 0.81 wt% SiO_2_HC1_s1 (section 4.1.1.2)

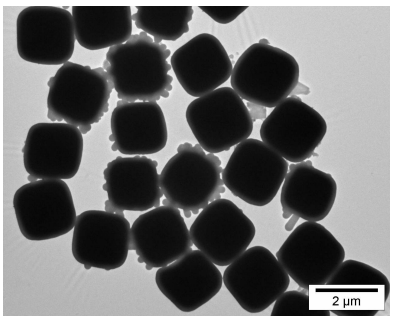

(a) After a few hours

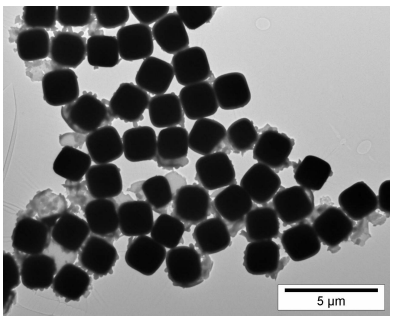

(b) After three days

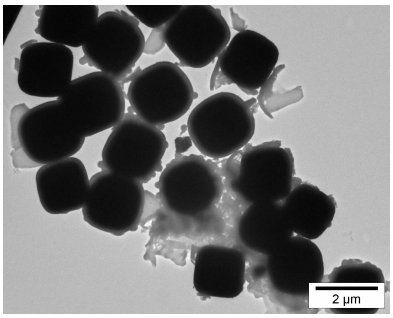

(c) After seven days

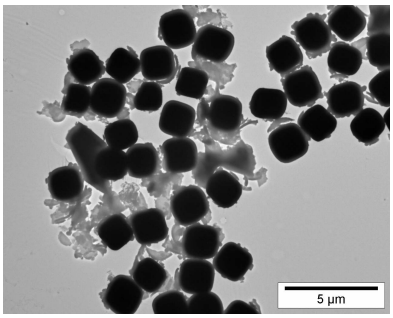

(d) After fourteen days

Figure A.3: 1 mL, 0.74 wt% SiO_2_HC2_s2 (section 4.1.7.2)

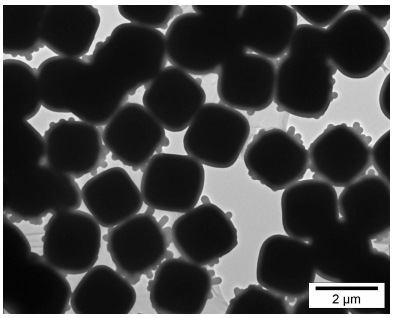

(a) After a few hours

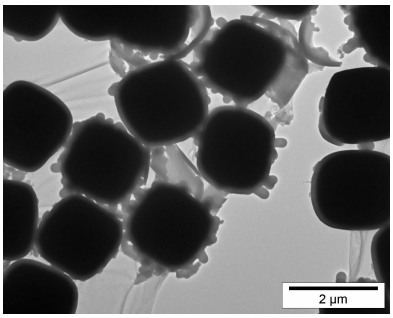

(b) After three days

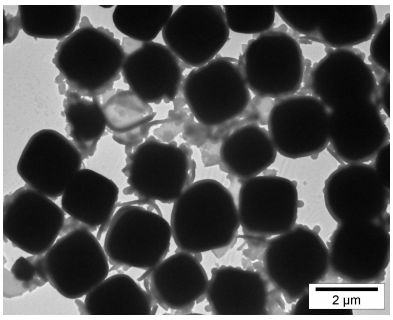

(c) After seven days

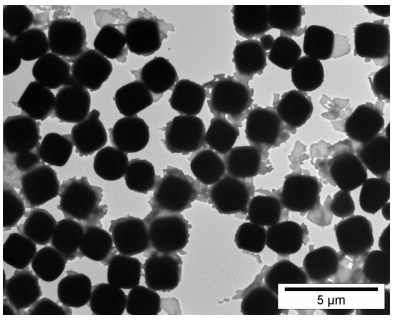

(d) After fourteen days

Figure A.4: 5 mL, 0.74 wt% SiO_2_HC2_s2 (section 4.1.7.2)

Appendix B

Nitrogen Physisorption Results

In this appendix the measured isotherms and the determined pore size distributions are given for each measured sample. Also the BET-surface area (per gram and per particle), the t-plot micropore area, the t-plot external surface area and the t-plot micropore volume (per gram and per particle) are given for the hematite and silica etched particles. In table B.1 the results are summarized for the hematite etched particles.

Table B.1: BET-surface area (per gram and per particle), the t-plot micropore volume (per gram and per particle) and the total pore volume (per gram and per particle) for the hematite etched cubes.

Sample	remaining hematite	BET (m^2/g)	BET (m^2/cube)	t-plot micropre vol. (cm^3/g)	t-plot micropre vol. (cm^3/cube)	Total pore vol. (cm^3/g)	Total pore vol. (cm^3/cube)
HC1_s2_ne	1	35	1.4×10^{-10}	0.007	2.7×10^{-14}	0.024	1.0×10^{-13}
HC1_s2_e1	0.25	68	7.0×10^{-11}	0.002	2.5×10^{-15}	0.222	2.3×10^{-13}
HC1_s2_e2	0.01	50	3.1×10^{-12}	0.003	1.9×10^{-16}	0.146	9.0×10^{-15}
Si13_HC1_s2_ne	1	51	2.5×10^{-10}	0.019	9.3×10^{-14}	0.031	1.5×10^{-13}
Si13_HC1_s2_I	0.19	175	2.9×10^{-10}	0.056	9.3×10^{-14}	0.201	3.3×10^{-13}
Si13_HC1_s2_II	0.05	308	3.3×10^{-10}	0.116	1.3×10^{-13}	0.210	2.3×10^{-13}
Si13_HC1_s2_hollow	0	294	2.9×10^{-10}	0.105	1.0×10^{-13}	0.188	1.8×10^{-13}

B.1 HC1_s2 (non-etched)

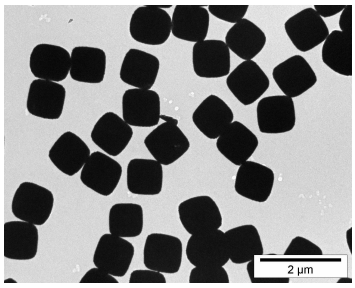

BET surface area: 34.8 m^2/g
t-plot micropore area: 13.9 m^2/g
t-plot external surface area: 20.9 m^2/g
t-plot micropore volume: 0.007 cm^3/g
Total pore volume: 0.024 cm^3/g

Figure B.1: HC1_s2 (non-etched)

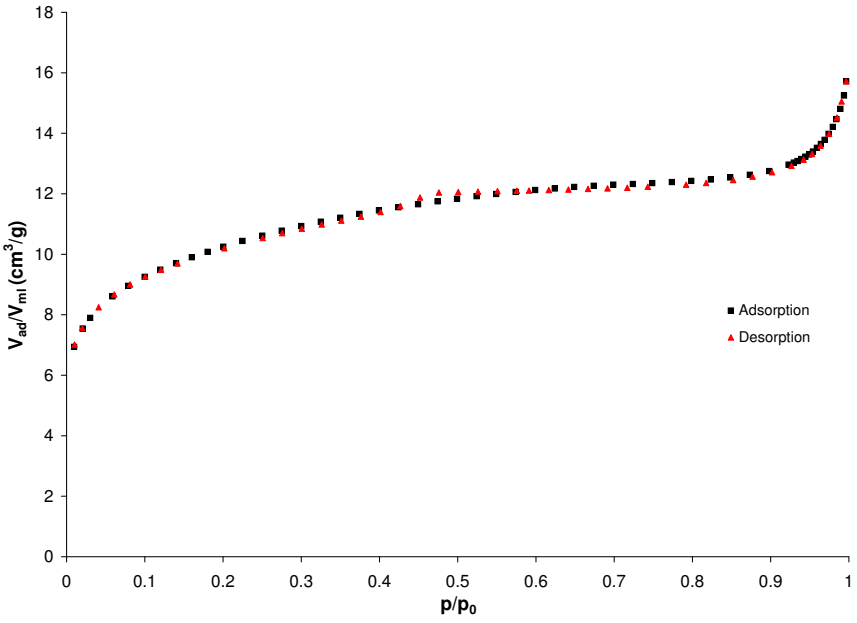

Figure B.2: Measured isotherm

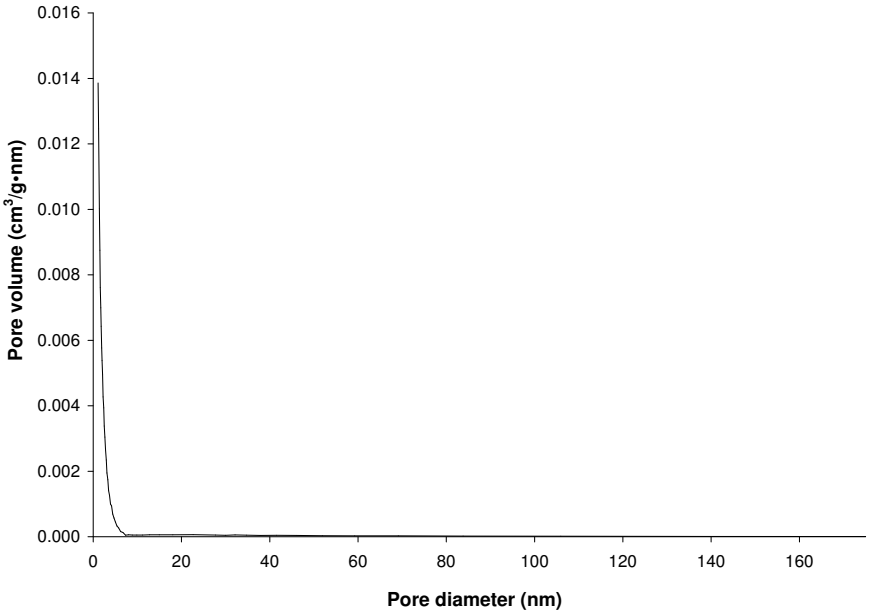

Figure B.3: Determined pore size distribution, according to the adsorption isotherm.

B.2 HC1_s2_e1

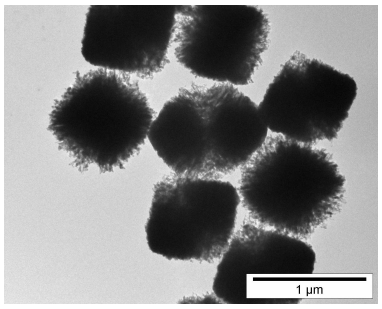

BET surface area: 67.9 m^2/g
t-plot micropore area: 6.3 m^2/g
t-plot external surface area: 61.7 m^2/g
t-plot micropore volume: 0.002 cm^3/g
Total pore volume: 0.222 cm^3/g

Figure B.4

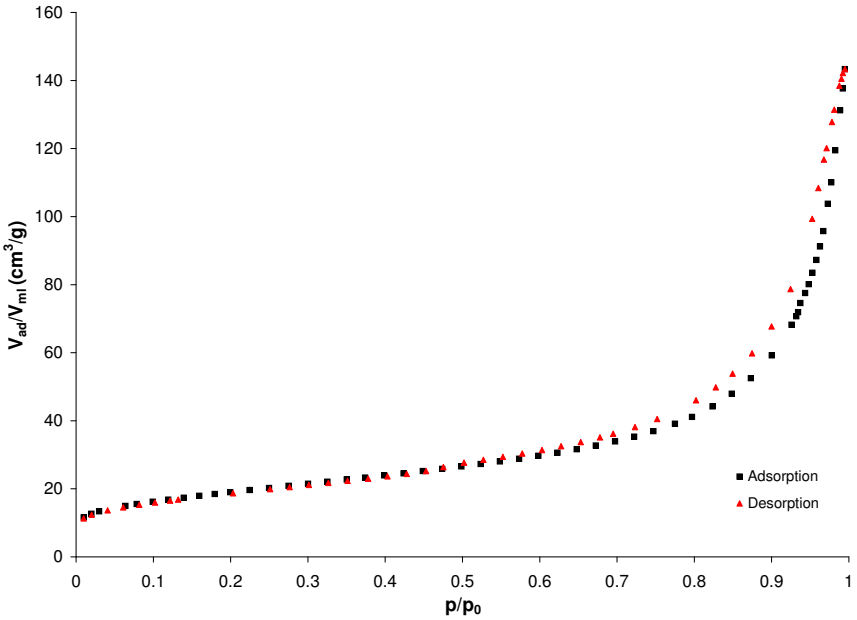

Figure B.5: Measured isotherm

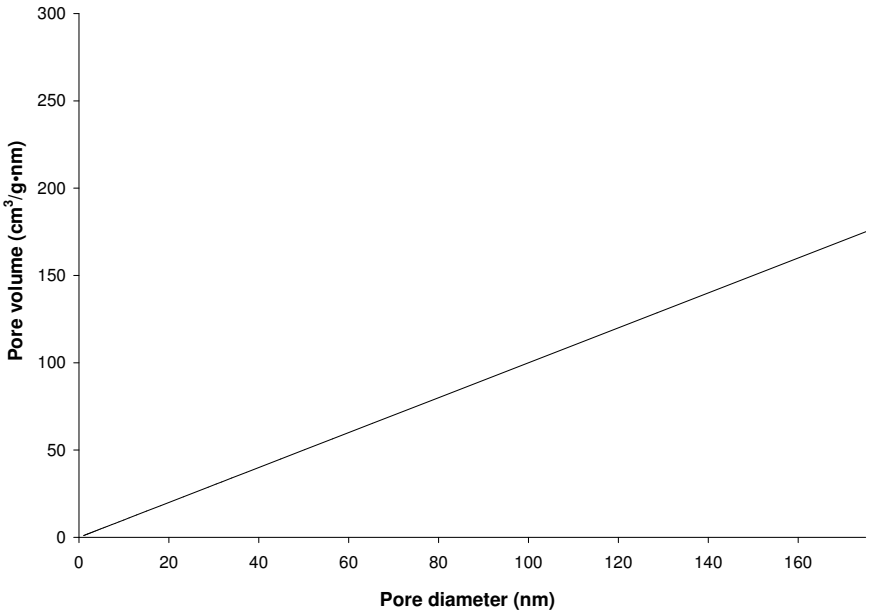

Figure B.6: Determined pore size distribution, according to the adsorption isotherm. This distribution gave a straight line, probably due to a calculation error of the computer program calculating the distribution. Therefore, below the distribution according to the desorption isotherm is given.

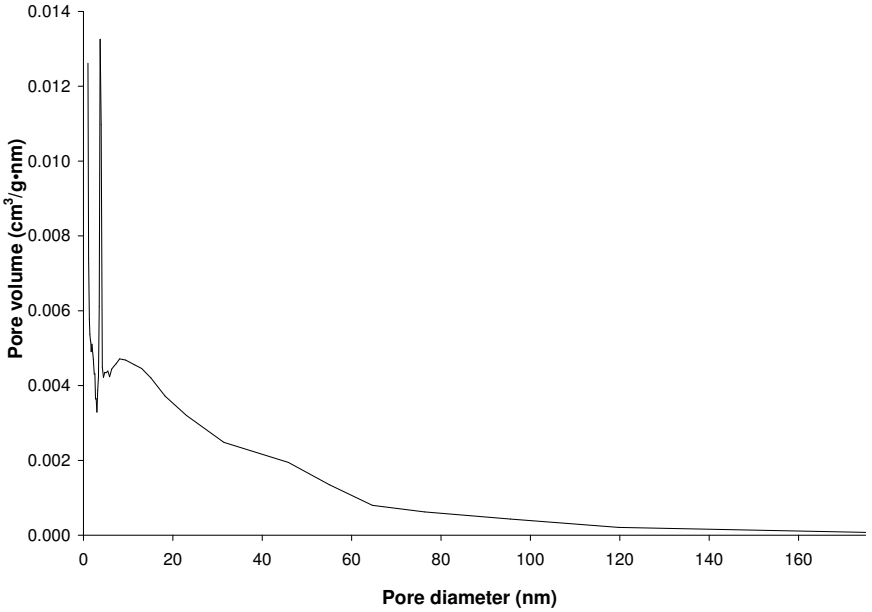

Figure B.7: Determined pore size distribution, according to the desorption isotherm.

B.3 HC1_s2_e2

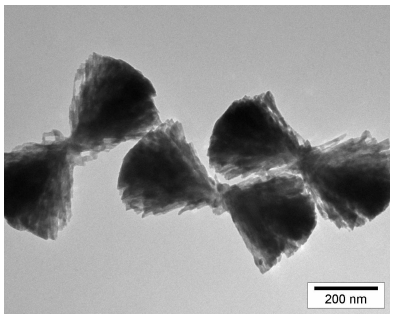

BET surface area: 49.6 m^2/g
t-plot micropore area: 7.2 m^2/g
t-plot external surface area: 42.4 m^2/g
t-plot micropore volume: 0.003 cm^3/g
Total pore volume: 0.146 cm^3/g

Figure B.8

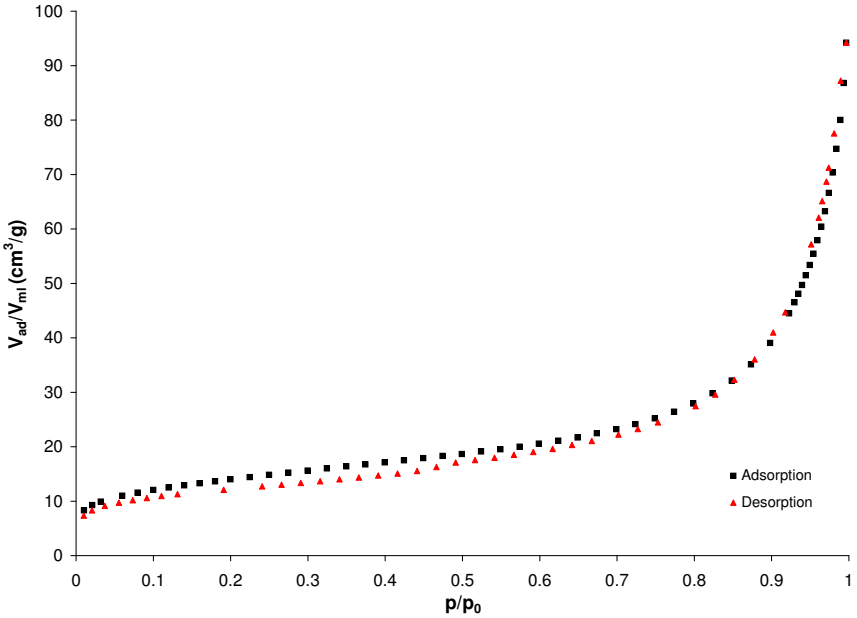

Figure B.9: Measured isotherm

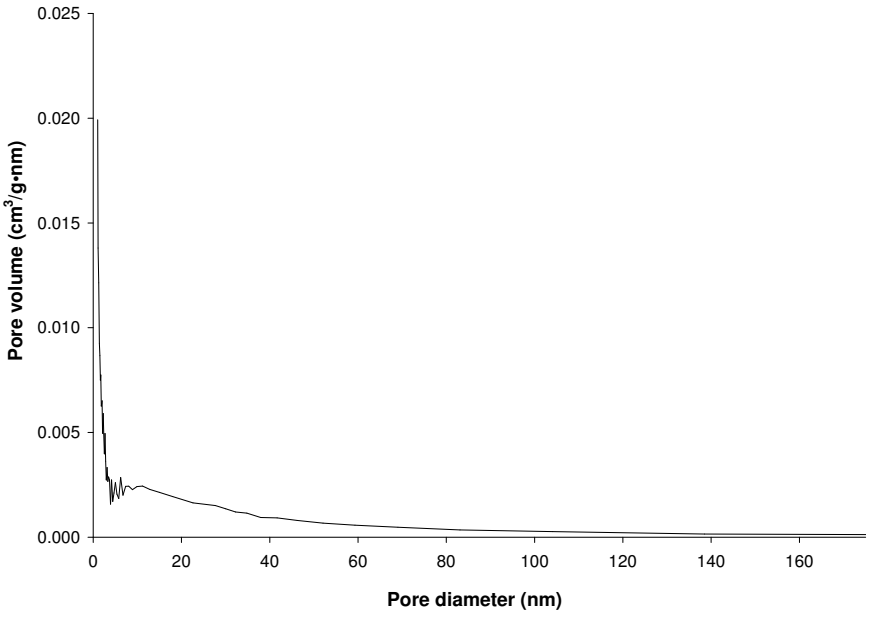

Figure B.10: Determined pore size distribution, according to the desorption isotherm.

B.4 Si13_HC1_s2 (non-ethced)

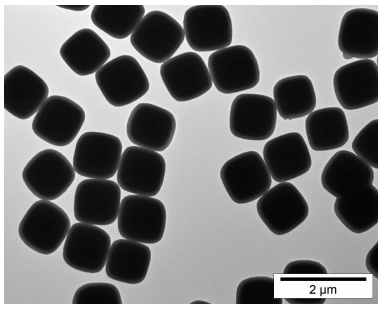

BET surface area: 51.2 m^2/g
t-plot micropore area: 38.3 m^2/g
t-plot external surface area: 12.9 m^2/g
t-plot micropore volume: 0.019 cm^3/g
Total pore volume: 0.031 cm^3/g

Figure B.11

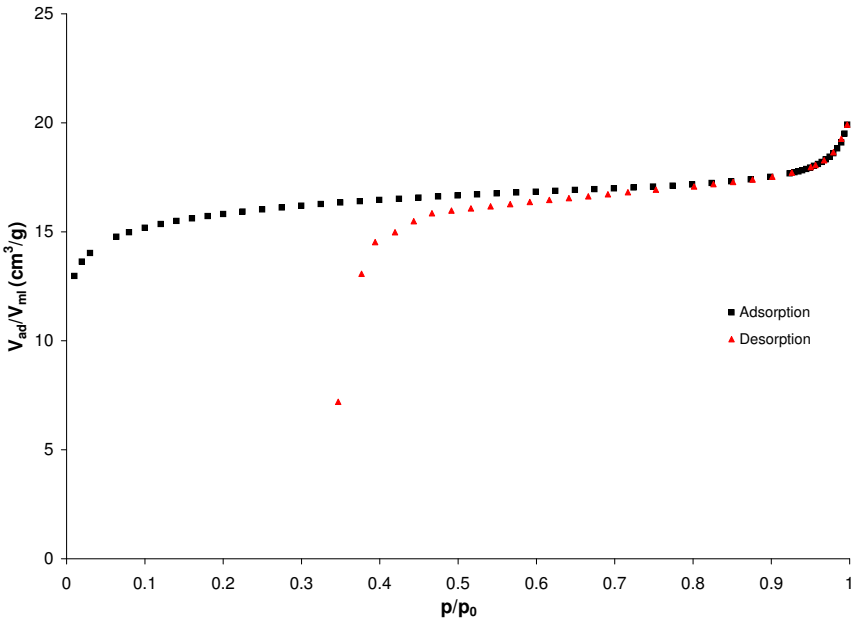

Figure B.12: Measured isotherm

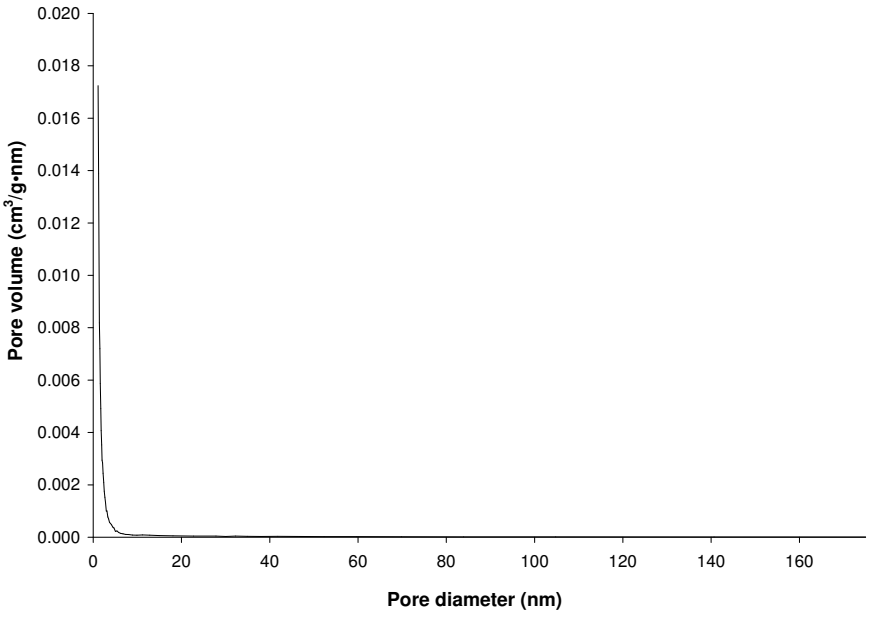

Figure B.13: Determined pore size distribution, according to the desorption isotherm.

B.5 Si13_HC1_s2_I

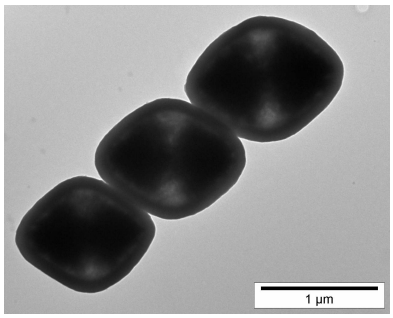

BET surface area: 175.4 m^2/g
t-plot micropore area: 115.1 m^2/g
t-plot external surface area: 60.4 m^2/g
t-plot micropore volume: 0.056 cm^3/g
Total pore volume: 0.201 cm^3/g

Figure B.14

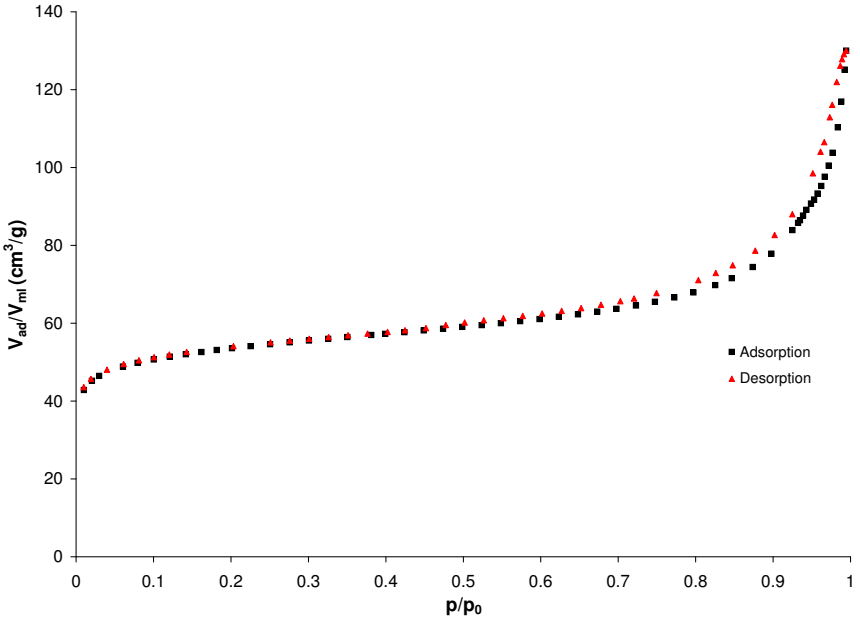

Figure B.15: Measured isotherm

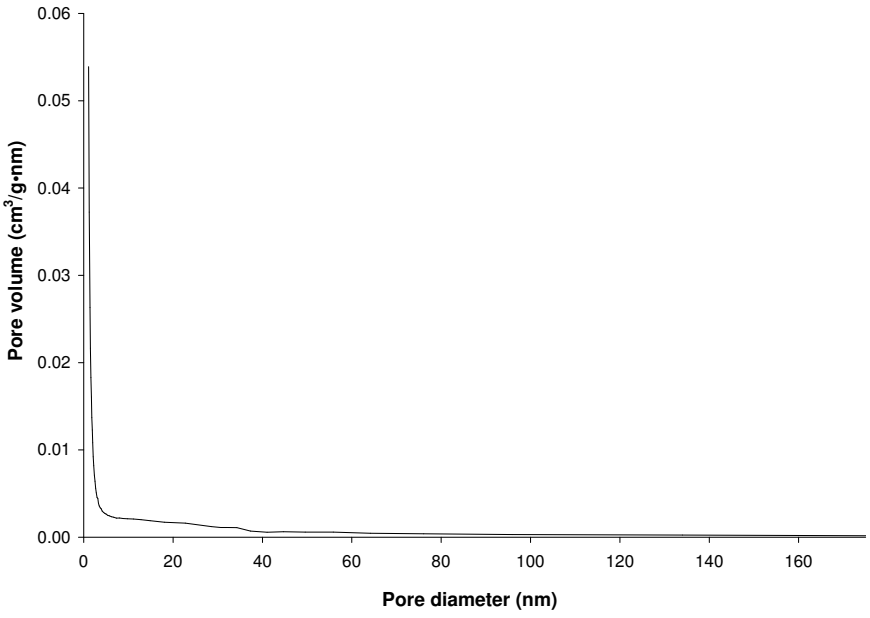

Figure B.16: Determined pore size distribution, according to the desorption isotherm.

B.6 Si13_HC1_s2_II

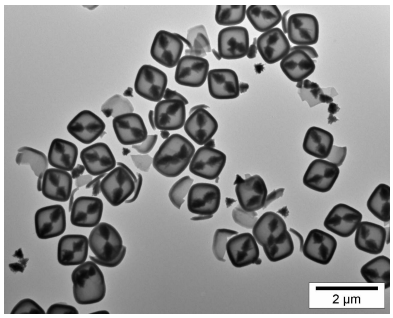

BET surface area: 307.5 m^2/g
t-plot micropore area: 237.2 m^2/g
t-plot external surface area: 70.3 m^2/g
t-plot micropore volume: 0.116 cm^3/g
Total pore volume: 0.210 cm^3/g

Figure B.17

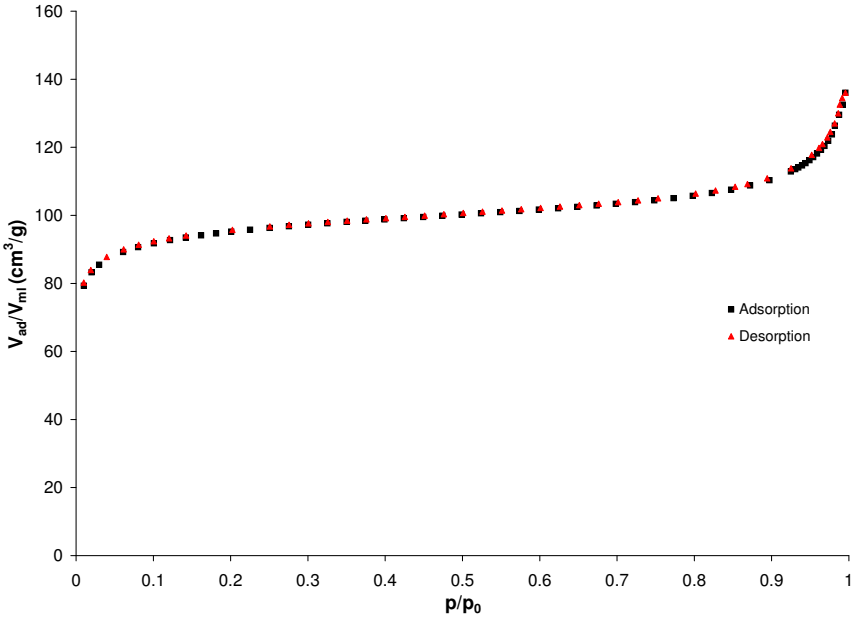

Figure B.18: Measured isotherm

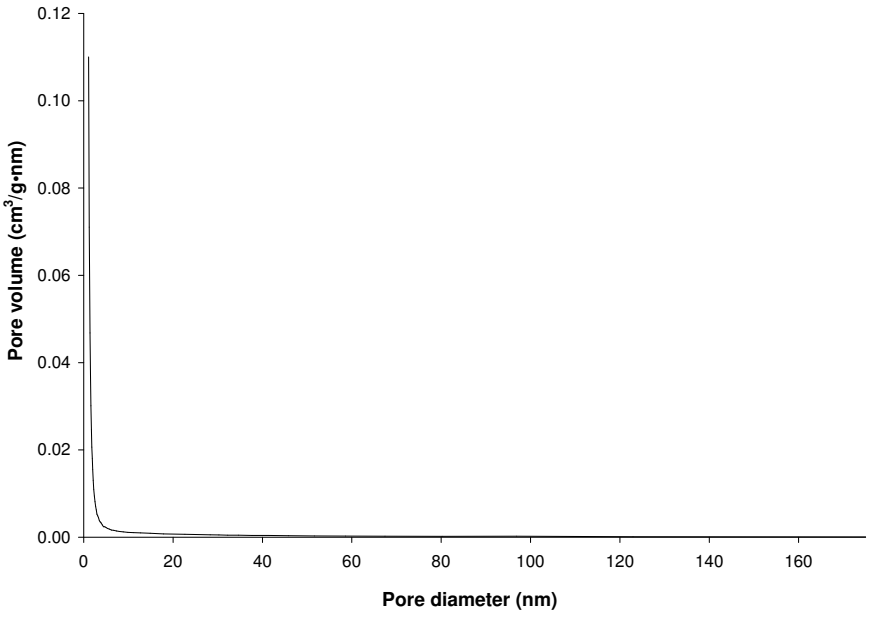

Figure B.19: Determined pore size distribution, according to the desorption isotherm.

B.7 Si13_HC1_s2_hollow

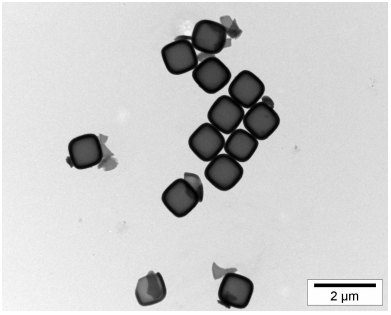

BET surface area: 293.7 m^2/g
t-plot micropore area: 214.9 m^2/g
t-plot external surface area: 78.8 m^2/g
t-plot micropore volume: 0.105 cm^3/g
Total pore volume: 0.188 cm^3/g

Figure B.20

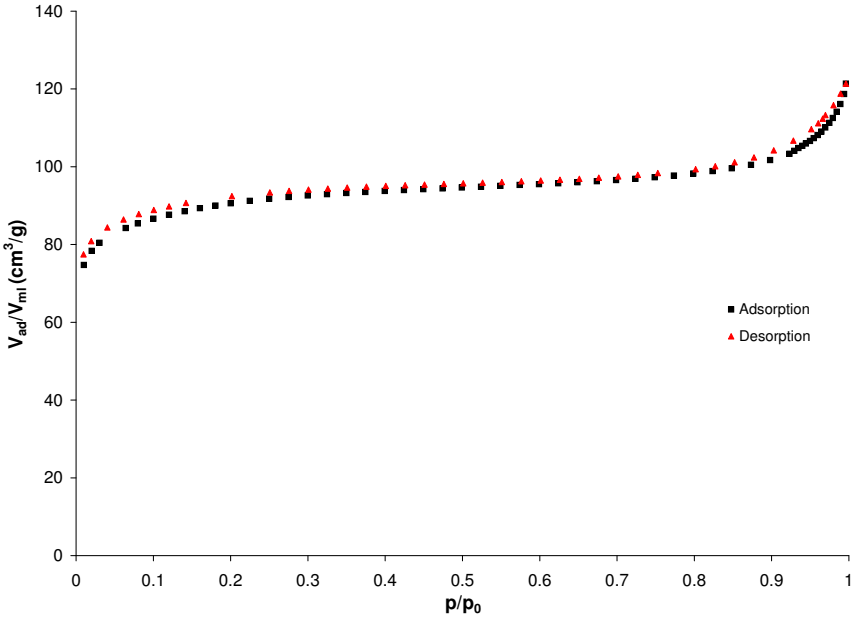

Figure B.21: Measured isotherm

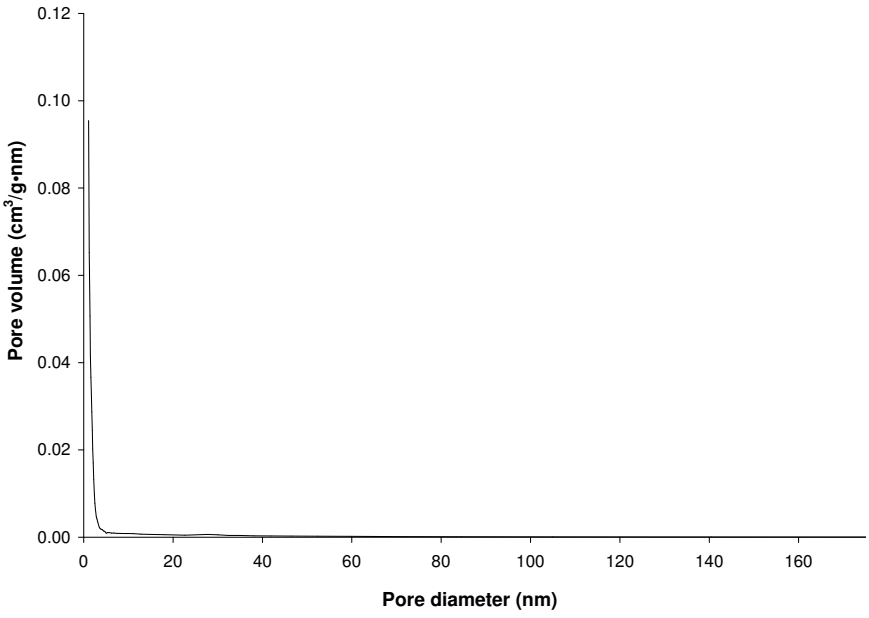

Figure B.22: Determined pore size distribution, according to the desorption isotherm.

B.8 SE_N_2_A

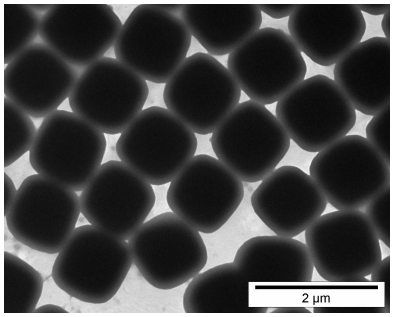

BET surface area: 57.5 m^2/g
t-plot micropore area: 39.6 m^2/g
t-plot external surface area: 17.9 m^2/g
t-plot micropore volume: 0.019 cm^3/g
Total pore volume: 0.035 cm^3/g

Figure B.23

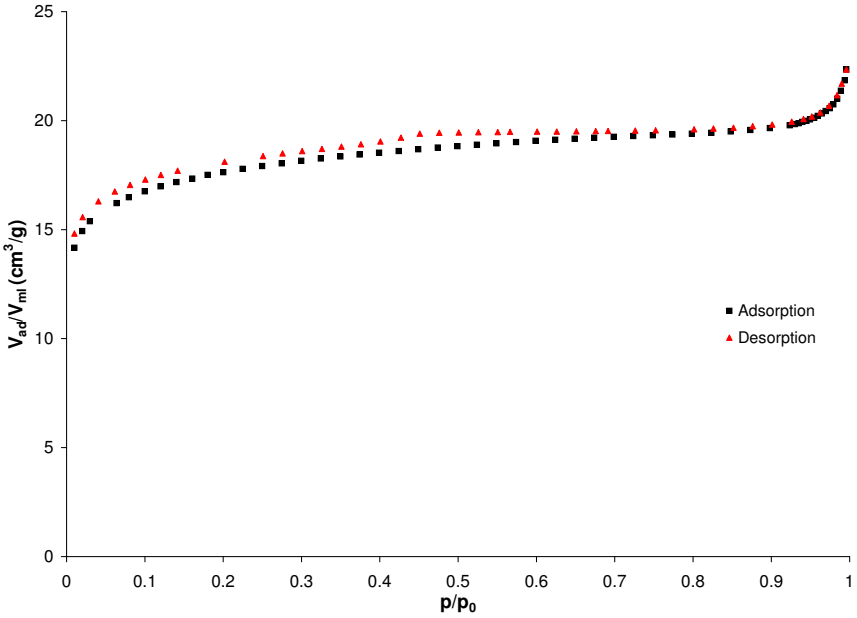

Figure B.24: Measured isotherm

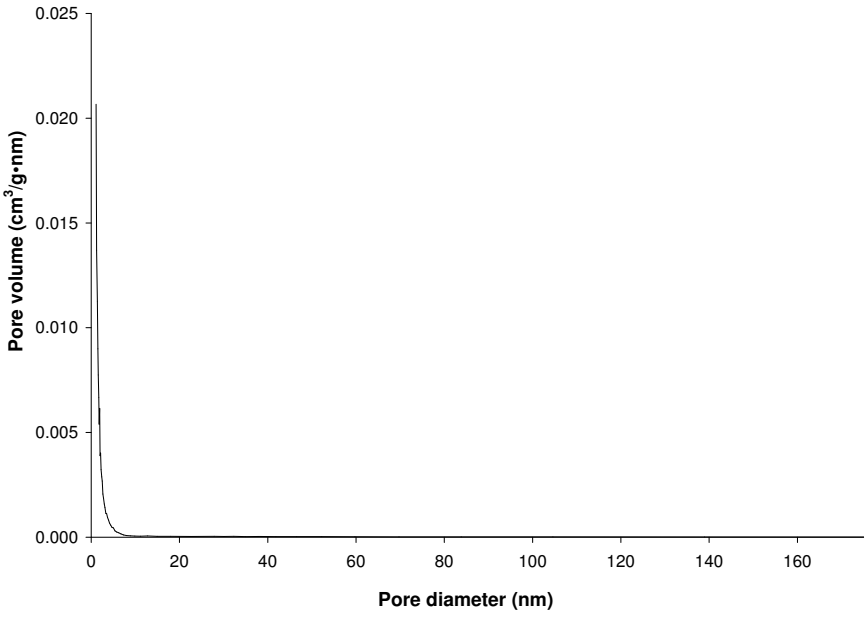

Figure B.25: Determined pore size distribution, according to the desorption isotherm.

B.9 SE_N_2_C

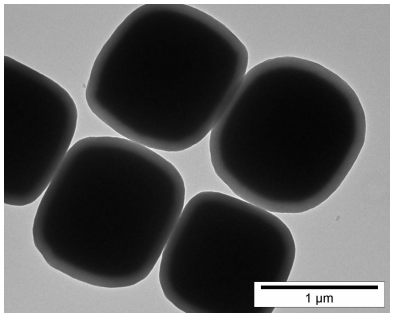

BET surface area: 103.8 m^2/g
t-plot external surface area: 110.2 m^2/g
Total pore volume: 0.066 cm^3/g

Figure B.26

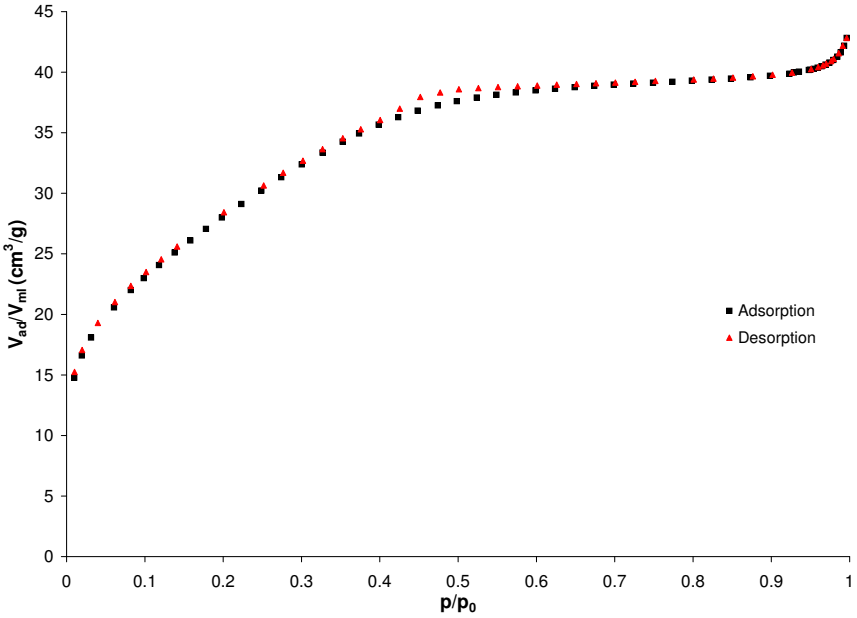

Figure B.27: Measured isotherm

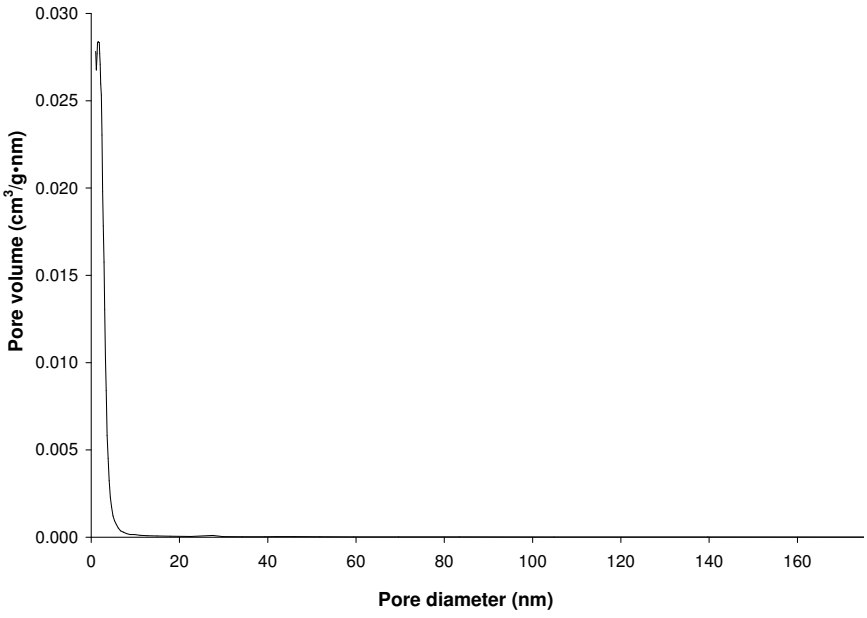

Figure B.28: Determined pore size distribution, according to the desorption isotherm.

B.10 SE_N_2_G

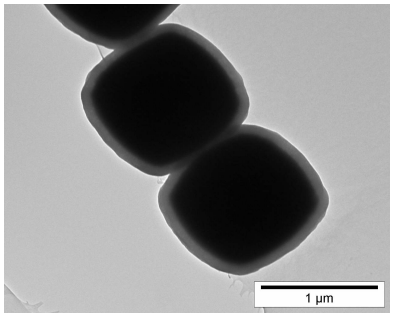

BET surface area: 34.5 m^2/g
t-plot external surface area: 34.7 m^2/g
Total pore volume: 0.076 cm^3/g

Figure B.29

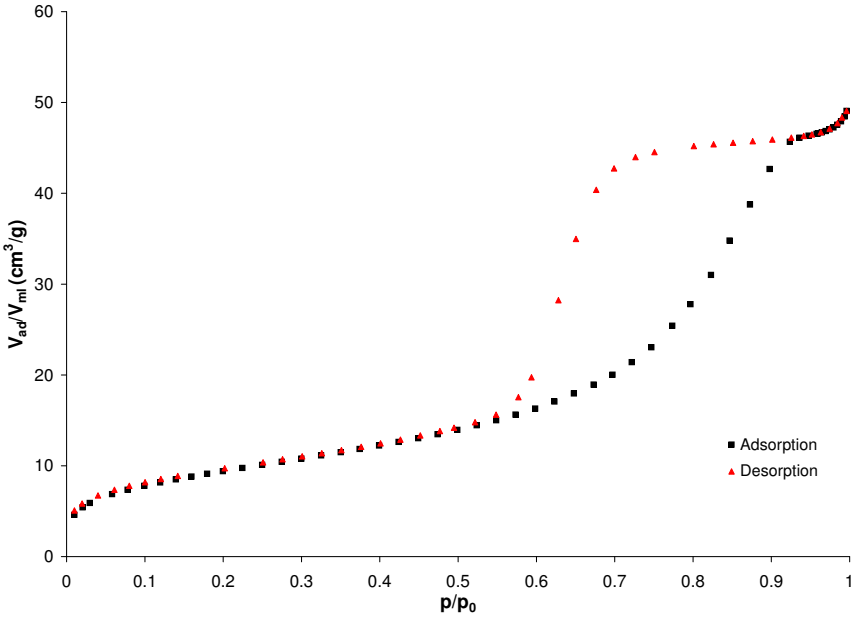

Figure B.30: Measured isotherm

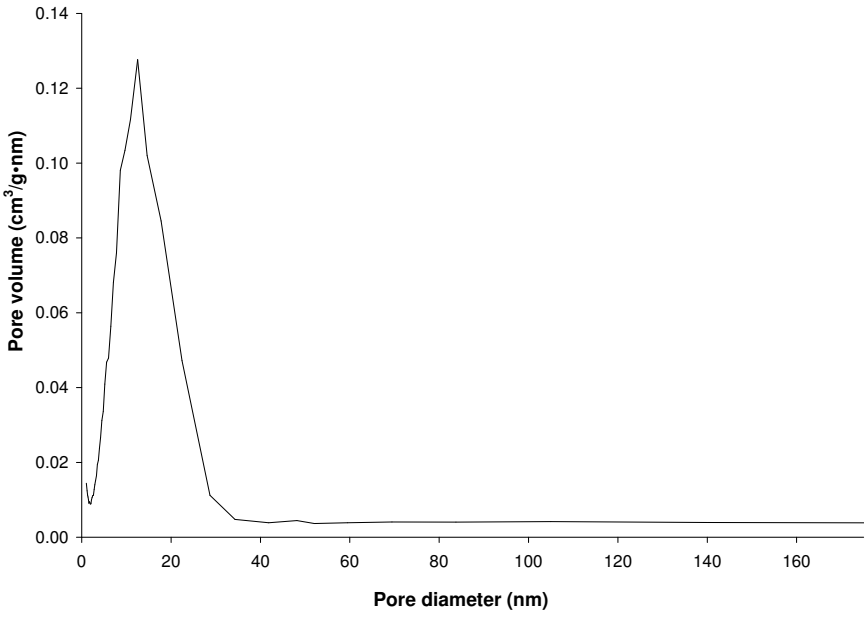

Figure B.31: Determined pore size distribution, according to the desorption isotherm.

Appendix C

Substrates versus Dispersed

In this overview SEM and TEM pictures are shown of dispersed and immoblized cubes, to compare the damaging of the silica shells. In the first column SEM pictures are shown of the substrates from section 4.3.2, the second column shows TEM pictures of cubes which were released from these substrates into the supernatant during the reaction. The third column shows TEM pictures of the same type of cubes however, these were used in dispersed form for the catalytic activity tests (section 4.2.3). As it can be seen, the silica shells of the particles in the third column, which did not have a heat treatment, are more severely damaged in comparison with the particles form the first and second column. The numbers correspond to the used cubes:

Sample	Figure	Cubes	Size (nm)
1	4.2	SiO_2_HC1_s1	743
2	4.3a	SiO_2_HC1_s1_1	743
3	4.3b	SiO_2_HC1_s1_2	743
4	4.17	SiO_2_HC2_s2	1784
5	4.18a	SiO_2_HC2_s2_1	1784
6	4.18b	SiO_2_HC2_s2_2	1784

SEM substrate | TEM supernatant substrate | TEM supernatant dispersed

1

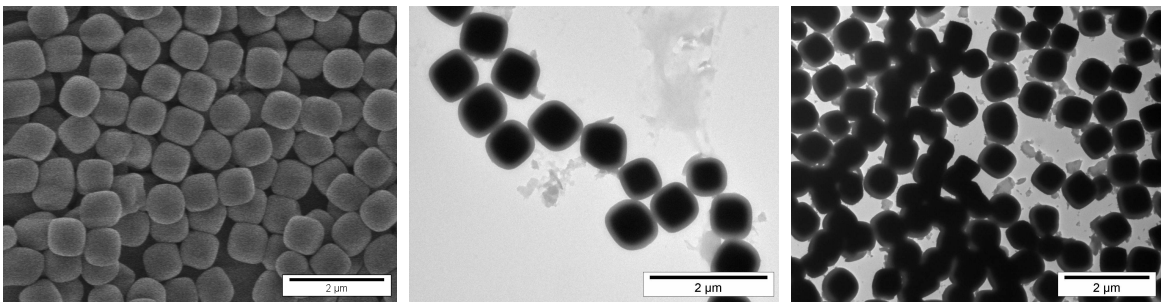

2

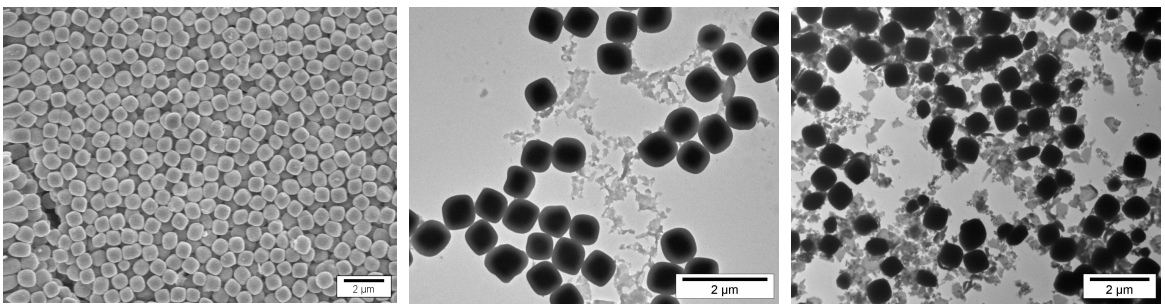

3

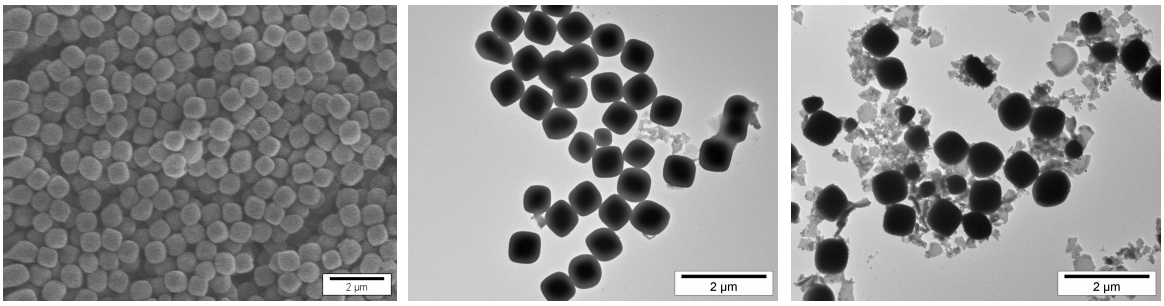

4

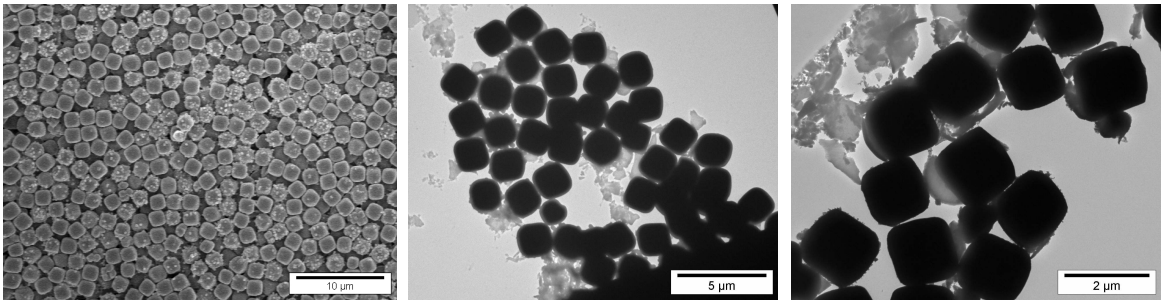

5

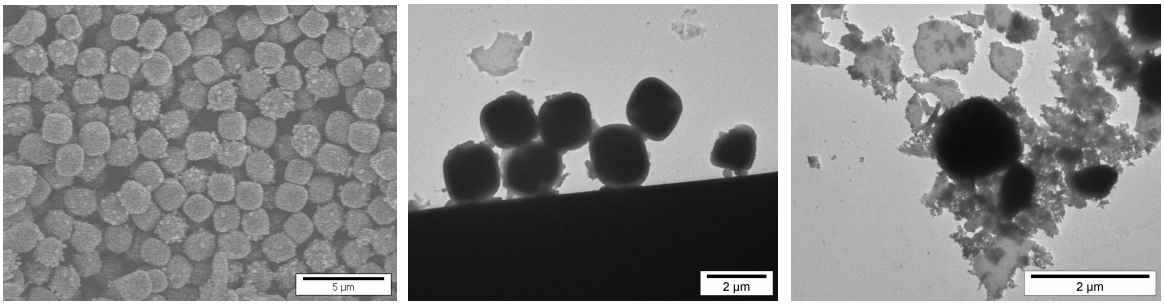

6